THE EFFECTS OF COCAINE SELF-ADMINISTRATION ON STRUCTURAL PLASTICITY OF ASTROCYTES

Anze Testen

A dissertation submitted to the faculty at the University of North Carolina at Chapel Hill in partial fulfillment of the requirements for the degree of Doctor of Philosophy in Neuroscience Curriculum in the UNC Scholl Of Medicine.

Chapel Hill
2021

Approved By:

Kathryn J. Reissner

Donita L. Robinson

Regina M. Carelli

Thomas L. Kash

Richard J. Weinberg

ABSTRACT

Anze Testen: The effects of cocaine self-administration on structural plasticity of astrocytes
(Under the direction of Kathryn J. Reissner)

One of the hallmark features of cocaine use disorder is susceptibility toward relapse following cessation of use. It is thus imperative to elucidate neurobiological factors of relapse, to inform more targeted treatment approaches. Previous studies have reported decreases in expression of astrocyte-associated proteins in the nucleus accumbens core following rat cocaine self-administration and extinction training, pointing to possible glial control of relapse vulnerability. Recent results from our laboratory have further revealed remarkable decreases in morphometric features of accumbens astrocytes, as well as decreased colocalization with neuronal synaptic elements. Here I explore the regional specificity of astrocytic responsiveness to cocaine self-administration, as well as the necessity of the withdrawal for its manifestation. Results indicate that the reduced astrocytic phenotype is specific for astrocytes in nucleus accumbens and are not observed in other brain reward centers following cocaine self-administration and extinction. Further, the extinction period was necessary for the development of the atrophic phenotype, with rats undergoing self-administration only not showing morphometric impairments.

To understand the subcellular nature of the atrophic phenotype, the second part of the study explored astrocyte branching complexity as well the number and density of accumbens astrocyte processes associated with two commonly utilized cocaine self-administration paradigms. To this end, novel 3-dimensional branching and Sholl analyses were employed as

well as end-point and segment analyses, in order to delineate between qualitative and quantitative changes to astrocyte structure following cocaine self-administration. Results showed similar directional changes to subcellular features of astrocytes, with a more severe atrophic phenotype across the analyzed features associated with longer cocaine access and prolonged abstinence. Lastly, segment analysis revealed changes in segment number but not average length, indicating atrophic phenotype is not due to astrocyte shrinkage but rather loss of branching complexity and segments.

In summary, this dissertation expands knowledge regarding structural plasticity of astrocytes following cocaine use and withdrawal, revealing specific vulnerability of nucleus accumbens astrocytes to cocaine self-administration, and a common observation of decreased interactions between astrocytes and synapses across self-administration paradigms, which is exacerbated by prolonged cocaine access and abstinence.

To my family for unconditionally supporting me on my intellectual journey and being my rock, and to J for being a rigorous peer and a loving partner.

ACKNOWLEDGMENTS

The work presented here is a culmination of the effort from the last 6 years with multiple brilliant scientists and colleagues contributing throughout this time. Thank you.

Firstly, to Ronald Y. Kim and Han "Jenny" Wang for contributing data for the complexity analysis and for diligently working on the branching algorithm, respectively. The advancement in knowledge presented here would not have been possible without you.

To Reissner lab family, past and present, including, but not limited to Marian, Kati, Ron, Emily, Janay, Eden, Tania, Thery and all the undergrad students, thank you for your encouragement, feedback, and help during the years. It is a joy working in a relaxed and collaborative, yet curiosity-stimulating environment.

To Kate, for giving me the space to run wild with my ideas yet still carefully guiding me so they became a reality. Thank you for all the lunches, cakes, adult beverages, and lab snacks that sustained my research in a very physiological way. And thank you for teaching with example how to be a great and generous PI and human being, yet still pursuing cutting edge competitive science. I hope in the future I can implement what I learned from you and, hopefully, make you proud.

To Donita, for guiding me from the interview weekend, through the first-year mentorship to the dissertation defense. Thank you for all the encouragement, advice, and many words of wisdom. Last but not least, thank you for introducing me to Kate.

To the dissertation committee members Drs. Carelli, Kash, and Weinberg: thank you for guiding me through the dissertation process and asking questions that elevated my science. Especially thank you guiding and helping me improve my planning and time management skills so

that I can be a successful scientist. I am wiser for going through this process with you.

Thank you also to the BBSP program, Neuroscience Curriculum and BIN program for supporting and housing me during my research.

TABLE OF CONTENTS

LIST OF FIGURES

LIST OF TABLES

LIST OF ABBREVIATIONS

AAV	Adeno-associated virus
AMPA	α-amino-3-hydroxy-5-methyl-4-isoxazolepropionic acid
ANOVA	Analysis of variance
DA	Dopamine
DAT	Dopamine transporter
DREADD	Designer receptors exclusively activated by designer drugs
DSM-V	Diagnostic and Statistical Manual of Mental Disorders
EDTA	Ethylenediaminetetraacetic acid
FDA	Food and Drug Administration
FR1	Fixed ratio 1
GAPDH	Glyceraldehyde 3-phosphate dehydrogenase
GFP	Green fluorescent protein
GFAP	Glial fibrillary acidic protein
GLT-1	Glutamate transporter type I
GluA1	Glutamate ionotropic receptor AMPA subunit type 1
GluA2	Glutamate ionotropic receptor AMPA subunit type 2
i.p.	Intraperitoneal
i.v.	Intravenous
iGluR	Ionotropic glutamate receptor
Lck	Lymphocyte protein tyrosine kinase
LgA	Long-access
mGluR	Metabotropic glutamate receptor
NAc	Nucleus accumbens

NAC	N-acetylcysteine
NGS	Normal goat serum
NIDA	National Institute of Drug Abuse
NMDA	N-methyl-D-aspartate
PB	Phosphate buffer
PBS	Phosphate buffered saline
PBST	Phosphate buffered saline + triton x-100
PFA	Paraformaldehyde
PPF	Propentofylline
PSD 95	Post synaptic density 95
Rac1	Ras related C3 botulinum toxin substrate 1
ROI	Region of interest
SA	Self-administration
ShA	Short-access
SUD	Substance use disorder
xCT	Catalytic subunit of the cystine-glutamate exchanger

CHAPTER 1: GENERAL INTRODUCTION

Substance use disorder

Substance use disorder (SUD) is a chronic relapsing brain disorder mainly characterized by neurobiological changes that lead to compulsive substance use as well as a loss of control over substance intake (Koob 2000). According to the Diagnostic and Statistical Manual of Mental Disorders (DSM-V), SUD is one of two substance related disorders, the other being substance-induced disorders (e.g. intoxication). To date there are 11 distinct criteria that are describing problems arising from SUD such as involuntary increases in dosage, inability to stop using, craving, tolerance and withdrawal (McLellan 2017). Mild disorder is diagnosed when 2-3 criteria are met, 4-5 indicates moderate and above 6 diagnosed criteria a severe SUD. Available statistics for 2017 reported 19.7 million people in the United States (above 7% of the population) met DSM-V criteria for SUD, including alcohol and prescription drugs (Uhl et al 2019). Around 40% of SUD cases were found to be illicit drugs. In 2019 CDC reported 70,630 cases where overdose was listed as official cause of death, with over 841,000 deaths reported since 1999. Notably, the numbers from 2019 were double the numbers reported a decade earlier. Besides the direct cost of human lives, SUD is recognized as a severe economic burden on a society; lost work productivity, law enforcement expenses, and healthcare resources associated with SUD have been estimated by NIDA to be upwards of $700 billion annually.

Pharmacological interventions are usually the prevailing approach for treating human diseases. Unfortunately, there are very limited options available for treatment of SUD. The FDA has approved just a handful of medications for SUD, namely acamprosate, disulfiram and

naltrexone for alcohol use; bupropion, NRTs and varenicline for nicotine use disorder; and buprenorphine for withdrawal symptoms as well as naltrexone methadone for relapse prevention for opioid use disorder (Kalin 2020, Liu & Li 2018). Cognitive behavioral therapy is also sometimes used although benefits are limited and temporary (Liu & Li 2018). Even though currently approved pharmacological treatments are moderately successful in reducing withdrawal symptoms and craving, no significant reduction is observed in relapse prevention. Incredibly, two thirds of patients seeking treatment for SUD relapsed within months and 85% of all users ultimately relapsed within a year of cessation of use (Sinha 2011).

Conspicuously absent from the list above are any medications or therapies approved for use disorder involving stimulants e.g., cocaine and amphetamine. A recent meta-analysis of pharmacotherapies that underwent randomized controlled trials (RCTs) for use in cocaine use disorder reported that the most tested compounds were antidepressants (38 RCTs) but all appear to have no efficacy in preventing cocaine use or on treatment retention (Chan et al 2019). Bupropion and topiramate extended abstinence but the general strength of evidence was considered low. Accordingly, exploring neurobiological substrates of relapse and candidate treatment targets should thus be a high priority. Unfortunately, due to high fail rate of tested compounds, most pharmaceutical companies have halted or scaled down their drug discovery programs catering the psychiatry field (Hyman 2013). There are multiple plausible reasons for that but the most obvious one, the failure of preclinical models, is most likely not the right one, although more attention to data robustness and data generalizability would indeed be welcomed (Bespalov et al 2016). This said, multiple preclinical models that were developed in the past employed a non-contingent mode of administration, where the drug is given by the experimenter. Behavioral sensitization to psychostimulants (Dafny & Yang 2006), interoceptive effects of a drug using drug discrimination paradigm (Jaramillo et al 2018), and motivational properties of

the drug tested with conditioned place preference (CPP) paradigm (Tzschentke 2007) are mostly performed using non-contingent drug administration. Humans, as well as vertebrate model organisms, voluntarily take drugs via multiple routes, including orally and intravenously (Spanagel 2017). If sudden unlimited access to heroin or cocaine is provided, laboratory animals readily lethally overdose (Nesse & Berridge 1997, Spanagel 2017). This is also frequently observed in drug users. It is widely accepted that drug and alcohol intake are common occurrence in mammals as well as other species (Sullivan & Hagen 2002). Thus, it is paramount that an effective drug administration model include the component of the voluntary drug taking. To this end, self-administration models (SA) that can encapsulate multiple evolutionary elements of drug taking, including overdose and (especially) relapse, are a gold standard in the field (Shaham et al 2003).

The drug self-administration paradigms as animal models of relapse

Perhaps the most used behavioral paradigm to model relapse particularly to cocaine is the extinction/reinstatement model (Bossert et al 2005, Bossert et al 2013). It consists of acquiring operant self-administration behavior and subsequently extinguishing it with extinction training, where previously active operandus (e.g., lever or nose poke) no longer results in delivery of the drug (or a drug-conditioned cue). Extinction training (Ex) usually lasts for 15 days, or until the behavior is sufficiently extinguished based on the predefined criteria. After successful extinction of the drug-taking behavior, the relapse potential (or drug seeking) can be measured using a reinstatement test, where animals are either injected with a bolus injection of a drug by administrator just before being placed in the operant chamber (drug-primed), or a drug-conditioned cue is reintroduced upon an active lever press (cue-primed). This model has been instrumental in studying neurobiological substrates underlying drug seeking and relapse (Dong et

al 2017).

Although powerful and reproducible model of relapse, the extinction/reinstatement model is often challenged for the inclusion of some use disorder elements not present in humans as well as the lack of others that are readily observable (Belin-Rauscent et al 2016). It is generally recognized that extinction training is not easily translatable to the human drug use condition, and its usefulness was questioned (Sanchis-Segura & Spanagel 2006) since users normally undergo a period of abstinence following cessation of use when being hospitalized for rehabilitation or while incarcerated. On the other hand, multiple well-recognized SUD elements in humans are not represented in the extinction/reinstatement paradigm, such as drug craving, tolerance and withdrawal. Therefore, alternative models have emerged to address translational shortcomings. This includes longer access of SA periods (typically 2h/day in the SA+Extinction model) coupled with home cage abstinence. The long access (LgA) and abstinence (Ab) model employs longer SA daily exposure to the drug (often cocaine) that reproducibly results in increased taking over time compared to more stable taking in the short-access (ShA) and extinction model (Li et al 2015). Increased drug taking reflects increase in drug craving as well as model development of tolerance (Ferrario et al 2005). Instead of the extinction training, LgA SA is followed by more translationally appropriate forced home cage abstinence (Ab) (usually between 30 and 45 days). Following the abstinence, seeking can again be assessed using a cue- or drug-primed seeking test (this time termed extinction test as opposed to reinstatement test since the drug-taking behavioral was never actually extinguished). The LgA+Ab paradigm is known to produce higher degree of seeking compared to ShA+Ex paradigm. This can not be explained exclusively by higher amount of drug taking during the SA period, since the drug seeking reproducibly increases with longer abstinence periods. This abstinence-length corelated increase in seeking has been termed incubation of craving, and was first described in cocaine use (Grimm et al 2001, Pickens et al

2011). It is also readily observable in human subjects thus translationally relevant (Parvaz et al 2016). The incubation of craving itself is not exclusive to cocaine. It was also reported in methamphetamine (Venniro et al 2017) and even with sucrose and palatable foods (Grimm 2020, Lu et al 2004).

To develop novel pharmacological therapies and better serve the patients, the neurobiological underpinnings of cocaine seeking and relapse must be understood. These investigations have revealed brain regions and associated molecular targets involved in the reward processing of acute cocaine administration, as well as changes in brain circuitry and molecular signaling governing the uncontrollable seeking and relapse vulnerability after repeated cocaine exposure (Kalivas 2007). Importantly, self-administration models have also been paramount in elucidation of the brain's innate reward circuitry, and is considered the gold standard for preclinical investigations of candidate therapeutic interventions (Belin-Rauscent et al 2016).

Neurobiological adaptations and glutamate homeostasis in the NAc following cocaine self-administration and withdrawal

The nucleus accumbens (NAc) is a central locus for reward processing, both adaptive and maladaptive. Located in the basal forebrain, it integrates projections from the limbic regions and projects to motor regions, thus being strategically positioned to control important aspects of motivated behavior (Mogenson et al 1980, Roitman et al 2005). Since cocaine is known to be a dopamine reuptake inhibitor, acute effects of cocaine exposure are largely mediated by elevated dopamine in the NAc (Cornish & Kalivas 2001a, Fowler et al 2001, Gatley et al 1997, Logan et al 1997, Volkow et al 1997a, Volkow et al 1997b, Volkow et al 1997c, Wang et al 1997). Interestingly, chronic exposure to cocaine leads to dysregulation in other neurotransmitter

signaling pathways, in particular glutamate (Cornish & Kalivas 2001a, Cornish & Kalivas 2001b, Kalivas & McFarland 2003, Kalivas et al 2003, McFarland & Kalivas 2001, Swanson et al 2001, Toda et al 2003). Glutamate concentrations are tightly regulated, and a critical balance is maintained between synaptic and extrasynaptic levels (Kalivas 2009, Knackstedt et al 2010a, Reissner & Kalivas 2010). Glutamate homeostasis is achieved mainly through the action of glial cells which can both mediate glutamate release and uptake (Bowers & Kalivas 2003, Tang & Kalivas 2003). In the extracellular space, basal levels of glutamate are regulated via the cystine-glutamate exchanger (xC-), which releases intracellular glutamate for the import of extracellular cystine, using 1:1 stoichiometric rate (McBean 2002).

Alongside Xc-, EAAT2/GLT-1, the most abundant high-affinity glutamate transporter, also plays a crucial role in maintaining glutamate homeostasis, by modulating synaptic glutamate levels. GLT-1 accounts for roughly ~90% of all synaptic glutamate clearance and it is, like Xc-, primarily expressed in astrocytes (Danbolt 2001, Kalivas 2009). Under physiological conditions, GLT-1 is responsible for the rapid uptake of synaptically released glutamate, maintaining a boundary between synaptic and extrasynaptic glutamate, as well as access to synaptic and extrasynaptic receptors (Kalivas 2009). Interestingly, cocaine ShA+Ex has been extensively reported to result in disruptions in glutamate homeostasis by downregulating the expression and activity of both the catalytic subunit of xC-,Xc-, and GLT-1 (Baker et al 2003, Kalivas 2009, Madayag et al 2007, Reissner & Kalivas 2010, Scofield & Kalivas 2014). Downregulation of Xc- results in decreased extracellular glutamate levels, reducing engagement of inhibitory presynaptic mGluRs, and leading to increased synaptic glutamate release and enhanced excitatory neurotransmission in the NAc (Scofield & Kalivas 2014). In addition, subsequent studies utilizing the LgA+Ab paradigm not only confirmed observations regarding glutamate homeostasis from the ShA+Ex model, but also showed both prolonged access and extended

abstinence exacerbate the observed effects of cocaine, showing more severe decreases in GLT-1 and Xc- protein expression (Fischer-Smith et al 2012, Kau et al 2008).

Because these transporter systems are expressed primary on astrocytes, these observationss put astrocyte function in the forefront of promising cellular and molecular targets for future pharmacological interventions. Based on data presented here, the most obvious approach was to restore Xc- and GLT-1 protein expression, thus contributing to the restoration of the glutamate homeostasis, leading to the reversal of augmented neurotransmission from the NAc. Intriguingly, drug screening tests looking for therapeutic candidates for various neurodegenerative disorders, yielded an unlikely result. Many beta-lactam antibiotics were shown to upregulate transcription and translation of the *SLC1A2* (gene for GLT-1) (Su et al 2003). One of them, ceftriaxone, was used to upregulate GLT-1 in animal model of ALS, delaying loss of neurons that usually arises due to high extracellular levels of glutamate (glutamate toxicity) (Rothstein et al 2005). When applied to the ShA+Ex paradigm, Ceftriaxone restored glutamate homeostasis and prevented relapse to seeking (Knackstedt et al 2010a). Two more drug candidate were tested, namely N-acetylcysteine (NAC) and propentofylline (PPF), a cysteine prodrug (precursor to glutathione) that enhances Xc-, and a phosphodiesterase inhibitor, respectively. NAC restore expression of both proteins of interest (Xc- and GLT-1) following cocaine ShA SA and extinction and reduced reinstatement behavior (Baker et al 2003, Reissner et al 2015). Similarly, PPF Xc-normalizes the cocaine-induced decrease in GLT-1 expression and reduce cue-induced reinstatement following ShA+Ex paradigm by a mechanisms requiring normalized GLT-1 expression (Reissner et al 2014).

Role of astrocytes in glutamate homeostasis in the NAc following cocaine self-administration and withdrawal

Beyond critical roles in glutamate homeostasis, the engagement of astrocytes in SUD remains largely unclear. Established as a full-fledged partner at the tripartite synapse (Araque et al 1999a, Araque et al 1999b), they are known to provide metabolic support to neurons (Eichberg et al 1976, Magistretti & Allaman 2018), buffer for electrolytes (Hertz 1981, Theparambil et al 2020), and control synapse formation (Banker 1980, Christopherson et al 2005, Eroglu et al 2009), maturation (Kucukdereli et al 2011), pruning (Chung et al 2015, Tasdemir-Yilmaz & Freeman 2014) and transmission (Corkrum et al 2020, Haydon & Carmignoto 2006) in health and disease (Siracusa et al 2019). All of these modulating properties are enabled due to the unique structural feature of astrocytes, their "spongiform" morphology (Reichenbach et al 2010). Spongiform morphology is a result of the extreme ramification of astrocyte structure where small peripheral astrocyte processes (PAP) account for 70-80% of the entire cell surface (Wolff & Nemecek 1970). PAP densely permeate the neuropil and associate with define neuronal structures (Halassa & Haydon 2010). Interactions and dynamics at the neuron-astrocyte interface account for most of the physiological functions of astrocytes listed above (Dallerac et al 2018, Durkee & Araque 2019, Santello et al 2019) thus making PAPs a cellular compartment of great interest (Derouiche et al 2002, Derouiche et al 2012). Interestingly, a single astrocyte can contact millions of neuronal elements (Fields et al 2014) within its own domain which is, in healthy brain, not invaded by neighboring astrocytes (Bushong et al 2004, Halassa et al 2007). Although separated physically, neighboring astrocyte still communicate heavily using gap junctions (Bennett et al 2003).

As previously established, Xc- and GLT-1, two important astroglial components involved in regulation of glutamate homeostasis, are downregulated following cocaine SA and extinction

or absintence (Reissner & Kalivas 2010). Both of them are located in PAP, although Xc- might be more enriched in the extrasynaptic part of the PAP (Bridges et al 2012, Rimmele & Rosenberg 2016). With stable interactions between astrocyte PAPs and surfaces of neuronal synaptic elements shown to be paramount for maintenance of brain homeostasis (Allen & Eroglu 2017), effects of cocaine SA and withdrawal on astrocyte morphology and plasticity, especially on the level of PAP, is critical to appreciate. Plasticity of cell processes is regulated by cytoskeletal proteins who are known to drive morphological changes in astrocytes during development, injury and disease (Schiweck et al 2018). Glial fibrillary acidic protein (GFAP), the most well know astrocyte-exclusive cytoskeletal protein in adult brain (Potokar et al 2020), was investigated in the past in a context of cocaine use and exposure but with inconclusive results. For example, 24h after acute cocaine injection as well as after 7 days of chronic administration, GFAP was shown to be increased in hippocampal tissue (Fattore et al 2002). Interestingly, there was no change in GFAP amount after 14 days of chronic cocaine injections although the GFAP tree, when stained with immunohistochemistry, showed less branching. GFAP is also not particularly useful cellular marker for astrocyte structural plasticity since it is not present in PAP (which present 70-80% of astrocyte surface) but rather only in primary and secondary astrocyte branches (Bignami & Dahl 1974). Most observations into astrocyte morphology following cocaine administration also used acute, non-contingent administration and no withdrawal period.

My research will thus focus on describing astrocyte structural plasticity following cocaine SA and withdrawal, using Lck-GFP as a reporter of structure complexity. Lymphocyte-specific protein tyrosine kinase (Lck) is a member Src family of tyrosine kinases and is usually found in lymphocytes. It possesses a special dual acylation motif which renders association with the plasma membrane (Zlatkine et al 1997). Fusing a fluorescent reporter protein like GFP to Lck

ensures complete surface labeling of a cell. This is unprecedentedly useful tool for studying cells with complexes surfaces, especially astrocytes, where it was shown that cytoplasm expression of fluorescent protein reporters or even cell filling does not report a complete cell morphology (Benediktsson et al 2005, Reeves et al 2011, Shigetomi et al 2010). Recently published study from our lab was the first to employ Lck-GFP to study astrocytes in NAc after ShA cocaine SA and extinction (Scofield et al 2016b). Astrocytes were found to be smaller, with less interfaces shared with neuronal synaptic elements. Interestingly, GFAP expression was also decreased 24h following last extinction day. This shines a new light on the role of astrocytes in drug use and withdrawal and implies that restoring downregulated transporters might not be sufficient to prevent relapse since the astroglial support is absent from the synapse altogether. It was also shown GLT-1 – positive PAP are present at the distance of 0-400 nm from the neuronal synaptic elements (Pannasch et al 2014) making it very likely any cocaine induced structural plasticity of astrocytes might deny synaptic elements sufficient astroglial ensheathment. To further investigate structural plasticity of astrocytes following cocaine SA and withdrawal, in Chapter 2 I utilize this approach to more deeply investigate the nature of the observed decrease in structure features and synaptic colocalization of astrocytes in the brain reward circuitry following cocaine ShA SA. In Chapter 3, I designed to investigate the exact nature of astrocyte plasticity changes observed in Chapter 2, with the focus shifting from morphometric analysis of the volume and surface on a single cell level to branching complexity and plasticity of individual PAPs. The scope was also broadened with the inclusion of LgA+Ab paradigm in order to delineate contribution of different SA paradigms to astrocyte plasticity changes. Collectively, the research described here is a comprehensive analysis of cocaine induced structural plasticity of astrocytes following SA and withdrawal with a goal do further the knowledge regarding the role of astrocytes in SUD and aid in development of new and successful behavioral and

pharmacological interventions.

CHAPTER 2: REGION-SPECIFIC REDUCTIONS IN MORPHOMETRIC PROPERTIES AND SYNAPTIC COLOCALIZATION OF ASTROCYTES FOLLOWING COCAINE SELF-ADMINISTRATION AND EXTINCTION[1]

Introduction

The rodent self-administration model of drug abuse has allowed for investigation of cellular consequences of drug use, as well as the circuitry and mechanisms that mediate motivated drug-seeking behaviors (Venniro et al 2016). For example, self-administration studies combined with pharmacological inactivation of brain nuclei and more recently optogenetics, have been instrumental in elucidating the neural circuitry engaged in different stages within the cycle of substance use, dependence, abstinence, and relapse (Cooper et al 2017, Saunders et al 2015). Further, genetic manipulation has revealed cell subtype specific roles in drug reward and motivation (Lenz & Lobo 2013), and self-administration studies have provided valuable insight into the subcellular signaling pathways and receptor dynamics which mediate drug use, dependence, and seeking (O'Connor et al 2011, Panlilio & Goldberg 2007, Scofield et al 2016a, Wolf 2016).

While use of this preclinical model has revealed considerable insight into drug-induced adaptations among neurons, relatively less is known about the consequences of self-administration on properties of astrocytes(Scofield & Kalivas 2014). Dysregulation of glutamate homeostasis, largely accomplished by astrocytes, was among the first astroglial adaptations observed in cocaine-withdrawn animals, a response that has now been reported

[1]This chapter previously appeared as an article in the journal *Frontiers in Cellular Neuroscience*. The original citation is as follows: Testen A, Sepulveda-Orengo MT, Gaines CH, Reissner KJ. Region-Specific Reductions in Morphometric Properties and Synaptic Colocalization of Astrocytes Following Cocaine Self-Administration and Extinction. *Front Cell Neurosci*. 2018 Aug 7;12:246. doi: 10.3389/fncel.2018.00246.

across numerous drug classes (Scofield et al 2016a). Specifically, impairments in glutamate homeostasis as a consequence of drug use and withdrawal are mediated by decreased expression and activity of the cystine-glutamate exchanger xC- and it's catalytic submit xCT, as well as the high affinity glutamate transporters GLT-1 and GLAST (Baker et al 2003, Kalivas 2009, Knackstedt et al 2010a, Reissner et al 2011). Notably, both system xC-, GLT-1, and GLAST are predominantly localized on astrocytes (Danbolt 2001, Huang et al 2004, Perego et al 2000, Roberts et al 2014). The regulation of these systems has been recognized as critical to drug seeking behaviors, illustrating functionally relevant roles for drug-induced adaptations to astrocytes.

Recently we reported that cocaine self-administration and extinction results in a decrease in surface area, volume, and presynaptic colocalization of astrocyte peripheral processes in the NAc core, suggesting impaired function and synaptic modulation by astrocyte processes (Scofield et al 2016b). The observation that peripheral processes of astrocytes colocalize significantly less with synaptic puncta in the NAc core raises important hypotheses regarding astroglial modulation of synaptic function in drug-withdrawn animals, and by extension, drug-seeking behavior. While the NAc is an important node within the reward circuitry, and is considered a limbic-motor integrator (Mogenson et al 1980), it is entirely unknown whether the observed phenomenon is restricted to the NAc core, or extends to other nuclei within the brain's reward circuitry. Toward that end, in the current study we assessed astrocyte morphometric properties and synaptic colocalization of peripheral processes in the NAc core, BLA, and PL. To capture and measure morphometric changes in astrocytes, a membrane-tagged Lck-GFP reporter was expressed under the control of the GfaABC1D promoter as reported previously (Scofield et al 2016b). Post-translational modification of a short amino acid sequence taken from the Lck and Fyn members of the Src family of protein tyrosine kinases leads to membrane association of GFP

and subsequent enhanced visualization of fine peripheral astrocyte processes (PAPs) over soluble protein reporters (Benediktsson et al 2005, Shigetomi et al 2013, Zlatkine et al 1997). The microinfusion of the viral vector was used to transduce the PL, NAc, and BLA of each rat. Animals were then trained in self-administration and extinction of cocaine or saline, and properties of astrocytes within these regions were subsequently assessed. We further assessed whether decreased synaptic colocalization of NAc peripheral processes would be observed using a post-synaptic marker, post-synaptic density protein 95 (PSD-95), in addition to a presynaptic marker, synapsin I, as reported previously (Scofield et al 2016b), and whether changes are observed 24 h after the last self- administration session.

Materials and Methods

Laboratory Animal Care and Surgical Procedures

Adult male Sprague-Dawley rats (200–250 g at arrival) were obtained from ENVIGO (formerly Harlan Labs, Indianapolis, IN, United States) and housed individually in a temperature- and humidity-controlled, AAALAC-accredited environment on a reverse light-dark cycle (7 p.m. to 7 a.m. lights on). The reverse light cycle was used in this study and others (Scofield et al 2016b) due to evidence that a reverse light-dark cycle can produce more stable behavioral responses in nocturnal rodents (Roberts et al 2002). All handling, surgeries and behavior were performed during the dark cycle. During the 1 week of acclimatization and an additional week of post-surgery recuperation, animals had ad libitum access to food and water. All experiments and procedures were approved by the University of North Carolina at Chapel Hill Institutional Animal Care and Use Committee (IACUC) and were in accordance with NIH guidelines.

On the day of surgery, rats were anesthetized with ketamine (100 mg/kg) and xylazine (7 mg/kg) followed by a single dose of the analgesic ketorolac (0.3 mg/kg). A silastic catheter was

surgically inserted into the right jugular vein, exiting from the back and ending with an exposed 22-gauge cannula (Plastics One, Roanoke, VA, United States). Catheters were flushed daily with the aminoglycoside antibiotic gentamicin (100 mg/ml, 0.1 ml) and heparin (100 U/ml, 0.1 ml) until the end of behavioral training. Immediately following catheterization, animals were stereotaxically microinjected with the lymphocyte protein kinase Lck-GFP reporter, packaged into the adeno-associated virus serotype 5 (AAV5), under the control of the GfaABC1D promotor (1.3 × 1013 virus particles/ml) (Scofield et al 2016b, Shigetomi et al 2013). Targeted areas were prelimbic cortex (PL, bilaterally; coordinates (mm): +3.2 anterior/posterior, +0.4 medial/lateral, -4.0 dorsal/ventral), basolateral amygdala (BLA, bilaterally; coordinates (mm): -2.8 anterior/posterior, +5.0 medial/lateral, -8.7 dorsal/ventral), and nucleus accumbens core (NAc, unilaterally; 6° angle, coordinates (mm): +1.5 anterior/posterior, +2.6 medial/lateral, -7.2 dorsal/ventral). Virus was microinjected using 26-gauge injection cannulas (Plastics One, Roanoke, VA, United States) in a single and dual configuration (1 µl per injection site, 0.05 µl/min injection rate) and left to diffuse for 15 min. Bilateral injections were made to PL and BLA, and unilateral injections to the NAc. After diffusion, microinjectors were slowly removed over 1–2 min.

Behavioral Training

Catheterized and microinjected rats were randomly divided into two groups, self-administering either saline (n = 20, total across experiments) or cocaine (n = 24, total). Saline-administering rats were not yoked to cocaine-administering rats. Training took place in modular rat operant chambers (Med Associates, Latham, NY) at the same time each day. Cocaine self-administration was performed on a fixed-ratio 1 (FR1) schedule of reinforcement during 2 h sessions. An active lever press produced a 0.2 mg intravenous (i.v.) infusion of cocaine (or saline) as well as an auditory and visual cues, followed by a 20 s time-out period. Cocaine intake

was capped for the first 3 days (maximum of 40 infusions) and unrestricted afterward. Threshold for minimum intake was 10 days of at least 10 cocaine infusions per day. When applicable, the self-administration phase was followed by 15 days of 2 h daily extinction sessions where cocaine, as well as contingent cues, were not available. Prior to the onset of behavioral training, rats received a single food training session (6 h), to facilitate acquisition of the operant task. Rats received 20 g of chow (45 g non-flavored pellets, BioServ, Flemington, NJ, United States) following each daily session throughout the study. Water was unrestricted. Cocaine was generously provided by the National Institute of Drug Abuse (NIDA) Drug Supply Program.

Tissue Processing

Rats were deeply sedated with pentobarbital 24 h after the last extinction or self-administration session, followed by transcardial perfusion using 200 ml of phosphate buffer (1× PB) and 200 ml of freshly made 4% paraformaldehyde (in 1× PB). The time point of 24 h after the last extinction session was chosen, so that adaptations in astrocytes present at the time of a typical reinstatement test could be observed. (Korogod et al 2015) compared cryo and chemical fixation of the mouse neocortex and concluded that chemical fixation, even though inferior for answering some anatomical questions, reveals better preservation of glial volume and more intimate glial coverage of the synapses. Brains were then extracted, post-fixed for 3 h in 4% paraformaldehyde (4°C), washed by excess amount of cold 1× PB and stored for 2 days in 30% sucrose solution (in 1× PB) at 4°C. Tissue was sectioned (100 μm) using a cryostat (Leica Biosystems Inc., Buffalo Grove, IL, United States) and stored at -20°C in 50/50 Glycerol/PB until staining. The complete areas of NAc, PL and BLA were collected.

Before staining, each selected section was inspected for sufficient expression and anatomical targeting. Immunohistochemistry was performed on free-floating sections. Sections were washed (3 min × 5 min) in 1× PBS to remove any residual glycerol and blocked for 1 h at

room temperature in 5% normal goat serum (NGS, Sigma-Aldrich, St. Louis, MO, United States) containing 1% Triton X-100 (Thermo Fisher Scientific, Waltham, MA, United States) in 1× PBS (1% PBST). Blocking solution was replaced with primary antibodies (all 1:500) in 5% NGS in 0.4% PBST: Rb anti-GFAP (Z0334, Dako) and Ms anti-PSD-95 (6G6-1C9, Thermo Fisher Scientific, Waltham, MA, United States). Sections were incubated for 72 h at 4°C with constant shaking and were turned over half way through.

To probe with secondary antibodies, sections were transferred to new 24-well plates and washed with cold 1× PBS (3 min × 10 min). Secondary antibodies (goat anti-Rb Alexa Fluor 647 (A32733, Thermo Fisher Scientific, Waltham, MA, United States) and goat anti-Ms Alexa Fluor 594 (A11032, Thermo Fisher Scientific, Waltham, MA, United States), all 1:1,000) were added to 5% NGS in 0.4% PBST and incubated 72 h at 4°C identically as for primaries. Sections were then once again washed three times with 1× PBS, mounted and immediately cover-slipped (Dapi-fluoromount-G, SouthernBiotech) to prevent desiccation.

Data Acquisition and Processing

To analyze astrocytes, optical sections of Lck-GFP-expressing cells were collected using a Zeiss LSM 800 confocal-scanning microscope (405, 488, 561, and 640 nm diode lasers; 2 Gallium Arsenide Phosphide (GaAsP) detectors) with a 63× oil-immersed objective (Zeiss, Oberkochen, Germany) and ZEN software suite (ZEN 2.3 (blue edition), Zeiss). Frame size was set to 1,024 × 1,024 pixels, bit depths to 16-bit, averaging to 4×, and z-step size to 1 μm. The imaging was restricted to previously mentioned regions (as marked in Figures 1, 2 with the white box) around A/P: 1.5, 3.2, and -2.8 for NAc, PL, and BLA, respectively. Astrocytes were imaged only if present in their entirety within the chosen region. Astrocytes bordering other regions or astrocytes being cut during sectioning in a z-dimension were not imaged. Cases in which viral injections missed their intended targets were not analyzed.

After acquisition, raw images were transferred to an image-processing workstation and deconvolved using AutoQuant software (v. X3.0.4, MediaCybernetics). A blind deconvolution algorithm with 10 iterations was run on each z-stack. The deconvolved output stack was directly imported to Imaris software (v. 8.4.1, Bitplane, Zürich, Switzerland) which was used to generate a 3-dimensional reconstruction of each individual astrocyte. Each individual cell was then isolated and a surface was built around it using Lck-GFP innate fluorescence signal. Surface area and volume were extracted from each individually built astrocyte surface. A special masked channel was generated using these surfaces, completely isolating the astrocyte Lck-GFP signal from Lck-GFP background. The masked channel was then used to perform colocalization analysis between the astrocyte Lck-GFP signal and the Alexa 594 signal, representing the PSD-95 post-synaptic neuronal marker. To remove the background, threshold for the PSD-95 channel was manually selected by taking repeated measurements of unambiguous puncta of fluorescent signal intensity on multiple optical slices. An average of these measurements was used as a final threshold for the PSD-95 channel. A new colocalization channel was generated which provided percentage of region of interest (ROI) colocalized with the PSD-95 channel (ROI was set as a masked Lck-GFP channel). It should be emphasized that fluorescence colocalization analysis is not a tool for detecting molecular interactions, but rather for assessing co-registry of two or more fluorophores within a given voxel. Accordingly, colocalization of Lck-GFP and PSD-95 signals serves as a proxy of astrocyte proximity to the neuronal post- synaptic terminal. The latter was checked by automatically counting PSD-95 puncta above a predetermined threshold within assigned 25 μm × 25 μm × 25 μm box for a subset of samples. Slides and files were encrypted during acquisition and manipulation to assure unbiased processing.

Statistical Analysis

Collected data were grouped into tables using Excel 2016 (Microsoft, Redmond, WA, United States) and analyzed using Prism (v. 7.02, GraphPad, La Jolla, CA, United States) and SAS (v. 9.4, SAS Institute, Cary, NC, United States). Independent variables were saline versus cocaine self-administration and time, and dependent variables were lever presses and infusions (for behavior), and surface area, volume, and synaptic colocalization for astrocytes. Variance is reported as SEM. For analysis of the active lever presses and infusions during self-administration and extinction training, we used repeated measures two-way ANOVA. Nested ANOVA analysis was performed on all groups for assessment of morphometric properties, synaptic colocalization and PSD-95 expression (Heimer-McGinn et al., 2013; Risher et al., 2014). The comparison of properties of saline-treated astrocytes across brain areas (Table 1) was performed using Tukey-Kramer post hoc analysis, and comparison of behavior between cocaine and saline-administering rats on specific days (Figure 1) was performed using Bonferroni post hoc analysis. $p < 0.05$ was considered significant.

Results

Cocaine Self-Administration and Extinction Training Leads to a Region-Specific Reduction in Astroglial Morphometric Features

Both active lever presses and cocaine infusions demonstrated main effects of group (cocaine versus saline) and time, and were significantly greater in cocaine-administering group by the 2nd day of SA, remaining elevated through self-administration [Figure 1A; infusions main effect of group $F(1,22) = 43.44$, $p < 0.0001$ and time $F(9,198) = 8.74$, $p < 0.0001$; self-administration active lever presses main effect of group $F(1,22) = 66.88$, $p < 0.0001$ and time $F(9,220) = 11.48$, $p < 0.0001$]. Main effects of group [$F(1,22) = 15.96$, $p < 0.001$] and time [$F(14,308) = 30.82$, $p < 0.0001$] were also observed across extinction, although post hoc

differences between groups were only observed on extinction day 1.

The Lck-GFP protein exhibited astrocyte-specific expression, and the virus spread enabled single cell imaging of isolated, spatially labeled astrocytes (Figures 1B, 2A,C). Slices were probed and imaged for the astrocytic marker GFAP, confirming that each imaged cell was indeed an astrocyte (Figure 1C). Cells were imaged only within targeted brain regions, as indicated by the white box in Figures 1B, 2A,C. Regions that were not transduced, failed to show adequate spread, or were not within the ROI were excluded from analysis.

After acquisition, astrocytes were reconstructed in 3D space and surfaces were built using the Lck-GFP signal in Bitplane Imaris (Figure 1D). The sequential analysis revealed that the astrocytes in the NAc of cocaine-extinguished rats exhibited significantly decreased surface area [saline 52,155 ± 1,935 μm2, cocaine 44,252 ± 1,605 μm2, $F(1,14) = 6.93$, $p < 0.05$] and surface-to-volume ratio [saline 2.983 ± 0.109 μm-1, cocaine 2.557 ± 0.072 μm-1, $F(1,14) = 4.79$, $p < 0.05$] compared to astrocytes from saline-experienced rats (Figure 1E). Surface area:volume ratio was assessed as a proxy for astrocyte complexity, since the branching of peripheral processes contributes more to the surface area than the volume of the cell (Hama et al 2004). Reduction in the number or length of these processes would thus report a lower ratio. There was no significant change observed in volume [saline 18,899 ± 1,347 μm3, cocaine 18,480 ± 1,137 μm3, $F(1,14) = 0.06$, $p > 0.05$; Figure 5].

Interestingly, none of these effects were observed in PL or BLA of the same rats (Figures 2B, D). No differences between astrocytes from the same saline- versus cocaine-extinguished rats were observed in surface area [PL saline 60,130 ± 2,270 μm2, cocaine 62,175 ± 2,084 μm2, $F(1,22) = 0.45$, $p > 0.05$; BLA saline 60,036 ± 2,203 μm2, cocaine 59,787 ± 2,066 μm2, $F(1,18) = 0.01$, $p > 0.05$], volume [PL saline 22,084 ± 976 μm3, cocaine 22,559 ± 953 μm3, $F(1,22) = 0.16$, $p > 0.05$; BLA saline 24,240 ± 950 μm3, cocaine 23,173 ± 967 μm3, $F(1,18) = 0.54$, $p >$

0.05] or surface area:volume ratio [PL saline 2.869 ± 0.073 μm-1, cocaine 2.970 ± 0.085 μm-1, $F(1,22) = 0.46$, $p > 0.05$; BLA saline 2.555 ± 0.067 μm-1, cocaine 2.779 ± 0.095 μm-1, $F(1,18) = 2.45$, $p > 0.05$].

We also probed for heterogeneity of astrocytes by comparing morphometric features of control animals across different brain regions (Table 1). Surface area:volume ratio of BLA astrocytes was significantly smaller compared to the NAc and PL (due to its significantly larger volume).

Cocaine Self-Administration and Extinction Training Leads to a Region-Specific Decrease in Colocalization Between NAc Astrocyte Processes and the Neuronal Post-synaptic Marker PSD-95

Previously we reported that colocalization of NAc astrocyte peripheral processes with a presynaptic marker, synapsin I, was significantly decreased in cocaine-extinguished rats (Scofield et al., 2016b). In the current study, we sought to determine whether this finding could be reproduced using a post-synaptic marker, PSD-95 (Figures 3A,B). We found that cocaine SA and extinction training resulted in a significant decrease in colocalization between GFP- and PSD-95-positive voxels in the NAc [saline 8.464 ± 0.469%, cocaine 6.623 ± 0.282%, $F(1,14) = 4.84$, $p < 0.05$], but not in the PL [saline 7.892 ± 0.309%, cocaine 8.339 ± 0.336%, $F(1,22) = 0.67$, $p > 0.05$] or BLA [saline 7.984 ± 0.344%, cocaine 8.443 ± 0.398%, $F(1, 18) = 0.31$, $p > 0.05$] of the same rats (Figure 3C).

Importantly, one possible reason that a change in colocalization could be observed is if there is a difference in expression of either GFP or PSD-95 between groups. The percentage of colocalization when compared across brain regions in control animals was almost identical (colocalization not dependent on a region) as was the expression of PSD-95 as assessed by number of PSD-95-postive puncta above threshold [Figure 3D; NAc saline 2,819 ± 162, cocaine

2,469 ± 261, F(1,14) = 0.72, p > 0.05; PL saline 3,172 ± 157, cocaine 3,361 ± 393, F(1, 22) = 0.06, p > 0.05; BLA saline 2,359 ± 181, cocaine 2,610 ± 233, F(1,18) = 0.47, p > 0.05]. We previously reported that cocaine self-administration and extinction had no effect of GFP-positive or synapsin I-positive puncta above threshold in the NAc core (Scofield et al 2016b); accordingly, the decrease in post-synaptic colocalization of astrocytes is not likely due to a change in expression of either colocalized components.

Extinction Training Is Necessary for Decreased Area, Surface-to-Volume Ratio and Neuronal Colocalization of NAc Astrocytes Following Cocaine Self-AdministrationPost-synaptic Marker PSD-95

To distinguish the temporal dynamics of the effects of cocaine self-administration on NAc astrocytes, a subsequent cohort of rats was sacrificed 24 h after the last SA session. Again, both active lever presses and cocaine infusions demonstrated main effects of group (cocaine versus saline) and time, and were significantly greater in cocaine-administering group by the 2nd day of SA, remaining elevated through self-administration [Figure 4A; infusions main effect of group F(1, 18) = 69.9, p < 0.0001 and time F(9,162) = 14.24, p < 0.0001; self-administration active lever presses main effect of group F(1, 18) = 19.69, p < 0.0001 and time F(9,162) = 13.10, p < 0.0001]. In this case, no significant changes were observed regarding astrocyte surface area [Figure 4B-left; saline 61,721 ± 2,770, cocaine 55,555 ± 2,447, F(1, 18) = 2.78, p > 0.05] and surface-to-volume ratio [Figure 4B-right; saline 2.305 ± 0.09 μm-1, cocaine 2.317 ± 0.08 μm-1, F(1,18) = 0.01, p > 0.05] as well as PSD-95 colocalization [Figure 4C-left; saline 12.754 ± 0.640, cocaine 12.212 ± 0.565, F(1, 18) = 0.40] and PSD-95 expression profile [Figure 4C-right, saline 3,236 ± 307, cocaine 3,621 ± 278, F(1, 18) = 0.86, p > 0.05].

Discussion

Cocaine Self-Administration and Extinction Leads to Reduced Morphometric Features and Synaptic Colocalization of NAc Astrocytes

Results provided herein reproduce and extend upon previously published findings regarding the effects of cocaine self-administration and extinction on NAc astrocytes (Scofield et al 2016b), and further indicate that the reduced synaptic colocalization in the NAc can be observed using both pre- and post-synaptic markers. These results also indicate that the effects of cocaine self-administration and extinction are specific to astrocytes in the NAc, and require a period of extinction or extended withdrawal. Previous studies have also found decreased astroglial protein expression specifically in the NAc by Western blot, including GFAP, xCT, GLAST, and GLT-1 (Knackstedt et al 2010a, Reissner et al 2011, Scofield & Kalivas 2014, Scofield et al 2016b), supporting our observation that the effects of cocaine self-administration and extinction on astrocytes may be specific to this node of the reward circuitry. It is possible that the lack of change in BLA and PL astrocytes after extinction training might have been the result of the recovery of the normal phenotype during the extinction period. Nonetheless, at this time period following extinction, the observed effect is specific to NAc astrocytes over PL or BLA astrocytes. Accordingly, these results raise intriguing questions about both the mechanism and functional role of NAc-specific adaptations. What is unique about astrocytes in the NAc? The answer may lie in regional differences among astrocytes, or in the cellular environment of the NAc across the progression of cocaine self-administration and extinction, or both.

Regarding regional differences among astrocytes, elaborate astroglial morphology prompted early interest in diversity and heterogeneity of astrocytes (McKhann et al 1997, Prochiantz & Mallat 1988, Wilkin et al 1990), yet these early findings were slow to be reexamined as compared to advances made within neuronal regional heterogenetity (Khakh &

Sofroniew 2015, Zhang & Barres 2010). However, recent studies show that astrocytes integrated within different circuits exhibit markedly different morphological, proteomic, transcriptomic and functional profiles (Ben Haim & Rowitch 2017, Chai et al 2017), although it remains a challenge to ascribe functional differences among astrocytes within different nuclei or circuits. Moreover, even within specific nuclei, astrocyte populations with different molecular markers and different cell fates can be observed (John Lin et al 2017, Schitine et al 2015). Our results indicate morphometric heterogeneity of astrocyte responsiveness within the reward circuitry that will help to isolate specific astroglial contributions to maladaptive reward processing following drug abuse.

Regarding the cellular environment of the NAc, acute exposure to many drugs, particularly psychostimulants, leads to robust hyperdopaminergia within the NAc, which over time results in adaptations in glutamatergic and GABAergic signaling that may well contribute to the region-specific effects observed here (Luscher 2016, Mameli & Luscher 2011). Over time and repeated exposures, series of adaptations are observed, including plasticity of glutamatergic synapses (Uys & Reissner 2011). In addition, some studies indicate cellular effects which occur across protracted periods of withdrawal. For example, (Fischer-Smith et al 2012) have observed an increase in the magnitude of GLT-1 protein suppression as a function of both cocaine use and withdrawal period. Accordingly, in order to determine whether the effects of cocaine self-administration on NAc astrocytes is a function of the pharmacological effects of cocaine, or is a function of withdrawal, we used a separate cohort of animals, to evaluate the effects of cocaine self-administration on morphometric properties and synaptic colocalization of NAc astrocytes. Indeed, no differences were observed between astrocytes from saline versus cocaine-experienced rats, supporting other studies which indicate that dynamic changes occur during a period of withdrawal from chronic self-administration. We cannot say conclusively whether the observed

changes in NAc astrocytes were a function of extended withdrawal or of extinction training itself. It is well established that extinction training modulates synaptic plasticity in the NAc, augmenting changes in glutaminergic receptor expression and function (Boudreau & Wolf 2005, Knackstedt et al 2010b, Lee & Dong 2011, Loweth et al 2014, Scofield et al 2016a, Self et al 2004, Wolf & Ferrario 2010). However, given that progressive reductions in GLT-1 are observed across protracted abstinence (Fischer-Smith et al 2012, Kim et al 2018b), we believe that it is most likely that the observed changes may be a function of abstinence over extinction.

A large body of evidence indicates that astrocytes play important roles in the modulation of synaptic and neuronal function, including synaptic strength, and neuronal excitability (Allen 2014, Barker & Ullian 2010, De Pitta et al 2016, Shibasaki et al 2014, Singh & Abraham 2017). Synaptic strength of glutamatergic projections onto NAc core medium spiny neurons is potentiated following withdrawal from chronic cocaine self-administration, and induction of long-term potentiation (LTP) and long-term depression (LTD) is impaired (Chen et al 2010, Martin et al 2006, Moussawi et al 2009). Further studies will be critical to test hypotheses regarding the functional consequences of decreased synaptic colocalization on synaptic and neuronal function and plasticity.

Limitations of the Study and Future Directions

While reduced surface area and surface area:volume ratios were observed in NAc astrocytes from cocaine-extinguished rats, we did not, however, observe the previously reported effect of cocaine self-administration and extinction on the overall volume of NAc astrocytes. One possible explanation for this observation could arise from the minor differences in tissue preparation and optical parameters leading to different baseline measurements. Notably, baseline surface area measurements of NAc astrocytes in saline-experienced rats were higher in the current study (approximately 5.0 × 104 μm2; Figure 1) compared to approximately 2.7 × 104

μm2 in the previous study (Scofield et al., 2016b), while baseline volume measurements were noticeably lower in the current study (1.5 × 104 μm3, data not shown) compared to approximately 3.1 × 103 μm3 in the previous study (Scofield et al 2016b). In particular, the lower baseline volume measurements in the current study could well mask decreases in volume of astrocytes from cocaine-extinguished rats. Also in the current study, slide-mounted slices were coverslipped while still wet to minimize potential morphological changes introduced by a drying process; in contrast, tissue sections were dried prior to slide mounting in the previously reported study. Measurement differences could also be attributed to differences in imaging parameters on different microscopes between the two studies (Zeiss LSM 800 compared to Leica SP5 confocal microscopes). In the current study, the increased sensitivity of the detector (GaAsP), improved light source (diode laser versus argon laser in a previous study), as well as smaller z-stack acquisition step (1 μm compared to 2 μm in the previous study) all enabled more precise reconstruction, which could certainly influence baseline measurements. While overall results presented herein corroborate the previously reported decline in morphometric properties of NAc astrocytes in cocaine-extinguished rats, these findings also illustrate the importance of relatively minor experimental variables in the overall quantitative results, which will be critical to consider in further experimentation moving forward.

It is also important to note that colocalization is a function of the voxel size, determined by the microscopy system, and in this case, colocalization reflects distances between fluorophores within approximately 250 nm. While super resolution and electron microscopy indicate that astrocyte–synapse interactions can occur within tens of nanometers (Heller et al 2017, Heller & Rusakov 2017, Panatier et al 2014), functionally relevant distances may well be higher. For example, astrocyte processes containing GLT-1 have been measured by immunogold electron microscopy at distances up to 400 nm from the active zone (Omrani et al 2009). Further,

a recent study using confocal colocalization analysis in the range of 10–600 nm observed changes in colocalization between peripheral processes and synapses following oxygen-glucose deprivation and in a genetic mouse model of Huntington's Disease (Octeau et al 2018). Moreover, changes reported here are observed for distances within 250 nm, including those much closer. Accordingly, decreases in colocalized signal include the most proximal interactions.

Appreciation of the responsiveness of non-neuronal cells and neuroimmune signaling to drugs of abuse has escalated considerably in recent years (Clark et al 2013, Cui et al 2014). While it has been known for some time that drug abuse can influence blood-brain barrier integrity and immunity, only in more recent years has it become evident that non-neuronal cells may contribute to drug reinforcement, dependence, and mechanisms of relapse (Lacagnina et al 2017, Nennig & Schank 2017, Pellegrino & Bayer 1998). While the current study is focused on investigation of the protracted effects of cocaine self-administration on astrocytes, we must consider this within the broader context of neuroimmune signaling within the brain. For example, microglia have been shown to become activated after non-contingent cocaine exposure (Little et al 2009). Cocaine exposure is also associated with increased expression of nuclear factor kappa B (NF-κB), a central mediator of immune responsiveness (Ang et al 2001, Russo et al 2009) which initiates the cascade leading to a decrease in antioxidant defense and an increase in reactive oxygen species, which in turn further promote microglial NF-κB activation (Block & Hong 2007). This and other neuroimmune pathways may well be engaged in the NAc by drug use, since it is known that activity of microglial NMDA receptors can activate NF-κB (Lipsky et al 2001, Munhoz et al 2008) leading to inflammation. Accordingly, continued investigation of both breadth and depth of non-neuronal and neuroimmune signaling following drug use will importantly expand on understanding of cellular mechanisms of drug use and addiction.

Within this context, results presented herein indicate a region-specific reduction of structure and synaptic colocalization of NAc astrocytes in cocaine-extinguished rats. This supports our previous report, as well as others indicating decreased expression and function of astroglial mediators of glutamate homeostasis following cocaine self-administration and extinction (Baker et al 2003, Fischer-Smith et al 2012, Knackstedt et al 2010a, Scofield & Kalivas 2014, Scofield et al 2016b). However, it is important to note that other studies have reported evidence for reactive astrocytes in the NAc following non-contingent cocaine administration (Kim et al 2018a). For example, evidence for increased GFAP expression and reactive astrogliosis has been reported following non-contingent administration of cocaine, alcohol, methamphetamine, and opiates (Bowers & Kalivas 2003, Friend & Keefe 2013, Udomuksorn et al 2011). Other studies have reported acute astrogliosis following a single non-contingent administration of cocaine, which is normalized following repeated administrations (Blanco-Calvo et al 2014), as well as an ER stress-induced astrogliosis following a single 12 h in vitro cocaine incubation (Periyasamy et al 2016). These differences illustrate important effects of pharmacodynamic responses to cocaine, and the importance influence of behavioral and administration approaches.

Relatively few studies have reported the effects of self-administered cocaine on properties of astrocytes. In addition to the report here and (Scofield et al 2016b), a recent study found no effect on the number of GFAP-positive cells in the NAc core following a 12 h binge cocaine self-administration session, 14 days after the cessation of 10 days of cocaine self-administration (Wang et al 2017). It remains to be determined how long-access cocaine self-administration or punishment-resistant self-administration affects astrocyte structure and physiology. Nonetheless, it is clear that there are measurable adaptations that occur in NAc astrocytes following cocaine exposure. Continued investigation moving forward will be critical

to determine the functional consequences of these adaptations, and the role(s) that astrocytes play in the behavioral pathology of compulsive drug seeking and relapse to use.

CHAPTER 3: CHANGES IN ASTROCYTE BRANCHING COMPLEXITY FOLLOWING COCAINE SELF-ADMINISTRATION AND ABSTINENCE

Introduction

Classically depicted as star-like, fibrous cells since early days of neuroscience, astrocyte morphology is now understood to be considerably more complex. Advanced imaging techniques have provided updated appreciation of astrocyte morphology from star-like to bush- or sponge-like, revealing a complex mesh of ramifications covering distinct territories and connecting to thousands of neuronal and vascular structures (Allen & Barres 2009, Barres 2008, Verkhratsky & Nedergaard 2018). The complex astrocyte structure belies their diverse and complex function, in particular at the interface of synaptic elements where astrocytes maintain ionic homeostasis, neurotransmitter recycling and provide metabolic support (Mahmoud et al 2019, Simard & Nedergaard 2004, Turner & Adamson 2011). These functions require close coverage of synaptic elements by peripheral astrocyte processes (PAPs), as well as plastic responsiveness to local physiological or pathological conditions (Becquet et al 2008, Lavialle et al 2011).

The structural plasticity of astrocytes and their processes is evidenced by directional responses to external stimuli. This plasticity can sometimes be regulated by changes in astrocyte volume. For example, under normal physiological conditions, CA1 hippocampal astrocytes can swell in response to physiological increases in extracellular potassium concentrations as well as shrink due to bicarbonate ion influx through activated $GABA_A$ channels (Florence et al 2012). However, the same plastic responses of astrocytes can also be instrumental in the development of pathologies. For example, in hypo-osmolar conditions, astrocytes can, due to the high-water

permeability, facilitate cellular edema. When this happens, intracellular glutamate can be released from astrocytes through volume-regulated anion channels (VRAC), elevating local neuronal excitability and contributing to seizures (Murphy et al 2017).

Besides volume regulation through osmotic pressure, astrocytes can change plasticity by assuming a reactive phenotype. Reactive astrocytes represent a pathological and typically inflammatory state induced by multiple stimuli raging from injury and trauma to autoimmune responses and neuro-degenerative diseases (Hamby & Sofroniew 2010, Sofroniew 2015, Sofroniew & Vinters 2010). The main characteristic of reactive astrocytes is an increase in GFAP gene expression, which results in increased immunoreactivity for GFAP and other markers. This manifests as an abnormal hypertrophy of GFAP-positive astrocytes and is characterized by the increased branching of the GFAP cytoskeleton (Escartin et al 2021, Kang et al 2014). In traumatic brain injury, reactive astrocytes are believed to develop due to environmental cues such as fibrotic extracellular matrix material (Okada et al 2018). Not limited to trauma, an increase in reactive astrocytes can also be detected via GFAP overexpression in post-mortem tissue of Alzheimer patients, as well as Huntington's Disease, Parkinson's Disease, and amyotrophic lateral sclerosis (ALS) (Kaur et al 2019, Khakh et al 2017, Philips & Rothstein 2014). In the majority of these conditions, astrocyte dysfunction arises due to accumulation of mutated proteins that alter astrocyte structural plasticity, leading to the invasion of nearby astrocytic domains and interruption of glia-neuron interface, causing local impairment of homeostatic functions (Kim et al 2018a).

In contrast, some experiences and conditions lead to measurable reductions in size and structural features of astrocytes, including mesial temporal lobe epilepsy as well as major depressive disorder (MDD) and chronic stress (Dossi et al 2018, Kim et al 2018a, Rajkowska & Stockmeier 2013). For instance, major morphometric features of astrocytes are decreased in size

in multiple cortical and limbic regions from postmortem brain of MDD patients (Rajkowska & Stockmeier 2013). Animal models of post-traumatic stress disorder (PTSD) and related mood disorders exhibit decreased volume of astrocyte somata as well as decreased number of peripheral processes and their branching complexity (Saur et al 2016, Webster et al 2005). Since a functionally integrated interface between astrocyte peripheral processes and neuronal synapses and vasculature is necessary for functional brain connectivity, decreased number and size of said processes may contribute to the connectivity deficits underlining MDDs. For example, astrocyte disfunction in prefrontal cortex of MDD patients was corelated to impaired astrocyte control of vasodilation leading to disrupted cerebral blood flow that regulated resting state connectivity (O'Leary et al 2021).

In addition to the disorders mentioned above, accumulating evidence indicates that responsiveness of astrocytes to drugs of abuse may also contribute to the pathology of substance use disorders (Cadet & Bisagno 2014, Miguel-Hidalgo 2009). Unlike with other psychiatric disorders discussed above, astrocyte phenotypes acquired through drug administration are not unified and can be substantially different based on a drug class, administration paradigm, time point, and brain region. For instance, acute and chronic non-contingent cocaine administration leads to increased GFAP expression in the hippocampus and striatum (Blanco-Calvo et al 2014, Fattore et al 2002) (likely through gliosis initiation and propagation (Periyasamy et al 2016)), while cocaine self-administration and extinction as well as prenatal drug exposure decrease GFAP in the nucleus accumbens core (Scofield et al 2016b, Testen et al 2018) and cortex (Lidow 1995), respectively.

Although short-access (ShA, 2h/day) cocaine self-administration (SA) followed by extinction and reinstatement provides a reliable and reproducible animal model of cocaine taking and relapse, limitations exist regarding the translational value of the model since it fails to

capture (at least to the degree) many human symptoms of substance use disorder such as drug craving, drug tolerance as well as withdrawal (Belin-Rauscent et al 2016, Sanchis-Segura & Spanagel 2006). These symptoms seem better addressed using a long-access self-administration protocol followed by home cage abstinence. This model comes closer to observed human behavior (limited extinction, abstinence following cessation of use) and better describes DSM-V criteria for substance use disorder diagnosis (Li et al 2015, Pickens et al 2011) (although alternatives have been proposed (Allain & Samaha 2019)) .

As reported in the previous chapter (Testen et al 2018) accumbens core astrocytes undergo significant decreases in morphometric features and interactions with synaptic elements following ShA self-administration and extension. However, the nature of these changes is not yet well understood. Here we used state of the art single cell structural analysis of previously collected and described astrocytes (Testen et al 2018) consisting of a novel three-dimensional branching and complexity analysis that will inform the degree of structural plasticity on the level of PAPs compared to the whole cell level of the previous dataset. The analysis also gives us the ability to determine if the observed cocaine-induced decreased phenotype of accumbal astrocytes is characterized by surface level alterations (shrinkage, retraction) or is correlated with quantitative changes to the astrocyte processes. The analysis was also performed on a second dataset collected using long-access (6h/day, LgA) cocaine self-administration and forced home-cage abstinence, to allow for direct comparison of two of the most commonly employed self-administration paradigms and their respective effect on astrocyte structural plasticity.

Materials and Methods

Animals and Surgical Procedures

Animal care and surgical procedures were identical to the previous chapter (30). Male

(200-250g) Sprague Dawley rats aged approximately 6-8 weeks were purchased from Envigo (Indianapolis, IN, United States) and individually housed in temperature and humidity controlled standard plexiglass cages on a reverse light-dark cycle (7 AM off, 7 PM on). All rats were allowed to acclimate to the animal facility for one week, where food and water were available ad libitum. All rats were then placed on a food restricted diet of ~ 20 g of chow per day. Food restriction lasted throughout all surgical, post-operative, and food-training procedures. Rats were then returned to an ad-libitum diet during self-administration which lasted throughout the duration of the study. All procedures were approved by the University of North Carolina at Chapel Hill Institutional Animal Care and Use Committee and followed the NIH Guide for Laboratory Animal Research.

For surgical procedures, animals were anesthetized with ketamine (100 mg/kg) and xylazine (7 mg/kg) and a silastic catheter was implanted into the right jugular vein as previously described (Kim et al 2018b, Sepulveda-Orengo et al 2018). Catheters were flushed daily with an antibiotic (gentamicin 5 mg/ml, 0.1 ml i.v.) and heparinized saline (100 U/ml, 0.1 ml i.v.) throughout all post-operative and self-administration procedures. Immediately following jugular vein catheterization, all rats were microinjected with Lck-GFP, under the control of the GfaABC1D promoter, packaged into the AAV5 serotype (6.1 x 10^{12} virus molecules/ml) by the UNC Viral Vector Core as previously described (Shigetomi et al 2013, Testen et al 2019, Testen et al 2018, Vivino et al 2016). Bilateral microinjections targeted the NAc (6° angle, AP +1.5, ML +1.8, DV -5.5) and virus was microinjected (0.1 µl/min, 1 µl per hemisphere) using 26-gauge guide cannula (Plastics One, Roanoke, VA). Microinjectors were left in place for 15 min to allow for virus diffusion and then slowly removed over 1-2 minutes. Before the start of self-administration procedures, patency of the catheters was examined by administering a sub-threshold dose of propofol (10 mg/mL, 0.05 mL).

Self-Administration Procedures

All self-administration procedures took place in standard sound-attenuated operant conditioning chambers (Med Associates, St. Albans, VT). Prior to the start of self-administration, all animals received one food-training session, where responding on the active lever resulted in the delivery of one 45 mg food pellet. Food training sessions lasted a minimum of 6 hours and criteria for food training was set at greater than 100 responses on the active lever. Rats then received 10 days of saline (0.9% NaCl) or cocaine (0.75 mg/kg/infusion) self-administration on an FR1 schedule for 6 hours/day for 10 consecutive days. Responding on the active lever resulted in the delivery of saline or cocaine (0.045 ml/infusion for a 300 g rat, over 2.18 seconds), accompanied by a tone (70 dB, 2.5 kHz) and illumination of a stimulus light above the active lever for five seconds. A 20-second timeout period occurred after every infusion, where active lever responding during this time resulted in no programmed responses. Responding on the inactive lever at any time also resulted in no programmed responses. Following 10 days of self-administration, animals remained in the home cage for 45 days and were handled twice per week.

Immunohistochemistry

For astrocyte imaging experiments, rats were euthanized 24 hours following the last day of abstinence. All rats were anesthetized with sodium pentobarbital and transcardially perfused with 1x phosphate buffer (PB), followed by 4% paraformaldehyde (PFA, in PB). Brains were extracted, post-fixed in 4% PFA for ~4 hours and then stored in 30% sucrose. Tissues sections (100 μm) from the NAc were collected using a cryostat (Leica Biosystems, Buffalo Grove, IL) and stored in 50% glycerol/PBS until staining.

For immunohistochemistry staining, free floating NAc sections were first washed (3 x 5 min) in 1x PBS containing 2% Triton X-100 (PBST) (Thermo Fisher, Waltham, MA). Sections

were then blocked in 5% normal goat serum (NGS, Sigma Aldrich, St. Louis, MO) in PBST for 1 hour at room temperature. Blocking solution was then replaced with primary antibodies (mouse anti-PSD-95 (Thermo Fisher, Waltham, MA) and rabbit anti-GFAP (Dako, Santa Clara, CA), both at 1:500) in 5% NGS in PBST. Sections were probed with primary antibodies for 72 hours at 4 °C and flipped halfway through the incubation period to allow for maximum penetration of primary antibodies. Secondary antibodies (goat anti-mouse Alexa Fluor 594 (Thermo Fisher, Waltham, MA) and goat anti-rabbit Alexa Fluor 647 (Thermo Fisher, Waltham, MA) were then added to 5% NGS in PBST. Sections were probed with secondary antibodies for 72 hours at 4 °C. Following incubation with secondary antibodies, sections were washed 3 x 10 min in PBST followed by one wash in 1x PBS. Sections were then mounted onto slides and coverslipped with DAPI Fluoromount-G (Southern Biotech, Birmingham, AL).

Astrocyte Image Acquisition and Processing

Image acquisition and processing of NAc astrocytes were identical to methods described previously (Testen et al 2019, Testen et al 2018). A Zeiss LSM 800 confocal-scanning microscope (405/488/561/640 nm diode lasers, 2 GaAsP detectors, 63x oil-immersed objective), along with the following parameters: 1024 x 1024 pixels, bit depth 16-bit, 4x averaging, 1µm z-step, was used for image acquisition. Only single, isolated astrocytes within the NAc were acquired. Astrocytes were not imaged if they were outside of the NAc, bordering other astrocytes, or cut within the z-plane during sectioning.

Following image acquisition, raw images were deconvolved using AutoQuant software (v. X3.0.4, MediaCybernetics) and imported into Imaris software (v 8.4.1, Bitplane, Zurich, Switzerland). Using the Lck-GFP signal from each astrocyte, each cell was reconstructed in 3-dimensions and a surface was built around each astrocyte to obtain measurements of surface area and volume. A masked channel was created to isolate the astrocyte Lck-GFP signal from

background and was then used to perform colocalization analysis between the masked Lck-GFP signal and PSD-95, represented by the Alexa 594 signal. A colocalization channel was then generated to obtain the percentage of masked Lck-GFP signal colocalized with PSD-95. All image acquisition and analysis was done blind to groups.

Astrocyte Filament Construction and Analysis

Astrocyte filament (wire model) construction was performed using deconvolved and isolated astrocyte-specific Lck-GFP signal as an input (Fig. 7 - I) via the native Imaris "Add new Filaments" function. "Autopath" algorithm was employed for the filament construction, utilizing the Fast-marching method (Sethian 1996). The maximal number of possible filament seed points was selected, using the lateral resolution of the imaging system (297 nm) as the only limiting factor. The nucleus of the selected astrocytes was utilized as the starting point for the filament construction. Since the astrocyte-specific Lck-GFP signal is readily colocalized with multiple surrounding neuronal nuclei, the automatic starting point selection can be impeded. To select the correct nucleus and thus a correct starting point for the filament construction, the colocalization between Lck-GFP and GFAP was performed in addition to the normally employed Lck-GFP and DAPI colocalization. Lck-GFP/GFAP colocalization reveals a complete astrocyte-specific GFAP cytoskeleton of the selected astrocyte while the Lck-GFP/DAPI colocalization informs about nuclei associated with the selected Lck-GFP positive astrocyte. If both analyses are performed correctly, the combination of both colocalizations should yield a single nucleus that is associated with both the Lck-GFP signal and GFAP cytoskeleton. Once the correct nucleus of each selected astrocyte was established, the starting point for the filament construction was manually seeded within it. Only a single starting point was allowed.

The obtained astrocyte filament (Fig. 7 - II) was used as the input for all 4 analyses, namely (1) 3D Sholl analysis, (2) custom branching analysis, (3) analysis of filament terminal

points and (4) segment analysis (all Fig. 7). For 3D Sholl analysis (1), an included stock algorithm was used with a custom graphical output (Fig. 7 – III). The Sholl sphere diameter was set to 1 μm to accommodate axial resolution. The in-house branching analysis (2) was initiated with an Imaris "XTension" file which allowed for a custom MATLAB script to ran parallel with the Imaris. The MATLAB script exported quantitative data (Sholl intersection) as an Excel file while the instructions for a graphical model were exported back to Imaris for visualization. The MATLAB branching analysis classified each bifurcation of the filament structure as either an arborization, continuation or termination node (Gillette & Ascoli 2015) where "arborization" node described the node where both child branches continued to bifurcate (Fig. 7 – IV.I). Similarly, "continuation node" described the node with one child branch was continuing to bifurcate and one was terminating (Fig. 7 – IV.II), while "termination node" was defined by the termination of both child branches (Fig. 7 – IV.III). The newly assigned bifurcation nodes and terminal points were then automatically binned based on their distance from the starting point as part of the incorporated 3D Sholl analysis. Filament's terminal points were analyzed (3) and used as a proxy for abundance of PAP (Fig. 7 – V). They were created using a stock Imaris algorithm and binned as a function of distance from the starting point, identical to the bifurcations. Segment data (4) was produced during the Sholl and bifurcation analysis and manually extracted to show the number of segments, as well as to calculate the total (Fig. 7 – VI.I) and average (Fig. 7 – VI.II) length of the segments. A segment was defined as a part of the astrocyte filament between the two distinct bifurcation nodes.

Statistical Analysis

Morphometric features of astrocytes, a total number of Sholl intersections, peak intersections, peak distances, bifurcations and terminal points as well as segment parameters were analyzed using nested ANOVA. When plotting parameters from all the four groups as a

function of distance from soma, the data was analyzed using 3-way repeated measure ANOVA with a behavioral paradigm and a drug as independent variables and a distance from soma as a continuous dependent variable. If the 3-way repeated measure ANOVA yielded significant three- or two-way interaction, the relationship was further explored using 2-way ANOVA followed by the Bonferroni multiple comparison post-hoc test. Area under the curve (AUC) measurements were compared using unpaired two-tail t-tests. The nested ANOVA was performed using SAS (v.9.4, SAS Institute, Cary, NC, US) while the Prism software (v.9.2.0, GraphPad Software, La Jolla, CA, US) was used for the rest of the statistics. Raw quantitative data for each astrocyte was exported and saved as an individual CSV file. These files were later collected and compiled into master Excel files (Microsoft, Redmond, WA, US) using custom macros. Individual data points on graphs represented individual astrocyte values. Variance was always reported as SEM. $p < 0.05$ was considered significant. Detailed nested ANOVA statistics can be found in Table 1, while the three- and two-way repeated measure ANOVA statistics can be found in Table 2.

Results

Severity of the cocaine-induced atrophic phenotype of accumbal astrocytes is contingent on the behavioral paradigm

The previous chapter examined the morphology of accumbens core astrocytes following short-access cocaine self-administration and extinction (Testen et al 2018), which exhibit a moderate decrease in astrocyte surface area and colocalization with neuronal elements. In comparison, when employing the LgA and abstinence paradigm, the atrophic phenotype is more pronounced, with a greater magnitude of effect (Kim *et al.,* unpublished data). When directly comparing both previously reported datasets (Fig. 6) there is indeed a statistically significant additional decrease in astrocyte surface area (Fig. 6A) (ShA(coc) 44,252 +/-1,564.59 μm^2, LgA(coc) 31,357 +/- 1,423.34 μm^2, $F(1,17)=37.17$, $p=0.0001$), volume (Fig. 6B) (ShA(coc) 18,579 +/-854.50 μm^3, LgA(coc) 11,720+/- 777.36 μm^3, $F(1,17)=35.26$, $p=0.0001$) and colocalization with neuronal PSD-95 (Fig. 6C) (ShA(coc) 6.623 +/-0.300 % of ROI, LgA(coc) 5.251 +/- 0.273 % of ROI, $F(1,17)=11.38$, $p=0.0036$) in the LgA cocaine group compared to ShA cocaine group. There was no statistically significant difference observed in in area (ShA(sal) 52,155 +/-2,342.40 μm^2, LgA(sal) 49,225 +/- 1,681.24 μm^2, $F(1,15)=1.03$, $p=0.325$), volume (ShA(sal) 18,750 +/-1,467.69 μm^3, LgA(sal) 19,532+/- 1,053.42 μm^3, $F(1,15)=0.19$, $p=0.671$) or neuronal colocalization (ShA(sal) 8.460 +/-0.403 % of ROI, LgA(sal) 7.939 +/- 0.289 % of ROI, $F(1,15)=1.10$, $p=0.310$) between saline groups in both paradigms, thus allowing for direct comparison of two unique atrophic phenotypes and their respective datasets.

Long-access cocaine SA and abstinence preferentially affects peripheral arborization patterning compared to short-access cocaine SA and extinction

The observed atrophic phenotypes of accumbens core astrocytes could be a result of

general, non-specific atrophy or shrinkage of astrocytes processes with no underlying quantitative changes to the arborization and branching, or could also be a result of PAP degradation and loss, producing a quantitative decrease in the number of arborizing elements and branching complexity. In order to address these alternative possibilities, we analyzed the arborization pattern of astrocytes using three-dimensional Sholl analysis. The ShA cocaine SA paradigm did not result in a significant decrease in the number of Sholl intersections following 10 days of extinction training (Fig. 8A) (ShA(sal) 7,844.13 +/- 295.77, ShA(coc) 7,038.22 +/- 261.12, $F(1,14)=4.17$, $p=0.0604$) while LgA cocaine SA showed a significant decrease in Sholl intersections following 45 days of forced home cage abstinence compared to saline control (LgA(sal) 8,025.09 +/- 319.79, LgA(coc) 5,654.14 +/- 329.33, $F(1,14)=26.68$, $p=0.001$). Comparing both drug self-administering groups, astrocytes from the LgA paradigm group showed significantly higher decrease in Sholl intersections compared to group preforming ShA training (ShA(coc) 7,038.22 +/- 272.00, LgA(coc) 5,673,55 +/- 274.02, $F(1,15)$, $p=0.0030$). Conversely, saline control groups did not exhibit paradigm-dependent changes (ShA(sal) 7,844.13 +/- 362.67, LgA(sal) 8,025.09 +/- 315.58, $F(1,13)=0.14$, $p=0.712$) confirming again a combination of drug and specific paradigm is needed to elicit distinct changes. No statistically significant difference between saline groups also allowed for direct comparison between cocaine groups done above.

To further investigate if the atrophy is homogeneously distributed throughout an astrocyte or localized to a certain region, we plotted the Sholl intersections as a function of a distance from soma (Fig. 3B). The number of Sholl intersections and thus complexity of astrocytes was not affected at the peak complexity for the ShA groups (Fig. 8B-I) (ShA(sal) 345.36 +/- 13.4351, ShA(coc) 308.07 +/-11.8611, $F(1,14)=4.33$, $p=0.0563$). Contrary, the peak value was decreased in the cocaine taking group in the LgA+Ab paradigm (LgA(sal) 367.54 +/-

15.5781, LgA(coc) 280.02 +/- 16.0432, F(1,14)=15.32, p=0.0016). There was no difference in peak intersections between both saline groups (ShA(sal) 345.36 +/- 17.8133, LgA(sal) 367.54 +/- 15.5, F(1,13)=0.88, p=0.3646) and both cocaine groups (ShA(coc) 308.07 +/- 12.3985, LgA(coc) 280.02 +/- 12.5849, F(1,15)=2.52, p=0.1331), respectively. It also seems the peaks of complexity stay relatively stable with both ShA+Ex (ShA(sal) 22.4906 +/- 0.9799 µm, ShA(coc) 22.6618 +/- 0.8651 µm, F(1,14)=0.02, p=0.8977) and LgA+Ab (LgA(sal) 20.7286 +/- 0.7726 µm, LgA(coc) 18.6364 +/- 0.7957 µm, F(1,14)=3.56, p=0.0801) behavioral paradigms showing no detectable drift of the complexity peak towards or away from soma. Interestingly, there was a small but statistically significant gap between the complexity peaks of both cocaine groups (ShA(coc) 22.6618 +/- 0.8397 µm, LgA(coc) 18.6364 +/- 0.8523 µm, F(1,15)=11.32, p=0.0043). No such gap was observed between both saline groups (ShA(sal) 22.4906 +/- 0.9114 µm, LgA(sal) 20.7286 +/- 0.7931 µm, F(1,13)=2.13,p=0.1685).

To identify the actual intervals of difference in the distribution of Sholl intersections along the astrocyte, we broke down datasets even further and compared individual distributions within specific behavioral and drug paradigm. Astrocytes from the ShA+Extinction paradigm (Fig. 8C-I) did not show statistically significant changes in distribution of Sholl intersections across the cell between saline and cocaine administering animals (see Table 3 for detailed statistics). This is consistent with the dataset of total intersections where ShA+Ex also did not show any changes. Interestingly there was a significant decrease in the area under the curve (AUC) in cocaine group (p=0.0079, graph insert), signifying a general decrease in complexity, although one that disappears when intersections are plotted across the distance from soma. Contrarily, the LgA+Abstinence paradigm (Fig. 8C-II) produced a significant decrease in Sholl intersections across the astrocyte length in the cocaine group across a wide interval (11-35 µm) that includes the peak and stretches to the periphery. The AUC measurement confirmed

decreased complexity of astrocytes in cocaine group (p=0.0001, graph insert). Interestingly, when comparing both cocaine groups (Fig. 8C-IV) we can see that the main decrease in Sholl intersections and thus complexity is not the result of the decrease at the peak complexity but rather well after the peak, at the more peripheral part of the astrocytes (25-46 μm). AUC of the LgA cocaine is significantly smaller then of ShA cocaine one (p=0.0001), with most of the area lost at the periphery. No difference was detected between both saline groups (Fig. 8C-III) as well as their respective AUC (p=0.3682).

Branching complexity of accumbal astrocytes is differentially compromised based on the cocaine self-administration paradigm

One of the structural hallmarks of astrocytes is their complex branching that results in the now well-recognized "bushy" morphology. To assess whether atrophic phenotypes that arise following cocaine SA are also characterized by changes in astrocyte branching, we performed a novel branching analysis able to discriminate between 3 distinct bifurcations. Arborizing nodes (Fig. 7 – IV.I) who contribute the most to the general complexity of astrocyte branching were decreased in number in cocaine SA groups in ShA+Ex (Fig. 9A-II) (ShA(sal) 654.00 +/- 27.443, ShA(coc) 560.81 +/- 24.277, F(1,14)=6.47, p=0.0234) as well as in LgA+Ab (LgA(sal) 599.62 +/- 23.459, LgA(coc) 437.64 +/- 24.150, F(1,14)=23.14, p=0.0003), although the cocaine-dependent decrease was significantly more severe with LgA paradigm compared to the ShA (ShA(coc) 560.81 +/- 21.958, LgA(coc) 437.64 +/- 22.283, F(1,15)=15.50, p=0.0013). There was no significant difference between the number of arborizing nodes between both saline control groups (ShA(sal) 654.00 +/- 29.491, LgA(sal) 599.62 +/- 25.719, F(1,13)=1.93, p=0.1880).

To further delineate the pattern of branching decrease, we plotted arborizing nodes as a function of distance from soma (Fig. 9A-I) and detected significant effects of both distance and drug on branching complexity (Table 3). When probing for intervals along the cell length that

where significantly altered in cocaine-taking animals, we observed a paradigm-specific pattern of decreased branching complexity. Cocaine self-administration produced a relatively narrow interval of decreased arborizing branching complexity in ShA+Ex paradigm (18-27 μm, p=0.0358), associated with the area of peak complexity (Fig. 9A-III). Conversely, LgA+Ab produces a wide interval of decreased arborizing branching complexity (Fig. 9A-IV) that, similarly to ShA+Ex, includes the peak of complexity, but also the majority of the peripheral length of the cell (8-32 μm, p=0.0006). Indeed, when comparing both cocaine groups (Fig. 9A-VI) we can observe a greater magnitude of decrease in arborizing complexity in LgA+Ab paradigm. The decrease is also in its entirety localized to the peripheral part of the cell and does not include the complexity peak (24-43 μm, p=0.0049). No difference was observed between the distribution of the arborizing nodes between the two control saline groups (Fig. 9A-V, p=0.1498).

A similar result was observed when analyzing continuing nodes (Fig. 7 – IV.II). Both ShA+Ex (Fig. 9B-II) (ShA(sal) 1,311.39 +/- 55.845, ShA(coc) 1,115.17 +/- 49.403, F(1,14)=6.93, p=0.0197) and LgA+Ab (LgA(sal) 1,205 +/- 46.821, LgA(coc) 867.39 +/- 48.199, F(1,14)=25.37, p=0.0002) behavioral paradigms resulted in a significant decrease in the number of continuing nodes following cocaine self-administration, with a significantly greater decrease observed with the LgA paradigm (ShA(coc) 1,115.17 +/- 43.371, LgA(coc) 867.39 +/- 44.014, F(1,15), p=0.0011). There was no difference observed between saline controls from the two paradigms (ShA(sal) 1,311.39 +/- 60.303, LgA(sal) 1,205.83 +/- 52.590, F(1,13)=1.74, p=0.2099).

When plotted as a function of distance from the astrocyte soma (Fig. 9B-I), the continuing branching nodes displayed a very similar pattern to the arborizing nodes, with the cocaine-associated decrease in the ShA+Ex paradigm being limited to the region of peak

branching complexity (Fig. 9B-III, 18-28 μm, p=0.0273) while extending further to the periphery in the LgA+Ab paradigm (Fig. 9B-IV, 11-33 μm, p=0.0003). When comparing both cocaine groups directly (Fig. 9B-VI), the statistically significant decrease in continuing branching complexity is observed at the distance interval of 25 to 46 μm from soma (p=0.0043). No difference in distribution of continuing nodes was observed between both control saline groups (Fig. 9B-V).

Lastly, terminal nodes (Fig. 7 – IV.III) were found to follow the same pattern of decrease with both paradigms, ShA+Ex (Fig. 9C-II) (ShA(sal) 772.41 +/- 33.301, ShA(coc) 660.65 +/- 29.460, F(1,14)=6.32, p=0.0248) and LgA+Ab (LgA(sal) 714.66 +/- 28.484, LgA(coc) 514.91 +/- 29.322, F(1,14)=23.88, p=0.0002) with the latter again displaying a larger decrease in the number of terminal nodes in the cocaine group (ShA(coc) 660.65 +/- 26.287, LgA(coc) 514.91 +/- 26.676, F(1,15)=15.14, p=0.0014). There was no significant decrease in the number of terminal nodes between the control saline groups (ShA(sal) 772.41 +/- 36.174, LgA(coc) 714.66 +/- 31.547, F(1,13)=1.45, p=0.2504).

The same pattern observed with previously described node types was also observed with terminal nodes when the number of terminal bifurcations was plotted as a function of distance from the soma (Fig. 9C-I). A decrease in branching complexity in cocaine self-administering group was observed around the peak of branching complexity (20-29 μm, p=0.0158) in the ShA+Ex paradigm (Fig. 9C-III) and around the peak as well as extending to the periphery of the cell (16-35 μm, p=0.0007) in the LgA+Ab paradigm (Fig. 9C-IV). Indeed, when plotted together, the interval of significant decrease in complexity between both cocaine groups (Fig. 9C-VI) is observed at the periphery, most distal from the soma (26-46 μm, p=0.0051). As before, no significant difference was observed in the density of terminal nodes between the two control saline groups (Fig. 9C-V).

We next analyzed the total number of bifurcations, regardless of the node type. Both ShA+Ex (ShA(sal) 2737.8 +/- 116.31, ShA(coc) 2336.64 +/- 102.89, F(1,14)=6.67, p=0.0217) and LgA+Ab (LgA(sal) 2520.11 +/- 98.54, LgA(coc) 1819.94 +/- 101.44, F(1,14)=24.51, p=0.0002) behavioral paradigms resulted in a significant decrease in the number of bifurcations in the cocaine groups compared to the respective control saline groups (Fig. 9D). This said, the accumbal astrocytes from LgA+Ab cocaine group show a larger decrease in branching complexity compared to cocaine-taking animals trained in the ShA+Ex paradigm (ShA(coc) 2336.64 +/- 91.39, LgA(coc) 1819.94 +/- 92.74, F(1,15)=15.75, p=0.0012). There was no difference in the number of branching nodes between both control saline groups (ShA(sal) 2737.80 +/- 125.69, LgA(sal) 2520.11 +/- 109.61, F(1,13)=1.70, p=0.2144).

As shown above, the self-administration paradigm as well as drug taking have an effect on the branching complexity through the decrease in the number of branching nodes. This said, cocaine and behavioral paradigms do not have a node-type specific effect and seems to affect all the different bifurcation in the same manner. Indeed, the percentage of a specific node types compared to the total number of bifurcations of the astrocyte processes remained remarkably stable, showing that the bifurcation decrease (when present) is uniform and non-discriminatory between the node types, with the ratio and percentages of individual node types being the same pre- and post-withdrawal (Fig. 9E).

Decreased number of peripheral astrocyte process endings poins to the downstream functional consequences of cocaine taking

To study abundance of PAP we analyzed filament ending points. Both behavioral paradigms, ShA+Ex (Fig. 10A) (ShA(sal) 2,922.96 +/- 125.75, ShA(coc) 2,501.46 +/-111.25, F(1,14)=6.30, p=0.0250) as well as LgA+Ab (LgA(sal) 2,703.51 +/- 106.46, LgA(coc) 1,946.39 +/- 109.59, F(1,14)=24.55, p=0.0002), showed a significant decrease in the number of filament

endings, indicating the possibility that structural changes may have a functional consequence in a form of diminished potential to interact with synapses and/or vasculature. As in the previously measured features, astrocytes from the LgA cocaine administering cohort revealed a larger magnitude of decrease compared to the ShA+Extinction group (ShA(coc) 2,501.46 +/- 98.64, LgA(coc) 1,946.39 +/- 100.11, $F(1,15)=15.60$, $p=0.0013$) with the saline control groups not being statistically significantly different (ShA(sal) 2,922.96 +/- 135.97, LgA(sal) 2,703.51 +/- 118.58, $F(1,13)=1.48$, $p=0.2455$).

The difference remained significant even when the terminal points were plotted as a function of distance from the soma (Fig. 10B). Interestingly, the distribution of decrease of the terminal points followed closely the decrease in complexity measured by Sholl (Fig. 8B) as well as the decreased branching complexity (Fig. 9 A-I, B-I, C-I) reaffirming again that both behavioral paradigms, even though distinct from each other in their power to produce a unique pattern of atrophy and decreased complexity, are still not able to specifically target any distinct feature of astrocyte morphology but rather control the degree of atrophic spread towards the periphery of the cell. This can be shown with the ShA+Ex behavioral paradigm (Fig. 10C-I) showing the decreased amount of terminal points around the peak of complexity (21-29 μm, $p=0.0374$) and with the LgA+Ab (Fig. 10C-II) showing the atrophic extension further to the periphery of the cell (16-36 μm, $p=0.0006$). This is confirmed when plotting both cocaine groups together (Fig. 10C-IV), clearly revealing the additional amount of decrease associated with the LgA+Ab paradigm is localized to the distal part of the cell (27-46 μm, $p=0.0050$). No difference was observed between both control saline groups ($p=0.1978$).

Atrophic phenotype as a result of paradigm-specific loss of peripheral astrocyte processes

To assess the state of the astrocyte filament tree in its entirety we summed together all the individual segments to reveal the total length of the astrocyte filament tree (Fig. 11A). Again, we

can observe a pattern where both behavioral paradigms, ShA+Ex (ShA(sal) 13,985 +/- 503.60 µm, ShA(coc) 12,387 +/- 445.51 µm, $F(1,14)=5.65$, $p=0.0323$) as well as LgA+Ab (LgA(sal) 13,189 +/- 493.47 µm, LgA(coc) 9,389 +/- 507.98 µm, $F(1,14)=28.78$, $p<0.0001$) resulted in a decreased total length of a astrocyte filament with the latter exhibiting more severe decrease in length then ShA (ShA(coc) 12,387 +/- 449.46 µm, LgA(coc) 9,389.48 +/- 456.12 µm, $F(1,15)=21.91$, $p=0.0003$) and saline control groups not showing any significant changes (ShA(sal) 13,985 +/- 567.69 µm, LgA(sal) 13,189 +/- 495.09 µm, $F(1,13)=1.12$, $p=0.3098$). The atrophic phenotype manifested by astrocytes after cocaine SA and withdrawal could theoretically be a result of general, non-specific shrinkage of the astrocyte filament tree and its processes or a quantitative loss of said processes. To address these two possibilities, we measured the average length of the segments to reveal a possible shrinkage of processes as well as the number of segments for each filament tree to inquire about the potential loss of segments/processes. Following the established pattern, we found that both, ShA+Ex (Fig. 11B) (ShA(sal) 5,700.52 +/- 243.63, ShA(coc) 4,859.45 +/- 215.52, $F(1,14)=6.69$, $p=0.0216$) and LgA+Ab (LgA(sal) 5,245.39 +/- 205.92, LgA(coc) 3,782.52 +/- 211.98, $F(1,14)=24.50$, $p=0.0002$) behavioral paradigms show significant decrease in the number of astrocyte segments/processes following cocaine taking with LgA paradigm once again displaying more severe phenotype compared to ShA group (ShA(coc) 4,859.45 +/- 190.99, LgA(coc) 3,782.52 +/- 193.82, $F(1,15)=15.66$, $p=0.0013$) and control saline groups not showing any significant changes in the number of segments (ShA(sal) 5,700.52 +/- 263.17, LgA(sal) 5,245.39 +/- 229.51, $F(1,13)=1.70$, $p=0.2151$). Conversely, no statistically significant difference was detected when comparing the average length of the astrocyte segments either when looking at the effects of cocaine within both paradigms (Fig. 11C) (ShA(sal) 4.903 +/- 0.087 µm, ShA(coc) 5.044 +/- 0.077 µm, $(1,14)=1.44$, $p=0.2503$; LgA(sal) 4.953 +/- 0.059 µm, LgA(coc) 4.845 +/- 0.061, $F(1,14)=1.60$,

p=0.2267) or effect of the paradigm itself (ShA(coc) 5.044 +/- 0.065 µm, LgA(coc) 4.845 +/- 0.066 µm, F(1,15)=4.54, p=0.0501; ShA(sal) 4.903 +/- 0.082 µm, LgA(sal) 4.953 +/- 0.071 µm, F(1,13)=0.21, p=0.6546). This points conclusively to the origin of the atrophic phenotype being the loss of processes and not their decrease in size.

Discussion

The presented study provides a comprehensive examination of qualitative and quantitative changes to astrocyte morphology following the cocaine self-administration and withdrawal. Two different SA paradigms were employed (ShA+Ex and LgA+Ab), both extensively used in addiction research. The LgA+Ab paradigm reliably produced a more atrophic astrocyte phenotype which was reflected in more pronounced reductions in astrocyte surface area and colocalization with post-synaptic neuronal elements compared to ShA+Ex. LgA+Ab also produced a decrease in astrocyte volume which was absent in ShA+Ex. To explore consequences of cocaine SA on astrocyte structure beyond morphometric features, we employed 3D Sholl analyses to compare the complexity of astrocyte processes network between both paradigms and respective saline controls. Even though morphometric astrocyte features were decreased with Sha+Ex, no quantitative changes were observed using Sholl analysis. Conversely, astrocytes from the LgA+Ab paradigm group exhibited a marked decrease in total Sholl intersections as well as distribution as a function of distance from nucleus. The decrease in intersections was wide and encompassed the proximal as well as the distal processes. Interestingly, there was no significant difference in both cocaine and saline groups undertaking LgA+Ab training in the distance from the nucleus where the peak complexity was achieved.

Besides the Sholl analysis, we also performed detailed branching analysis encapsulating three different bifurcations as well as analysis of processes end points. We found similar results

across these experiments, showing smaller and narrower decreases in branching complexity and end points between saline and cocaine taking animals trained in ShA+Ex paradigm compared to LgA+Ab. There was no specificity in effect for either drug or paradigm type on individual bifurcation sub-type. This said, all bifurcation types as well as PAPs endings showed a reproducible pattern of the LgA+Ab cocaine group showing decreased values at the more peripheral side of the cell compared with the ShA+Ex group, thus revealing for the first time subcellular specificity of cocaine-induced effects on accumbal astrocytes. These effects contributed to the atrophic phenotype of astrocytes which is ultimately achieved by the decrease in the number of PAPs and not their shrinkage or retraction.

Comparison of effects from two commonly employed behavioral models of cocaine

Astrocytes from the cocaine group that underwent LgA+Ab paradigm training showed an exacerbated atrophic phenotype compared to the cocaine group from the ShA+Ex paradigm. Differences in behavioral and synaptic alteration after ShA and LgA cocaine self-administrations has previously been reported. For example, LgA cocaine self-administration is known to not only increase the total drug taken due to the increased administration time compared to ShA, but also increases the rate of taking and early drug loading (Ahmed & Koob 1998). Higher rates of motivation to obtain drug (Paterson & Markou 2003) as well as greater susceptibility to reinstatement after abstinence were also reported (Knackstedt & Kalivas 2007). On a molecular level, LgA is associated with region-specific increases in dendritic spine density in the NAc core (Ferrario et al 2005) and decrease in dopamine 2 receptor expression (Mantsch et al 2004). Beside higher cocaine intake, LgA animals also underwent forced home cage abstinence. This type of withdrawal is associated with incubation of cocaine craving, in which behavioral evidence for drug craving does not diminish over time but rather increases progressively over a

period of months (Grimm et al 2001). The molecular bases of this phenomenon were very early on connected to the unique time courses of protein expression of multiple components of the reward circuitry (Kalivas 2004, Nestler 2001, Wolf 2003). In recent years this knowledge has been expanded with new research showing a broad range of molecular changes, from upregulation of NMDA receptor subunits GluN1 and GluN2A following cocaine SA (Smaga et al 2020) to decreased dopaminergic tone in VTA following LgA and abstinence (Salin et al 2021). This said, most changes seem to be related to glutaminergic system in striatum, confirming LgA, similarly to ShA, might mainly disturb glutamate homeostasis thus again implicating astrocytes (Mahmoud et al 2019, Scofield & Kalivas 2014).

Astrocyte morphology was indeed more severely impacted in the LgA+Ab paradigm (Fig. 6), showing decrease in the density of processes (Sholl analysis) (Fig. 8), their branching complexity (Fig. 9), end point number (Fig. 10) as well as the number of processes itself (Fig. 11). Although the use of Lck-GFP to label elaborate astrocyte morphology is not new to the field (Benediktsson et al 2005, Shigetomi et al 2013) it is mostly used to extract morphometric feature of labeled astrocyte (Kruyer et al 2021, Scofield et al 2016b, Testen et al 2019, Testen et al 2020, Testen et al 2018) and not as a reporter for structural model building. This is to our knowledge the first use of Lck-GFP for tracing astrocyte processes for use in 3D Sholl and branching analysis. All previous studies employed a myriad of different model-building approaches, from early 2 D manual trancing (Bushong et al 2003, Butt et al 1994) and thresholding (Hashemi et al 2008, Narayan et al 2007, Pirici et al 2009) to advance 3D models using angular variance (Bjornsson et al 2008), edge (Benesova et al 2009) and root (Kulkarni et al 2015) detection as well as structural tensor analysis (Budde & Frank 2012). The only point of similarity, it seems, was the fact that all of them used simple GFAP immunohistochemical staining as an input for their model-building algorithms. Although verified and powerful in their own right, these

algorithms required already existent filament-like structure (like GFAP) to be used as a foundation of tracing, thus ruling out Lck-GFP membrane-tagged images. Unfortunately, this severely limited the power and usefulness of these analyses since upwards of 90% of the astrocyte complexity was lost. To this end we used Imaris with its build-in Fast marching algorithm (Sethian 1996) which used a space-filling component to build a filament and simultaneously traces it. With this setup, Lck-GFP astrocyte images were a viable input. The only other optical setup that was capable of capturing the similar degree of complexity was dye-filling of astrocytes. Besides being significantly more involved and lower yield, dye-filling also reported significant loss of structural astrocyte information compared to membrane-tagging (Reeves et al 2011). In addition to optical approaches, serial block-face electron microscopy (SBF-EM) was employed recently in order to elucidate astrocyte structural complexity (Cali et al 2019). A 750,000 μm^3 (100x100x75µm) block of somatosensory cortex tissue from a single juvenile rat (P14) was imaged with 20 nm accuracy. 186 cell bodies were reconstructed from the block, 22 of them were identified as astrocytes based on nuclei morphology. Out of 22, 4 were partially (or close to fully) reconstructed. Incredibly, they report between 1,853 and 6,240 individual astrocyte branches for the least and most branched cell, respectively. Unfortunately, it is not immediately clear if they refer to only terminal branches (the ones ending in PAP) or did their counting include every child branch of every bifurcation (referred in our study as a "segment"). If the latter is true, the number of branches (upper limit) was very close to the number of segments reported here (average of both saline control groups: 5,464). This is encouraging and would imply that the imaging method described here, combined with the reconstruction pipeline produces one of the most detailed insights into astrocyte complexity still obtainable with the optical confocal microscope that is lacking any pseudo (e.g., Zeiss Airyscan 2) or real super-resolution capabilities. As for SBF-EM study, even the most branched astrocytes

were assessed to be just 78% complete so significant part of the astrocyte was still missing, reaffirming that electron microscopy still delivered the most detailed image view of astrocyte complexity and thus remains a gold standard (Cali et al 2019).

When astrocyte intersections were plotted as a function of a distance from soma, a clear pattern was established where astrocytes from cocaine ShA group showed decrease in Sholl intersections at the peak complexity compared to its saline counterparts while astrocytes from LgA cocaine group showed the same decrease in Sholl intersections at the peak intersections but also at the more peripheral (distal) part of the cell, the furthers from the soma. Emergence of distribution changes in Sholl intersections as a function of distance were again allowed due to detailed reconstruction of astrocytes. Studies utilizing GFAP as a marker or astrocyte dye filling observed no changes in intersection distribution across distance although the density of the processes was increased (Naskar & Chattarji 2019) implying the minimum threshold of complexity must be reached by the traced reconstruction in order to be informative of the spatial distribution of intersections.

Both obtained phenotypes of Sholl intersection decrease are fascinating. ShA cocaine SA shows peculiar decrease that is exclusive to the peak complexity. This was unusual since decreases in complexity in astrocytes and neurons are usually not limited to the certain cellular subregion (Bird & Cuntz 2019). To our knowledge no other SUD or other neuropsychiatric disorder produces similar phenotype of decreased complexity. This said, only recently a subpopulation of oxytocin-positive astrocytes was discovered in the central amygdala of rats and mice (Wahis et al 2021). These astrocytes had a significant increase in the number of Sholl intersections that was limited to the peak of complexity compared to the nearby oxytocin-negative astrocytes. This discovery added to the growing evidence of regional and subregional diversity of astrocytes (Khakh & Deneen 2019) but it might be also implying that cocaine usage

fundamentally changes the nature of affected astrocytes.

On the other hand, LgA cocaine taking and abstinence revealed a markedly different phenotype of Sholl intersections compared to the ShA+Ex. LgA+Ab phenotype was characterized by the similar peak decrease previously observed in ShA+EX, but it also exhibited an additional component, a decrease further to the periphery. This type of the phenotype was observed before, and it is correlated with astrocyte maturation and age. During maturation, rodent astrocytes naturally extend to the periphery and become more complex. But this trend is reversed at some point and astrocytes of 24-36 months old animals show decreased peripheral complexity (Bondi et al 2021, Klein et al 2020, Popov et al 2021). Astrocytes from rats undergoing LgA cocaine SA followed by abstinence thus resemble, based on Sholl analysis, aged atrophic astrocytes. It is not possible at this point to precisely delineate contributions of each behavioral component to the observed atrophic phenotypes since both paradigms employ different withdrawals and are characterized by the different amounts of cocaine taking. This said, the astrocyte phenotype observed in the cocaine group experienced in LgA+Ab is clearly more severely impacted which correlates nicely with increased cocaine seeking and higher degree of imbalance in glutamate homeostasis observed in LgA+Ab paradigm. Similarly, to the Sholl analysis, the analysis of branching showed identical phenotypes with almost identical intervals of decreased astrocyte branching complexity. This is not a big surprise since branching complexity directly results in higher number of Sholl intersections. Thus, both analyses showing almost identical outcome adds validity to our analysis.

Cocaine induced structural changes of astrocyte complexity

To our knowledge this was the first time branching analysis, able to differentiate between individual bifurcations (Gillette & Ascoli 2015), was applied to a non-neuronal cell type.

Interestingly, almost half of all bifurcations (~48%) was classified as continuing nodes (one terminating, one continuing child branch). Abundancy of this node type assures that the filament tree continues while at the same time producing significant number of terminal branches, ending in terminal points (i.e., PAP) thus enabling the hallmark astrocyte morphological complexity. Also amazingly, the ratio of different node types is extremely consistent across behavioral paradigms as well as drug administration, strongly implying this specific ratio is necessary for astrocytes to successfully achieve needed arborization and through it, functional relevance.

On a molecular level, branching is dependent on the properties of cytoskeleton elements. Astrocyte express microtubules, actin, as well as intermediate filaments GFAP and vimentin (Potokar et al 2007). Among those listed, actin is the only one present in all of the processes and thus changes to actin branching have a direct and immediate effect on astrocyte branching (Schiweck et al 2018). For a new actin branch to arise, the Arp2/3 complex must bind to the actin "mother" filament and initiate a growth of a new child branch by enabling G-actin to attach at the 70º degree angle (Smith et al 2013). Downregulation of Arp2/3, subunit Arp3 or Arp2/3 activator N-WASP by siRNA resulted in a reduced branching complexity in cortical astrocytes (Murk et al 2013). Although the actin cycling and branching was studied in a context of neuropsychiatric disorders (Blanpied & Ehlers 2004, McGee & Bredt 2003) a very limited knowledge exists regarding the effect of cocaine on its dynamic. 3-week withdrawal from repeated cocaine administration resulted in the increase of F-actin through phosphorylation changes to actin binding proteins (ABPs) (Toda et al 2006). It is yet to be determined if restoring normal acting cycling in NAc would affect reinstatement after extended cocaine use and withdrawal. Further research should focus on restoring acting branching in astrocytes in hope of mitigating seeking and reinstatement.

Besides decreases in Sholl intersections and branching, we saw a similar pattern of

decrease in the number of filament endings. For all intent and purposes, terminal points described here can serve as a proxy for PAP and thus finally connect atrophic structure of astrocytes to the dysregulated function. A single astrocyte can interface with upwards of 600 synaptic elements (Halassa et al 2007) but interestingly, the astrocytes do not invade each other's territory under normal circumstances, a phenomenon known as astrocyte tiling (Bushong et al 2002, Eilam et al 2016). It quickly becomes clear that each decrease in astroglial synaptic coverage is thus not mitigated by nearby astrocytes. The lack of built-in redundancy thus makes the whole brain areas susceptible to dysregulation. Besides missing PAP proxies, we also found the whole filament segments were missing, exacerbating the atrophic phenotype of astrocytes. At the same time, the average length of segments was not changed in cocaine animals compared to the saline control, confirming this is a permanent atrophic phenotype and not a temporary retracted one. Activity-dependent plasticity of astrocytes was reported previously in which hippocampal LTP would induce mobility of PAP, making them temporarily unavailable to regulate synaptic function (Perez-Alvarez et al 2014). Recently this mechanism was expanded, showing that NKCC1 transporters present on PAPs as well as cofilin (actin controlling protein) were involved in activity-triggered retraction of the PAP (Henneberger et al 2020). Interestingly, retracted PAPs enabled leakage of glutamate from synaptic cleft thus activating extrasynaptic NMDARs. This elegant mechanism, located in CA1 has thus a potential to exert effect on nearby synapses, potentially contributing to the local signal integration. This finding adds to a body of literature indicating that PAPs are extremely plastic and that their plasticity is integral to synaptic function. To this end it is extremely worrisome to discover a significant decrease in the number of astrocyte endings capable of forming functional tripartite synapses.

Mechanisms have recently been reported that can also increase the coverage of synaptic elements by PAP. One month of caloric restriction diet was shown to increase the coverage of

CA1 synapses by PAP (Popov et al 2020). Increased coverage in return prevents potassium and glutamate spillover thus preventing extrasynaptic NMDARs to tail of burst-induced EPSCs. Interestingly, no changes were reported in the number of PAP or in GLT-1 expression, implying no quantitative changes to PAP were made thus this approach would likely have a limited effect on mitigating disfunction of the glutamate homeostasis in the NAc following extended cocaine use and withdrawal.

Recently, a new study showed that endocannabinoid might warrant more exploration as a new intervention of choice to mitigate cocaine induce plasticity changes in NAc. A diacylglycerol lipase (DAGL), an enzyme known to synthesize endocannabinoid 2-AG, was found to be increased in NAc core following prolonged 30-day abstinence (Mitra et al 2021). Conveniently, monoacylglycerol lipase (MAGL), which hydrolyzes 2-AG was decreased at the same time. Since 2-AG is known to regulate phosphorylation, using DAGL and MAGL inhibitors, researchers were able to bidirectionally regulate cocaine seeking. At the same time, synthetic cannabinoid R-(+)-Methanandamide (MethAEA) was able to restore mGluR2/3 function and mGluR5-mediated astrocytic glutamate release which in turn inhibited reinstatement of cocaine seeking (Zhang et al 2021).

The results presented here describe in detail the nature of previously reported atrophic phenotype. Both tested self-administration paradigms (ShA+Ex and LgA+Ab) examined here showed significant decrease in filament density, branching complexity and number of endpoints (PAPs) as well as branching segments. LgA+Ab paradigm showed additional cocaine induced changes compared to ShA+Ex, extending further to the periphery. This knowledge reenforces the important role of astrocyte plasticity in substance use disorder and can inform development of more targeted pharmaceutical approaches. The novel analyses presented also offer a new toolbox for astrocyte research that can be readily applied to different fields.

CHAPTER 4: GENERAL DISCUSSION

Summary of Results

The two studies presented here offer novel insights into the structural plasticity of astrocytes associated with cocaine self-administration. Building upon previous research in the laboratory (Scofield et al 2016b), we first set out to reexamine morphometric features of NAc astrocytes following ShA cocaine SA and extinction, using Lck-GFP membrane- tethered fluorescent reporter. We reproduced the observation that accumbal astrocytes exhibit an atrophic phenotype following cocaine ShA+Ex, characterized by a decrease in the surface area and colocalization with neuronal synaptic elements. The atrophic phenotype was exclusive to the NAc and was not observed in astrocytes from two other brain regions in the reward circuitry, the mPFC PL and BLA. This illustrates that NAc astrocytes are uniquely impacted following cocaine ShA+Ex and thus warrant further attention for functional contributions to behaviors associated with relapse. Interestingly, this study also revealed that an extinction or withdrawal/abstinence period is necessary for manifestation of the atrophic phenotype, as no effect of cocaine were observed 24 h following the final SA session.

While results from the first study revealed a reduction of astrocyte surface area and colocalization with synaptic elements, no effect of cocaine was observed on astrocyte volume. This might seem paradoxical at first, however considering that PAPs account for 70-80% of the entire cell surface (Wolff & Nemecek 1970) it quickly becomes clear that atrophy of the PAPs would contribute more significantly to the change in surface area while not significantly effect the cell volume. Atrophy of the PAPs would also explain the decrease in colocalization with

synapses, leading to deprivation of neuronal synaptic elements of its glial partner thus boosting extrasynaptic glutamate, collapsing glutamate homeostasis and promoting drug seeking (Henneberger et al 2020, Kalivas 2009).

While astrocytes are increasingly acknowledged as an important element in SUD (Wang et al 2021), the effect of cocaine self-administration on astrocyte complexity and branching has not yet been explored. To this end, the second part of the study re-focused from the cellular to the sub-cellular scale in order to examine PAP complexity and their contribution to the atrophic phenotype observed following cocaine SA and extinction/withdrawal. To do this, the data set from Chapter 2, as well a second data set employing the LgA+Ab paradigm were used to further explore effects of cocaine SA on branching complexity. The LgA+Ab reliably produced a more severe atrophic astrocyte phenotype, which was reflected in more pronounced reductions in astrocyte surface area and colocalization with post-synaptic neuronal elements compared to ShA+Ex. To further explore consequences of cocaine SA on astrocyte structure beyond morphometric features, we employed 3D Sholl analyses to compare the complexity of astrocyte processes. Even though morphometric astrocyte features were decreased with ShA+Ex, no quantitative changes were observed using Sholl analysis. Conversely, astrocytes from the LgA+Ab paradigm group exhibited a marked decrease in total Sholl intersections as well as distribution as a function of distance from nucleus. The decrease in intersections was wide and encompassed the proximal as well as the distal processes.

Besides the Sholl analysis, we also performed detailed branching analysis encapsulating three different bifurcations as well as an analysis of process end points. We found similar results across these experiments, showing smaller and narrower decreases in branching complexity and end points between saline and cocaine taking animals trained in ShA+Ex paradigm compared to LgA+Ab. There was no specificity in effect for either drug or paradigm type on individual

bifurcation sub-type. This said, all bifurcation types as well as PAP endings showed a reproducible pattern of the LgA+Ab cocaine group showing decreased values at the more peripheral side of the cell compared with the ShA+Ex group, thus revealing for the first time subcellular specificity of cocaine-induced effects on accumbal astrocytes. These effects indicate that the reduced structural features of astrocytes associated with cocaine SA, in particular LgA and prolonged abstinence, are driven by a selective impairment of astrocyte collectively at peripheral processes, rather than overall shrinkage across the entirety of the cell.

Relationship to human postmortem studies

Results from this and other animal self-administrations studies are especially informative and important since postmortem human studies which, even though highly relevant and a valuable resource (Maatouk et al 2019, Stockmeier & Rajkowska 2004), are often confounded by factors including polydrug use, comorbid psychiatric conditions, previous life experiences, and a recent history of use. For example, human postmortem studies of NAc astrocytes of cocaine overdose victims show increase in astrocytes size and GFAP expression (Hemby et al 2005, Tannu et al 2007). The same 50% increase in GFAP protein expression was confirmed using non-human primates (NHP) (Tannu et al 2010). Importantly, NHP studies were designed to enable snapshot in the brain proteomics immediately after cocaine taking thus ensuring to avoid any kind of withdrawal before sacrificing animals. Unfortunately, this is also the case for the postmortem human studies, since most examined samples from overdose victims and victims of suicide with drugs in their system (Hemby et al 2005, Tannu et al 2007) . Besides the lack of withdrawal, other confounding factors such as cocaine adulterants (Gameiro et al 2019, Knuth et al 2018) as well as poly-drug use cases (Akhgari et al 2021) make interpretation of postmortem data from cocaine users challenging, particularly if one is interested in understanding prolonged

effects of cocaine use across a period of abstinence. Even without the presence of any substances, astrocyte-related genes, including GFAP, continued to be upregulated 24h following human brain tissue resection, implying inherent bias of postmortem tissue analysis to overreporting astrocyte morphological features due to a rapid onset of gliosis following death (Dachet et al 2021). Thus animal self-administration models still remain critical for understanding effects of single-use drug in a controlled environment (Lynch et al 2010).

Circuit and cell subtype specificity of interactions of astrocytes with synapses

Important aspects of experience-dependent astrocyte plasticity still remain unaddressed. One of them is specificity of astrocyte ensheathment of specific cell types and circuits within the NAc. Colocalization of PAPs with synaptic elements was explored in Chapter 1 using PSD-95 immunohistochemistry as a proxy for post-synaptic excitatory terminals. This said, the source of these terminals is not determined in the study. Medium spiny neurons within the NAc are generally distinguished as either positive for expression of either dopamine receptor D1 or D2, with a limited proportion positive for both (Gagnon et al 2017). It is currently unknown whether reduced synaptic colocalization of astrocytes is observed at either, or both of these subpopulations. Further, with the NAc being one of the main hubs and an integrator for glutaminergic projections, it would be informative to explore potential projection-specific atrophy of PAPs. A non-comprehensive list of areas involved in the reward circuitry that are known to send their glutamatergic projections to the NAc core includes but it is not limited to the ventral tegmental area (VTA), PFC (PL), hippocampus (dorsal), thalamus (ILT), mesencephalon (limited glutaminergic projections from SNpc and SNpr) as well as amygdala (central) (see (Scofield et al 2016a) for review). A second limitation of this approach could be considered the limited resolution of our colocalization analysis. With the use of conventional confocal

microscope our maximum achievable lateral resolution was ~250 nm. PAPs are found at the distance of 0-400 nm from the synapse (Octeau et al 2018, Omrani et al 2009) thus we were not able to distinguish between and examine a certain subpopulation of most synaptically proximal PAPs that are arguably the most important for maintenance of glutamate homeostasis (Henneberger et al 2020).

To explore potential projection-specific change in plasticity of accumbal astrocytes as well as to increase the resolution of our approach to study their relationship with excitatory projections, we have implemented the Neuron-Astrocytes Proximity Assay (NAPA) in our lab (Octeau et al 2018). The assay relies on Förster resonance energy transfer (FRET), a quantum phenomenon in which emission light from a fluorophore is able to excite a second fluorophore. To achieve this, fluorophore wavelengths must be compatible, as well as the fluorophores must be no more then 10 nm apart. To satisfy both projection-specificity and increased resolution, we microinjected AAV to express a neuron-specific membrane-tethered reporter and FRET acceptor into the PFC, and an astrocyte-specific receptor and FRET donor in the NAc. In this way, we will be able to assess astrocyte interaction with glutamatergic cortical projections exclusively as well as examine the most proximal subpopulation of PAPs and their response to the cocaine SA and withdrawal. In the future, this approach can be used to systematically interrogate incoming NAc projections from various regions of interest that are involved in cocaine reward processing such as the VTA and BLA, and determine their relationship with accumbal astrocytes and their PAPs.

Regulation of information processing by NAc astrocytes

As stated in Chapter 1, the main goal of this research was to examine the effects of cocaine self-administration on astrocytes, as a means to develop hypotheses regarding the

contribution of astrocytes to mechanisms of cocaine seeking and relapse. Here we established that accumbal astrocytes are uniquely affected by cocaine self-administration and extinction/withdrawal, with atrophy of PAPs resulting in decreased glial coverage of glutamatergic synapses. Future studies should thus attempt to prevent or reverse the atrophy of accumbal astrocytes following cocaine SA and withdrawal, and restore glial synaptic coverage in order to reestablish glutamate homeostasis. One possible approach is to target cytoarchetectual components of the astrocytes. Structural features of cells are regulated by changes in cytoskeletal proteins; interestingly, actin is the only cytoskeletal protein present in PAPs (Schiweck et al 2018). Ras-related C3 botulinum toxin substrate 1 (Rac1) is a protein belonging to the Ras superfamily of small GTPases that controls growth and motility of PAPs through regulating actin dynamics (Kalman et al 1999). Recently, a photoactivatable version of Rac1 (PA-Rac1), expressed exclusively in astrocytes via viral delivery, was used to temporarily induce structural alteration in astrocyte structure (most likely PAPs) in BLA during fear conditioning and thus attenuate the formation of fear memory (Fan et al 2021, Liao et al 2017). Expressing PA-Rac1 in the NAc and activating it during a critical period of dysfunction of glutamate homeostasis thus has potential to restore the glial coverage of synapses.

Reestablishment of astrocyte coverage at the synapses would normalize the synaptic pathology induced by cocaine taking to an extent. But, as previously reported, synaptic pathology following cocaine self-administration was first described as downregulation of the glutamate transporter GLT-1 (Kalivas 2009). It is thus reasonable to expect that any successful mitigation of glutamate homeostasis dysregulation will necessitate a two-pronged approach, where reestablishment of the astroglial coverage of the accumbal synapses will have to be accompanied by the upregulation of the GLT-1 in astrocyte-specific manner. Indeed, overexpression of GLT-1 in accumbal astrocytes alone failed to attenuate cocaine reinstatement

(Logan et al 2018), presumably due to the lack of sufficient glial coverage of the synapses. In addition to glutamate uptake, astrocytes also control excitatory synaptic transmission through release of factors including glutamate, ATP, and others (Li et al 2020). Release of glutamate has been repeatedly reported to stimulate presynaptic inhibitory mGluR receptors (Kofuji & Araque 2021, Scofield et al 2015), and astroglial release of ATP similarly exerts a brake on synaptic strength through Gi-coupled presynaptic A1 receptors (Corkrum et al 2020, Martin-Fernandez et al 2017). Notably, excitatory synaptic strength in the NAc is potentiated subsequent to SA and extinction/abstinence. Thus, normalization of both structural and functional modulation of synaptic function by astrocytes carries the potential to normalize synaptic function, and limit the excitatory dive in this limbic-motor integrator, the NAc, associated with persistent drug seeking.

In summary, the study presented here describes a region-specific pathological atrophic phenotype of accumbal astrocytes following cocaine SA and extinction/withdrawal, and its direct connection to elimination of PAPs which correlates with two different, commonly utilized behavioral models of cocaine abuse. The results underscore the significant and long-lasting effect of cocaine self-administration on astrocyte complexity, and should aid behavioral and pharmacological approaches aimed at mitigating cocaine seeking and relapse. Moreover, the novel branching complexity analysis employed herein can be used in future studies to evaluate experience-dependent effects on astrocytes throughout the brain.

FIGURES AND FIGURE CAPTIONS

Chapter 2 “Region-Specific Reductions in Morphometric Properties…” Figure 1

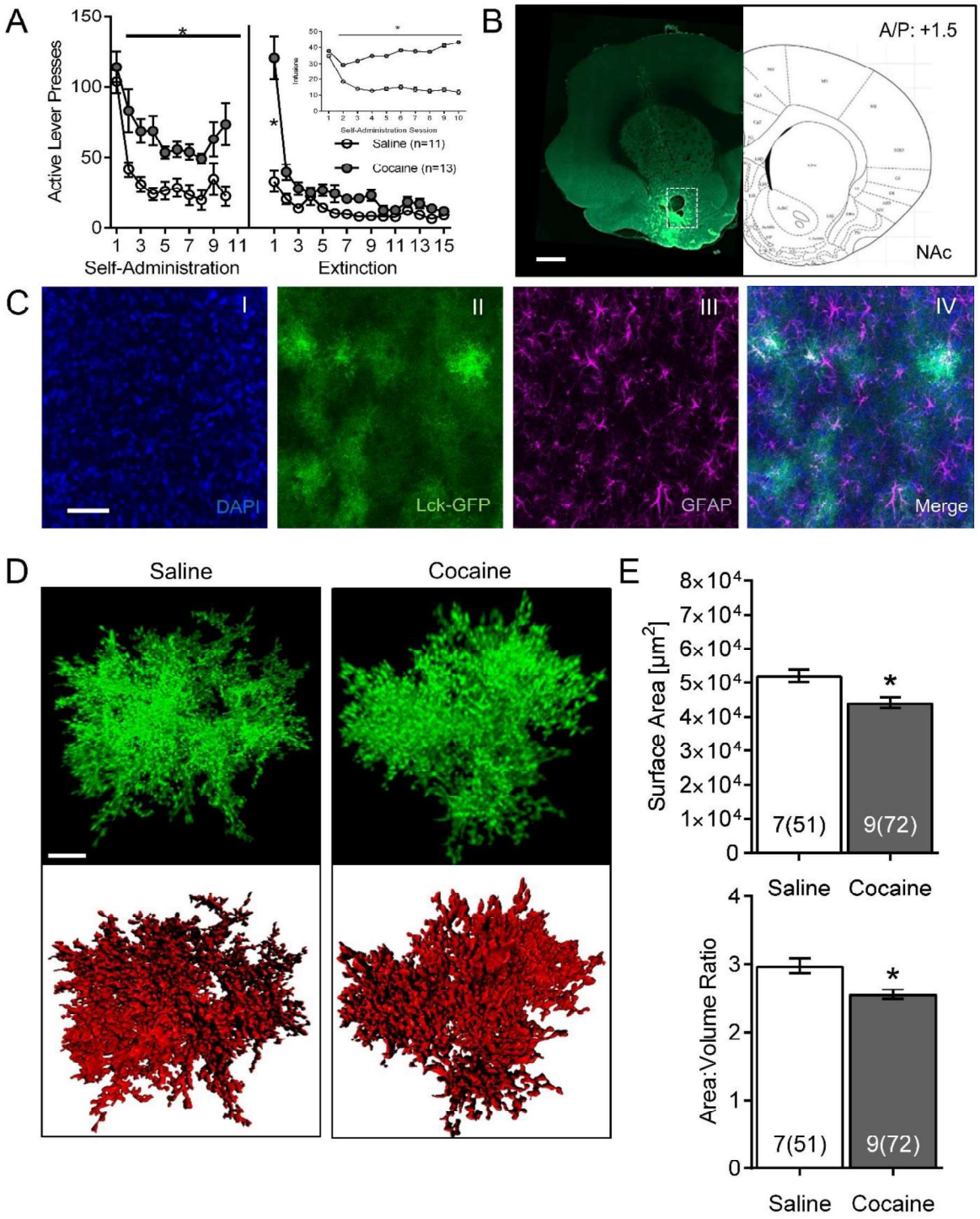

Figure 1. *Cocaine self-administration and extinction reduces astrocyte surface area and surface area:volume ratio in the NAc core.*

(A) Active lever presses by session across self-administration (10 days) and extinction (15 days) training. Insert: number of infusions during self-administration sessions ($^{*}p < 0.05$ by two-way ANOVA). **(B)** Scan of a brain slice showing the intensity and the range of expression of the AAV5 GfaABC1D-Lck-GFP. The white dotted box shows the area of NAc from which astrocytes were selected for imaging. 10× magnification, scale bar: 1 mm. **(C)** Multiple intensity projection (MIP) of an area within the NAc showing Lck-GFP expressing astrocytes (II) as well as staining for DAPI (I), GFAP (III), and merged image (IV). Colocalization between GFAP and Lck-GFAP is shown in white. 20× magnification, scale bar: 50 μm. **(D)** Representative isolated astrocytes from saline and cocaine-experienced rats imaged in the NAc. Lck-GFAP signal is shown in green and surface rendering used for volumetric measurements in red. 63× magnification, scale bar: 10 μm. **(E)** Astrocyte surface area and surface area:volume ratio in NAc are significantly decreased in cocaine-administering rats compared to saline-administering rats. Bar insert: number of animals and number of cells (in parentheses). $^{*}p < 0.05$ by nested ANOVA.

Chapter 2 “Region-Specific Reductions in Morphometric Properties…” Figure 2

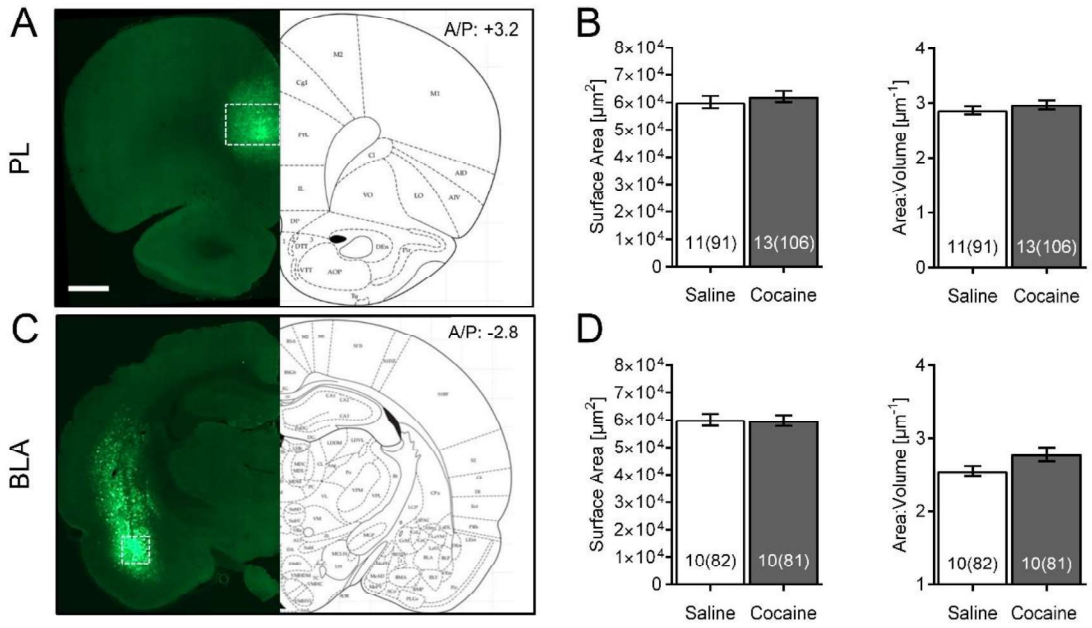

Figure 2. *Cocaine self-administration and extinction does not affect morphometric features of PL or BLA astrocytes.*

(A) Scan of a brain slice showing the intensity and range of expression of the AAV5 Lck-GFP. The white box shows the area of PL where imaging was performed. 10× magnification, scale bar: 1 mm. **(B)** No significant difference was observed in astrocyte surface area and surface area:volume ratio in the PL following cocaine self-administration and extinction. Bar insert: number of animals and number of cells (in parentheses). **(C)** Lck-GFP expression in BLA. The white box shows the area where imaging was performed. **(D)** No significant difference was observed in astrocyte surface area and surface area:volume ratio in the BLA following cocaine self-administration and extinction. Bar insert: number of animals and number of cells (in parentheses).

Chapter 2 “Region-Specific Reductions in Morphometric Properties…” Figure 3

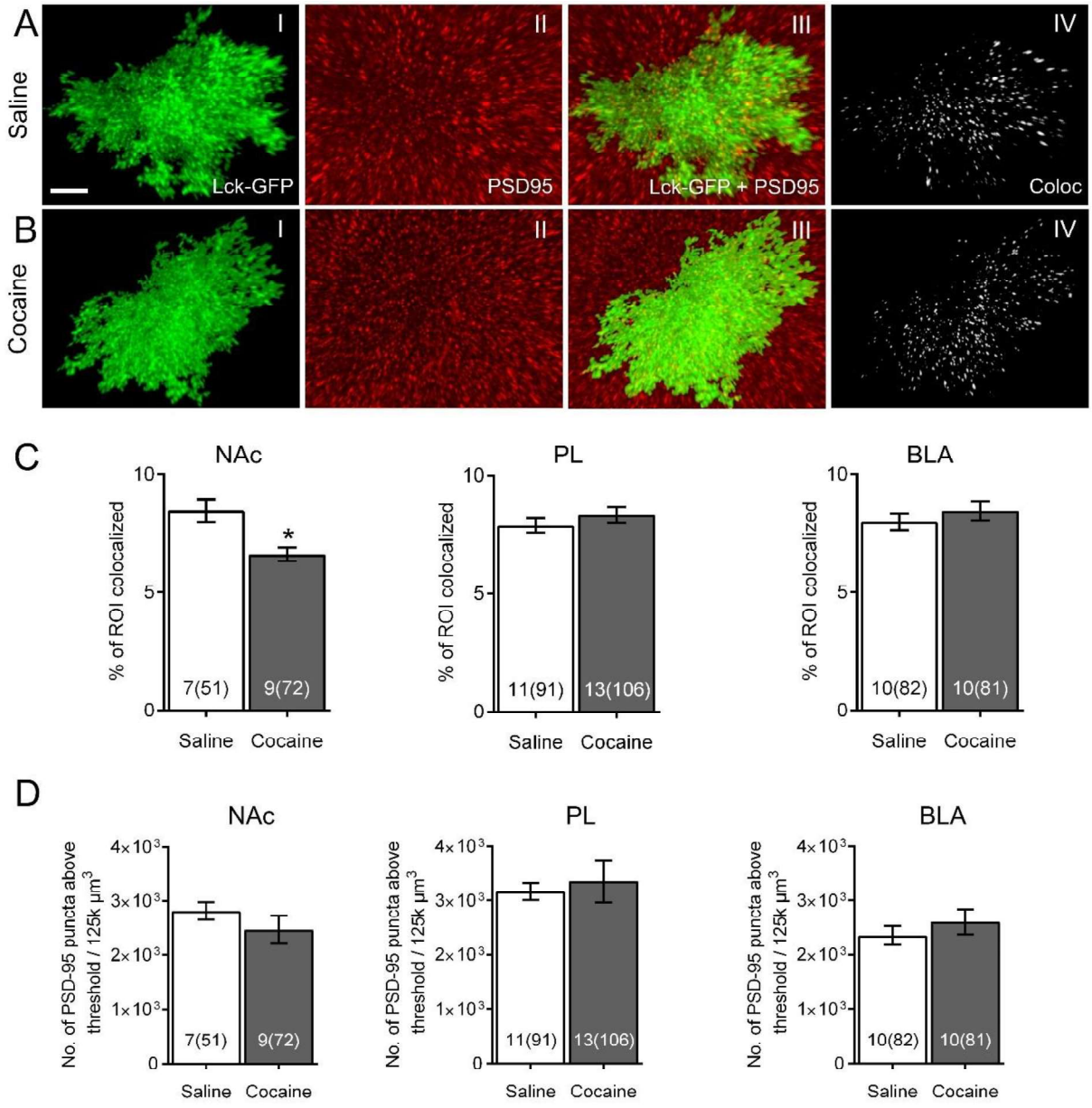

Figure 3. *Colocalization between astrocytes and post-synaptic marker PSD-95 following cocaine SA and extinction in NAc, PL, and BLA.*

(A) Isolated Lck-GFP signal from a single NAc astrocyte (I) from a saline-experienced rat and the same area, stained for neuronal post-synaptic marker PSD-95 (II). Both signals were overlapped (III) and Imaris was used to isolate the PSD-95 signal colocalized with Lck-GFP

(IV). **(B)** Same as in **(A)**, an astrocyte from a cocaine-extinguished rat. **(C)** Imaris was used to evaluate the percentage of isolated astrocyte Lck-GFP signal (ROI) colocalized with the PSD-95 signal. Significant difference in % of ROI colocalized between cocaine- and saline-administering rats was found in the NAc, but not in the PL or BLA regions. Bar insert: number of animals and number of cells (in parentheses). **(D)** Automated counting of PSD-95 positive puncta above the previously determined threshold level showed no difference in PSD-95 expression in any of the selected brain regions following cocaine versus self-administration and extinction. Bar insert: number of animals and number of cells (in parentheses). $^{*}p < 0.05$ by nested ANOVA.

Chapter 2 “Region-Specific Reductions in Morphometric Properties…” Figure 4

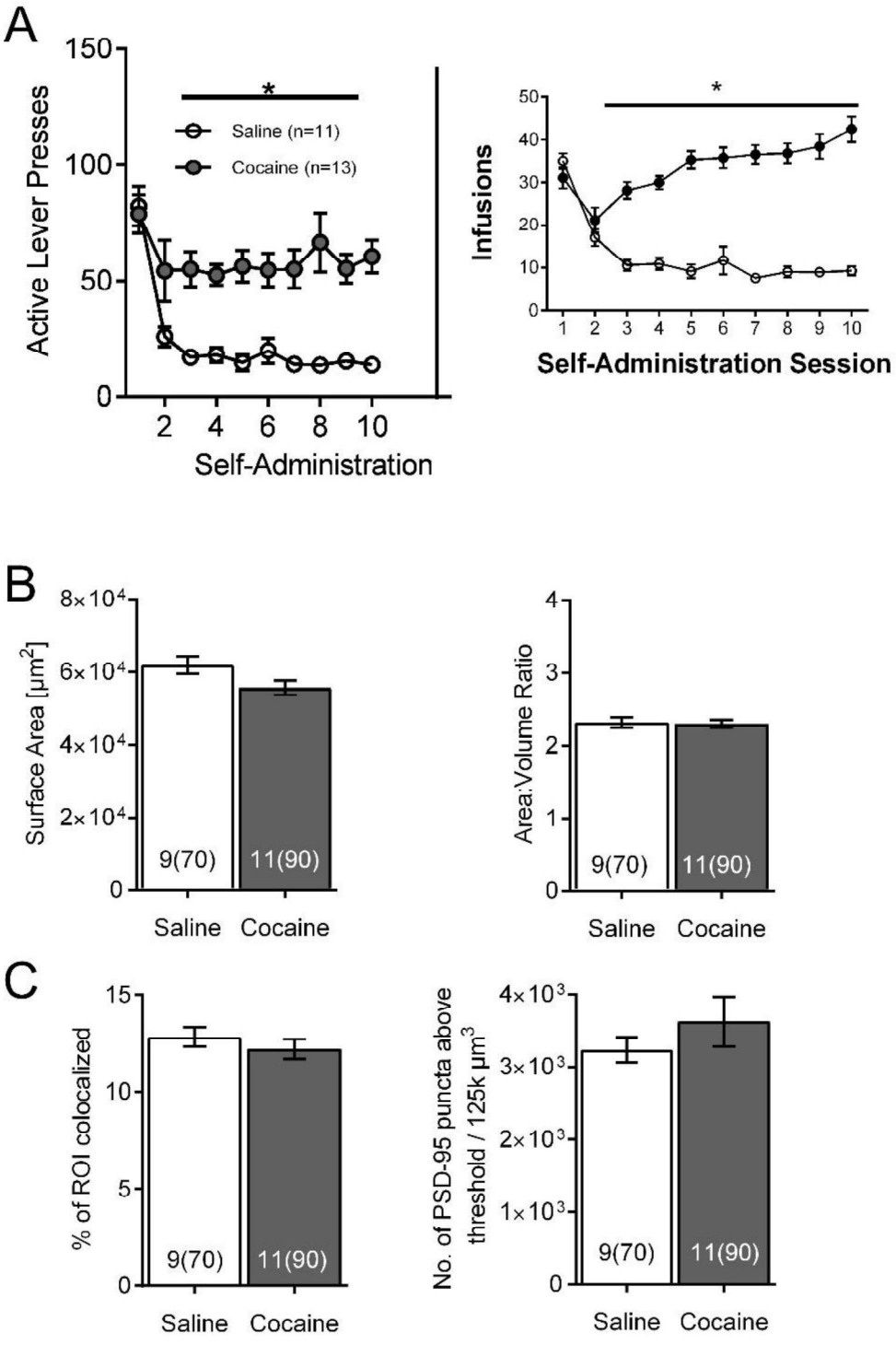

Figure 4. *The effects of cocaine self-administration on NAc astrocytes are not observed 24 h following the last self-administration session.*

(A) Active lever presses and cocaine infusions by session across self-administration (10 days) ($^{*}p < 0.05$ by two-way ANOVA). **(B)** No significant differences were observed in surface area (left) or surface area:volume ratio (right) in NAc astrocytes following cocaine versus saline self-administration. Bar insert: number of animals and number of cells (in parentheses). **(C)** No significant differences were observed following self-administration in NAc astrocyte:PSD-95 colocalization (left) or in the PSD-95 expression (right). Bar insert: number of animals and number of cells (in parentheses).

Chapter 2 “Region-Specific Reductions in Morphometric Properties…” Figure 5

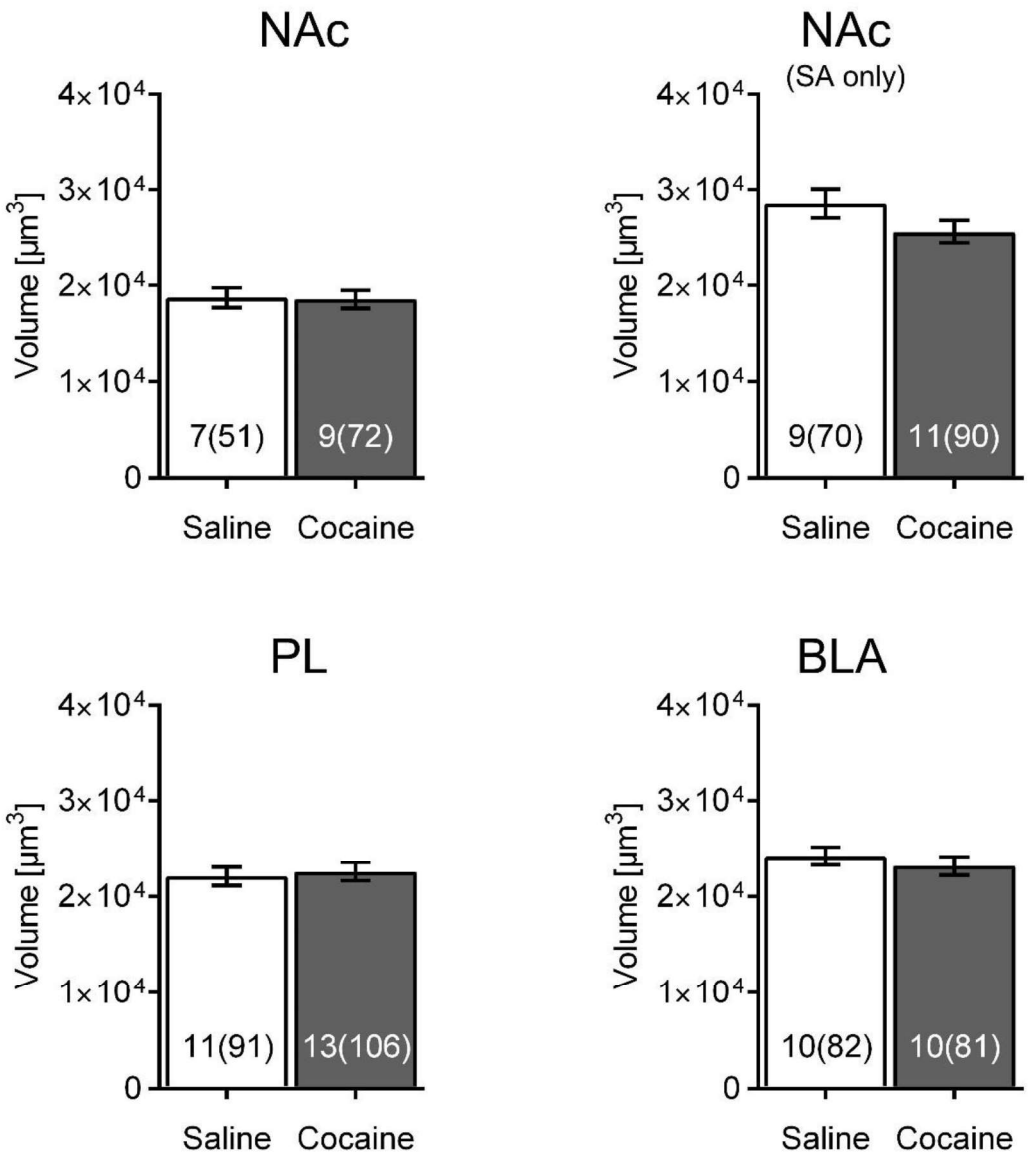

Figure 5. *Astrocyte volume is not affected in any of the explored brain regions following cocaine self-administration, regardless of the extinction training*

Volume of analyzed astrocytes did not change significantly in any of the studied brain regions following cocaine self-administration and extinction nor did it change after self-administration alone. Bar insert: number of animals and number of cells (in parenthesis).

Chapter 2 “Region-Specific Reductions in Morphometric Properties…” Table 1

	Surface area (μm^2)	Volume (μm^3)	Surface area: volume ratio (μm^{-1})
NAc	52,502 ± 3,114	19,259 ± 1,458	2.936 ± 0.114
PL	59,884 ± 2,441	22,016 ± 1,175	2.865 ± 0.090
BLA	59,225 ± 2,549	23,748 ± 1,220*	2.570 ± 0.094**

*Collected values from saline-extinguished rats from NAc, PL, and BLA. *Significantly different compared to NAc, **significantly different compared to NAc and PL. *, ** $p < 0.05$.*

Chapter 3 “Changes in Astrocyte Branching Complexity …” Figure 6

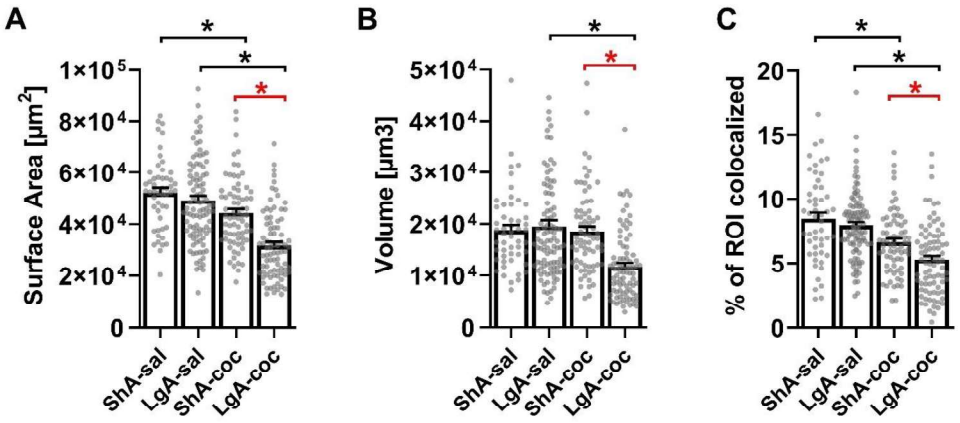

Figure 6. *Long access cocaine self-administration and abstinence produces more pronounced atrophic phenotype in NAc core astrocytes compared to the short-access cocaine self-administration*

(A) Both explored self-administration paradigms showed statistically significant decrease in astrocyte surface area in cocaine groups compared to the respective saline control groups (black asterisk). The decrease observed in LgA cocaine group was also significantly higher than the decrease associated with ShA cocaine group (red asterisk). There was no difference between both saline control groups. (B) Decrease in the volume of NAc astrocytes following cocaine self-administration was observed only in LgA paradigm (black asterisk) but not in ShA or between both saline control groups. Correspondingly, the difference between both cocaine groups is also significant (red asterisk). (C) Similarly, to the surface area, astrocyte colocalization with neuronal synaptic marker PSD95 was significantly decreased following cocaine self-administration within both paradigms when compared with their respective saline controls (black asterisk). Decrease in colocalization in cocaine-taking groups was significantly more pronounced when using LgA paradigm compared to ShA (red asterisk). * $p < 0.05$ as measured by the nested ANOVA.

Chapter 3 “Changes in Astrocyte Branching Complexity …” Figure 7

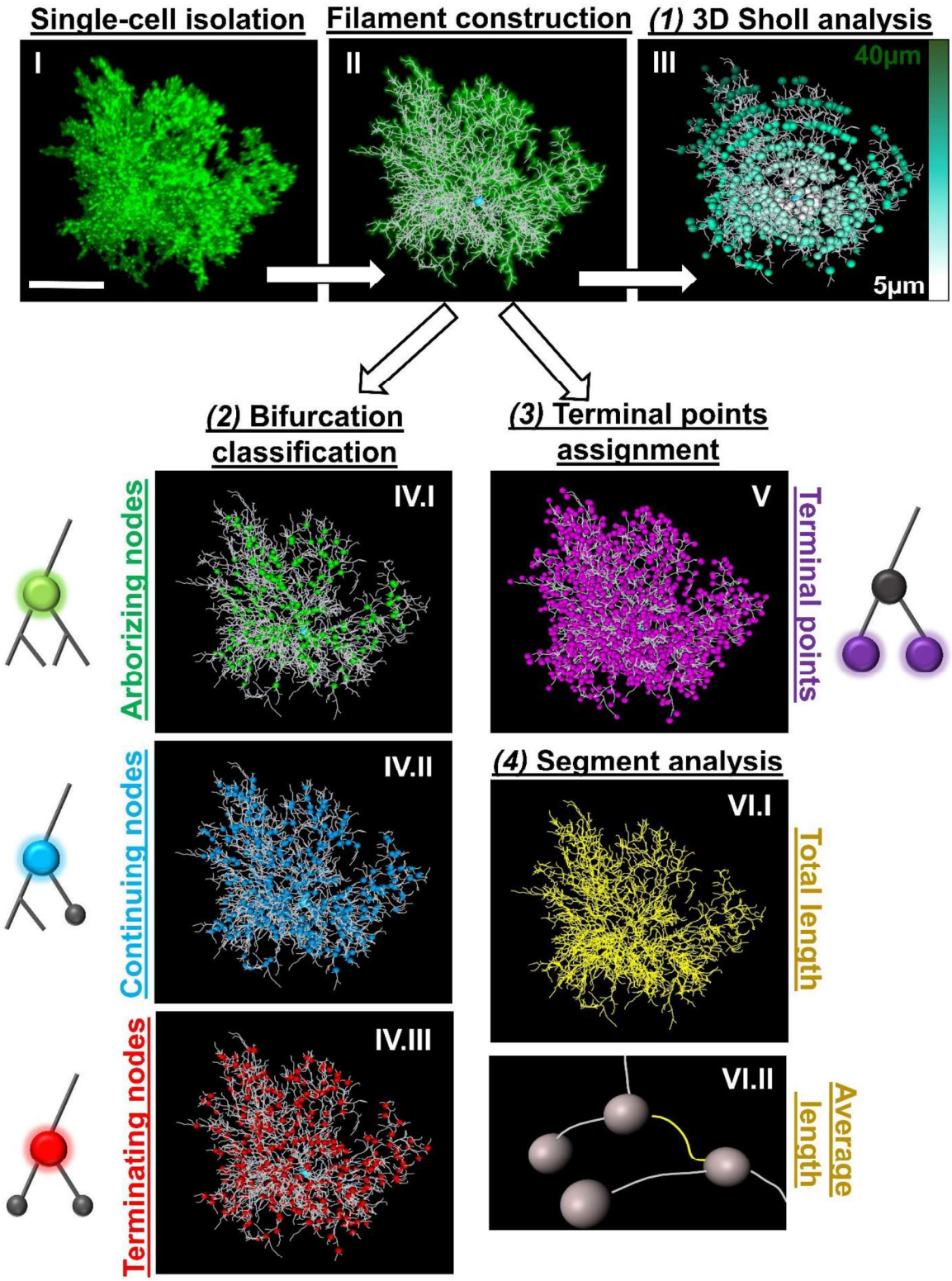

Figure 7. *The filament analysis pipeline*

After extracting morphometric and colocalization measurements from isolated accumbal astrocytes (frontiers, ron), the same isolated Lck-GFP signal (I) was used to build the skeleton of the filament using IMARIS software and its fast-marching algorithm (II). Four analyses were performed on the newly build filament constructs: (1) a 3-demensional Sholl analysis with 1 µm step size (III) (step size defined as an increase in sphere radius; the graphical representation shows intersections at every 5 µm for greater clarity), (2) bifurcation classification and analysis where each filament bifurcation was described as exactly one of three possible node types: arborizing node, where both child branches continue to bifurcate (IV.I), continuing node, where one child branch continues to bifurcate yet the second one terminates (IV.II) and terminating node, where both child branches terminate following the initial bifurcation (IV.III), (3) terminal point (filament ending) assignment where the number and distribution of filament endings (acting as proxies for PAP endings) was analyzed (V) and (4) the segment analysis where individual segments (defined as parts of the filament between two bifurcation nodes) were analyzed (VI.I-II). Scale bar: 20 µm

Chapter 3 “Changes in Astrocyte Branching Complexity …” Figure 8

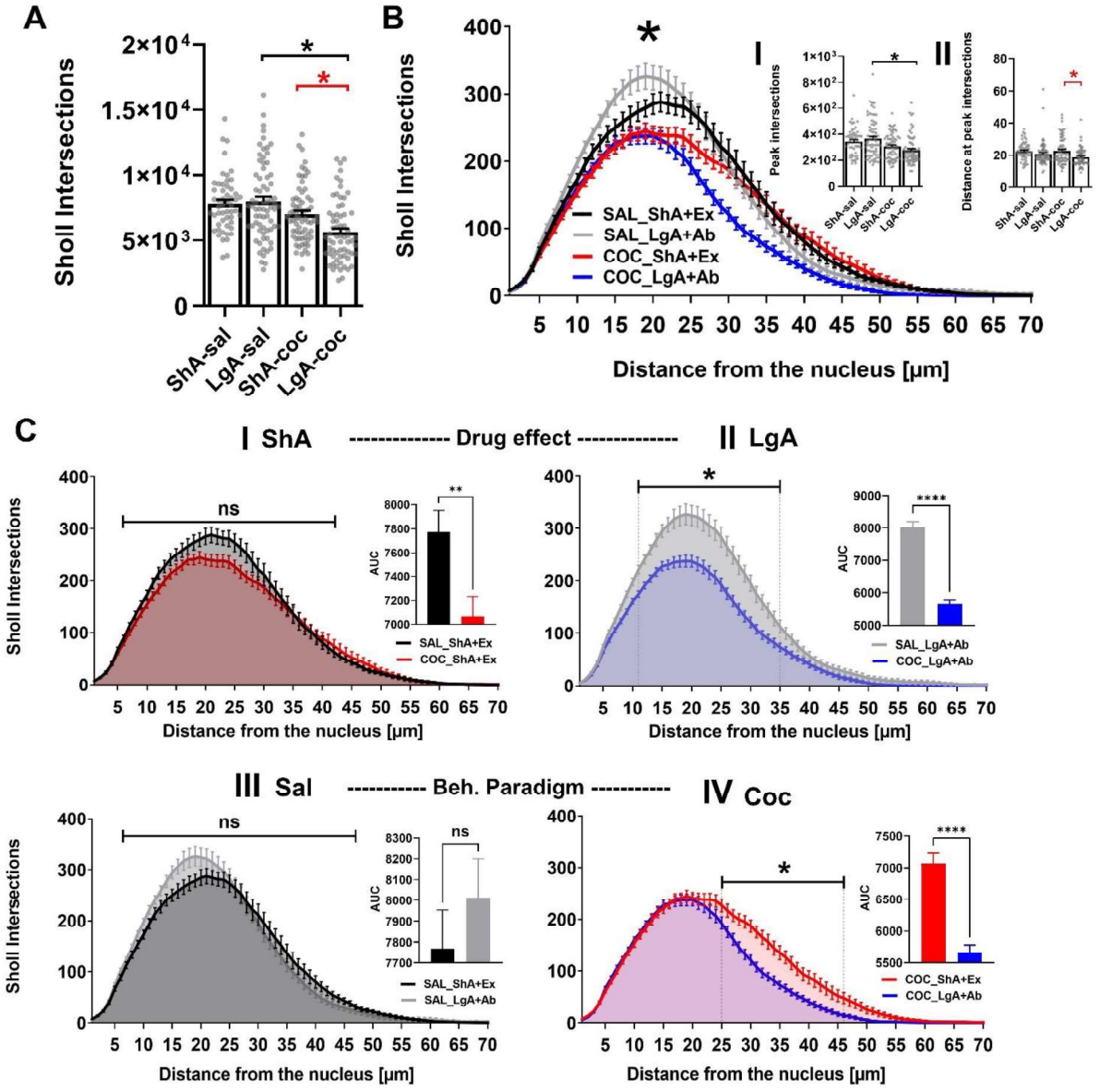

Figure 8. *The increased severity of the anthropic astrocyte phenotype associated with the long access cocaine self-administration and abstinence is a result of decreased complexity at the cell periphery*

(A) LgA cocaine SA and abstinence, but not ShA and extinction, paradigm results in a significantly decreased complexity of accumbal astrocytes as identified by the Sholl analysis

(black asterisk). Correspondingly, both cocaine groups also show significant difference (red asterisk). (B) Distribution of Sholl intersections plotted as a function of distance from the nucleus. Inserts: (I) Significant difference in peak intersections values detected between LgA cocaine-taking group and its respective saline control (black asterisk). No difference detected in the ShA group. (II) When comparing both cocaine groups, there was a statistically significant shift between distances where peak intersection values are observed (red asterisk). (C) Sholl intersections plotted as a function of distance, separated into two groups, using either drug or paradigm as a variable. No difference in astrocyte complexity shown in the ShA (I) and saline (III) pairings, respectively. LgA paradigm shows sizable decrease in complexity in cocaine-taking group (interval 11-35 μm) (II). The same LgA cocaine group also shows decrease in complexity when compared to the ShA cocaine group (interval 25-46 μm) (IV). Inserts show corresponding AUC. * $p < 0.05$ as measured by the nested ANOVA (A, B-I,II), * $p < 0.05$ as measured by the 3-way repeated measure ANOVA (B), * $p < 0.05$ as measured by the 2-way ANOVA followed by the Bonferroni multiple comparison post hoc test (C), **$p<0.01$, ****$p<0.0001$ as measured by unpaired two-tail t-test (C – AUC inserts).

.

Chapter 3 “Changes in Astrocyte Branching Complexity …” Figure 9

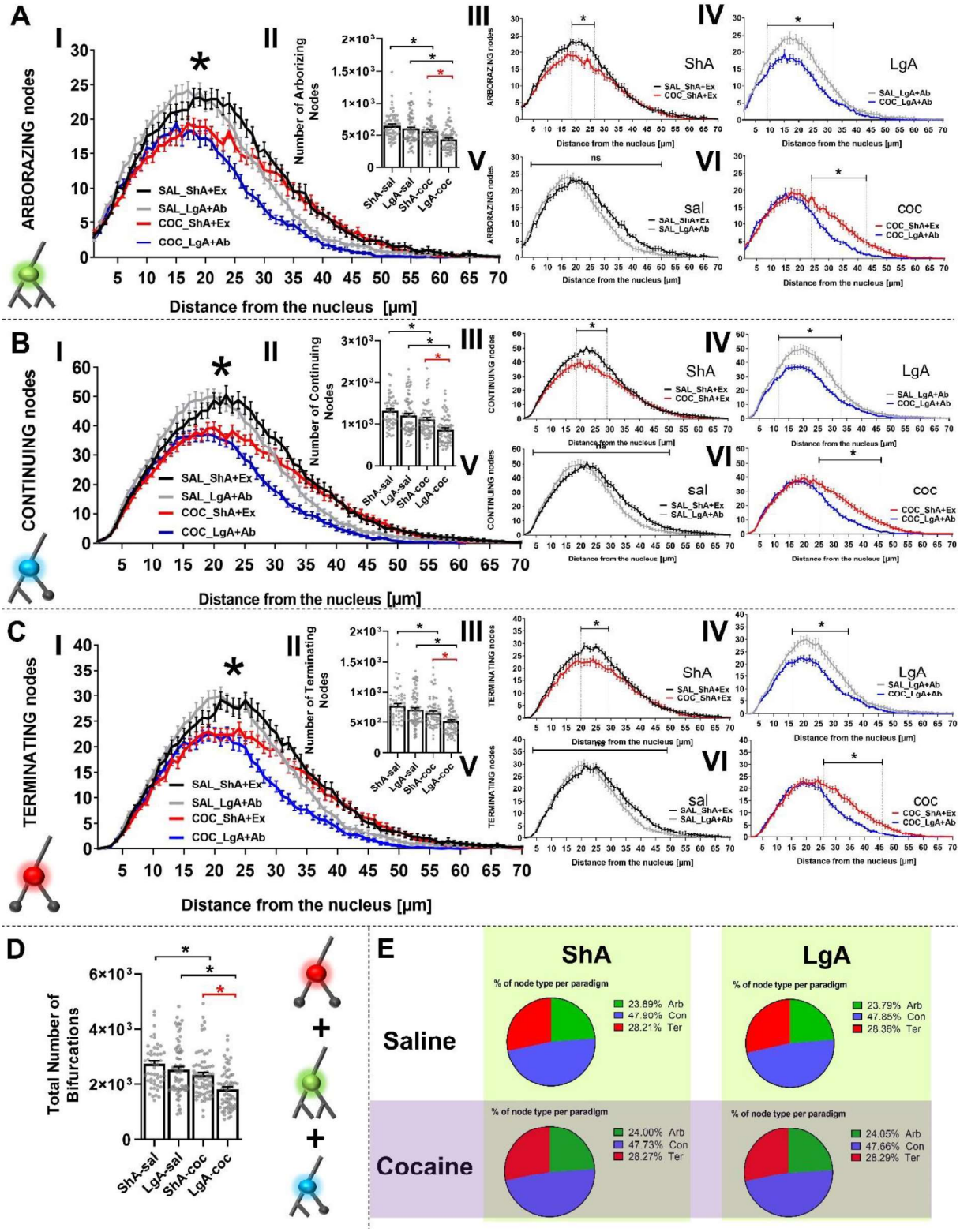

Figure 9. *LgA cocaine self-administration and abstinence decreases the number of bifurcations in accumbal astrocytes regardless of the branching type*

The number of (A) arborizing, (B) continuing and (C) terminating nodes was decreased in cocaine self-administrating animals (II) compared to respective saline control animals in both SA paradigms (black asterisk) but it was more pronounced in LgA cocaine animals (red asterisk). The decrease in branching complexity varied across groups as a function of distance (I) and all three bifurcation types followed a similar pattern of bifurcation distribution in space, with the ShA-cocaine group showing loss of branching nodes at the peak of branching complexity compared to its respective control saline group (III) and LgA-cocaine group extending its atrophic phenotype to the periphery (IV). This was confirmed with direct comparison of cocaine groups (VI). No difference was detected in saline groups (V). The same pattern was retained when combining all the different bifurcation (D). Throughout the different drug and behavioral paradigms, the percentages of individual node types stayed remarkably stable (E). * $p < 0.05$ as measured by the 3-way repeated measure ANOVA (A-C - I), * $p < 0.05$ as measured by the nested ANOVA (A-C – II, D), * $p < 0.05$ as measured by the 2-way ANOVA followed by the Bonferroni multiple comparison post hoc test (A-C – III-VI).

Chapter 3 “Changes in Astrocyte Branching Complexity …” Figure 10

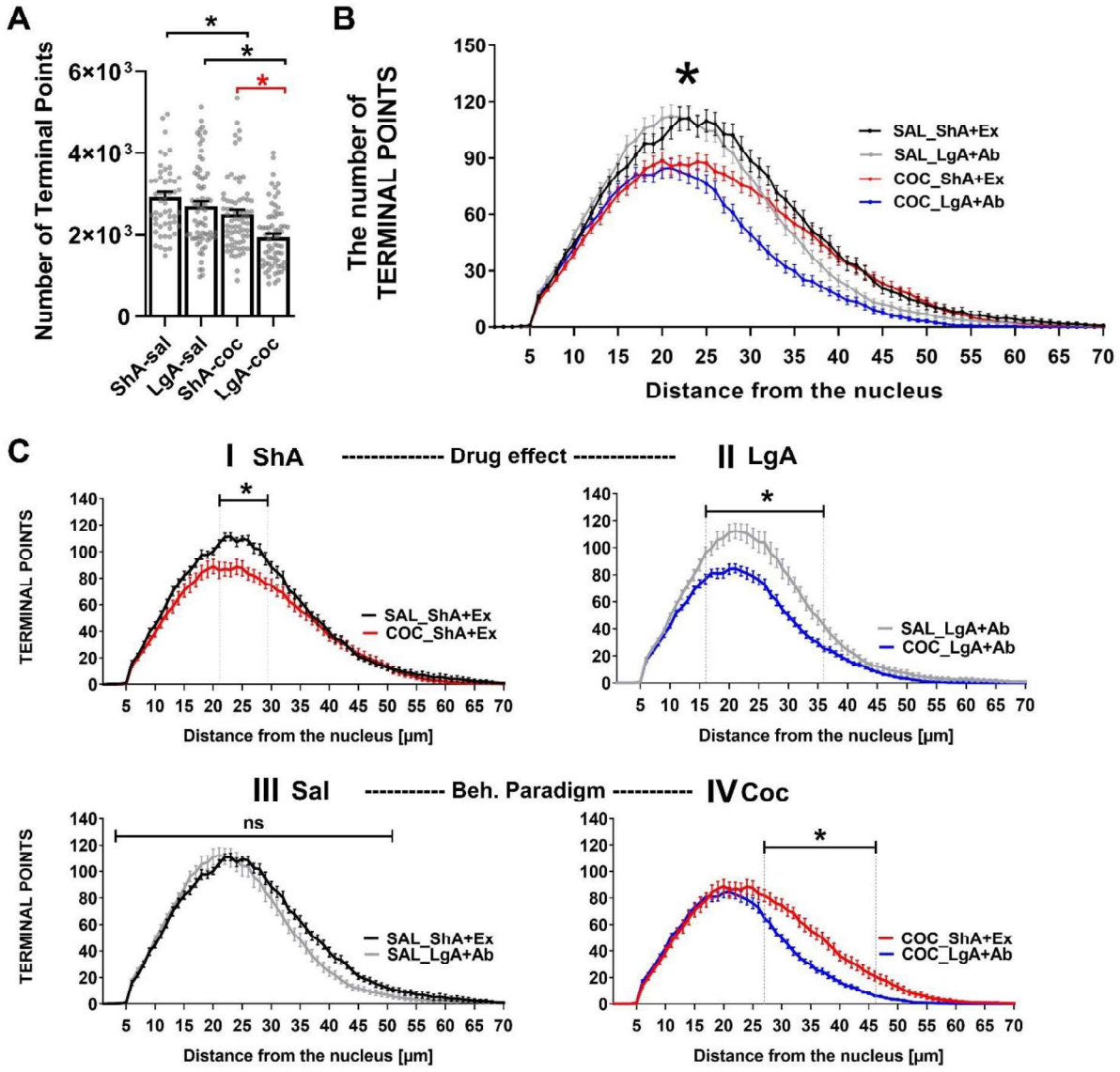

Figure 10. *LgA cocaine self-administration and abstinence results in a decrease in the number of filament endings of accumabal astrocyte.*

(A) Filament endings (terminal points), a proxy measurement for astrocyte PAPs, were significantly decreased in cocaine self-administrating animals compared to saline self-administrating animals in both SA paradigms (black asterisk), but the decrease was significantly more pronounced in LgA (red asterisk) (B) Distribution of terminal points plotted as a function

of distance from the nucleus. (C) Filament endings plotted as a function of distance, separated into two groups, using either drug or paradigm as a variable. ShA cocaine group shows a decrease in astrocyte filament endings around the peak value (I) while a decrease in LgA cocaine group extends further along the periphery (II). This is clearly shown when comparing both cocaine groups directly (IV). No difference in astrocyte filament ednings shown between both respective saline control groups (III). *$p < 0.05$ as measured by the nested ANOVA (A), * $p < 0.05$ as measured by a 3-way repeated measure ANOVA (B), * $p < 0.05$ as measured by two-way ANOVA followed by the Bonferroni multiple comparison post hoc test (C).

Chapter 3 “Changes in Astrocyte Branching Complexity …” Figure 11

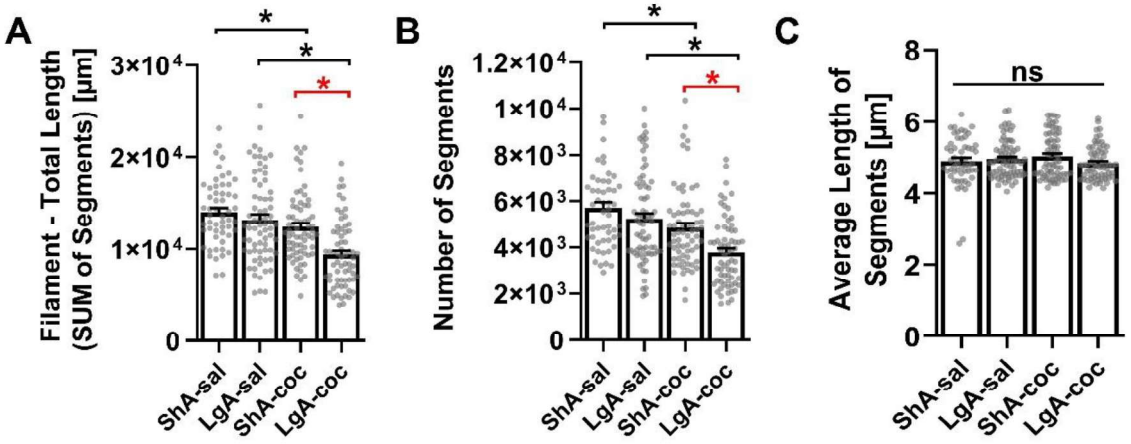

Figure 11. *The decrease in the accumbal astrocyte filament model’s length is a result of filamentsegments loss and not the shortening of the segments.*

(A) The total length of the astrocyte filament models (the sum of the filament segments) as well as (B) the number of segments were significantly decreased in cocaine self-administrating animals compared to saline self-administrating animals in both SA paradigms (black asterisk), but the decrease was significantly more pronounced in LgA (red asterisk). (C) The average length of individual segments was not changed across the groups thus not contributing to the decrease in total filament length. * $p < 0.05$ as measured by the nested ANOVA.

Chapter 3 “Changes in Astrocyte Branching Complexity …” Table 2

		variable	ShA (sal v coc)					LgA (sal v coc)				
		DRUG	mean	SEM	DF	F-value	p-value	mean	SEM	DF	F-value	p-value
Sholl intersections	total (SUM)	sal	7844.13	295.77	14	4.17	0.0604	8025.09	319.79	14	26.68	**0.0001***
		coc	7038.22	261.12				5654.14	329.33			
	Intersections peak	sal	345.36	13.4351	14	4.33	0.0563	367.54	15.5781	14	15.32	**0.0016***
		coc	308.07	11.8611				280.02	16.0432			
	distance at peak	sal	22.4906	0.9799	14	0.02	0.8977	20.7286	0.7726	14	3.56	0.0801
		coc	22.6618	0.8651				18.6364	0.7957			
	AUC	sal	7770	183.1	14	1.245	**0.0079***	8011	189.1	14	2.555	**0.0001***
		coc	7067	164.1				5666	118.3			
Arborazing nodes	total number (SUM)	sal	654	27.4431	14	6.47	**0.0234***	599.62	23.4599	14	23.14	**0.0003***
		coc	560.81	24.2776				437.64	24.15			
Continuing nodes	total number (SUM)	sal	1311.39	55.8451	14	6.93	**0.0197***	1205.83	46.8216	14	25.37	**0.0002***
		coc	1115.17	49.4035				867.39	48.199			
Terminating nodes	total number (SUM)	sal	772.41	33.3015	14	6.32	**0.0248***	714.66	28.4845	14	23.88	**0.0002***
		coc	660.65	29.4602				514.91	29.3224			
Bifurcations (all nodes)	total number (SUM)	sal	2737.8	116.31	14	6.67	**0.0217***	2520.11	98.5449	14	24.51	**0.0002***
		coc	2336.64	102.89				1819.94	101.44			
Terminal points	total number (SUM)	sal	2922.96	125.75	14	6.3	**0.025***	2703.51	106.46	14	24.55	**0.0002***
		coc	2501.46	111.25				1946.39	109.59			
Filaments	length - total	sal	13985	503.6	14	5.65	**0.0323***	13189	493.47	14	28.78	**0.0001***
		coc	12387	445.51				9389.48	507.98			
Segments	total number (SUM)	sal	5700.52	243.63	14	6.69	**0.0216***	5245.39	205.92	14	25.47	**0.0002***
		coc	4859.45	215.52				3782.52	211.98			
	length - average	sal	4.9037	0.08767	14	1.44	0.2503	4.9536	0.05942	14	1.6	0.2267
		coc	5.0441	0.07755				4.8458	0.06117			

		variable	Coc (ShA v LgA)					Sal (ShA v LgA)				
		DRUG	mean	SEM	DF	F-value	p-value	mean	SEM	DF	F-value	p-value
Sholl intersections	total (SUM)	sal	7038.22	272	15	12.49	**0.003***	7844.13	362.67	13	0.14	0.7127
		coc	5673.55	274.02				8025.09	315.58			
	Intersections peak	sal	308.07	12.3985	15	2.52	0.1331	345.36	17.8133	13	0.88	0.3646
		coc	280.02	12.5849				367.54	15.5			
	distance at peak	sal	22.6618	0.8397	15	11.32	**0.0043***	22.4906	0.9114	13	2.13	0.1685
		coc	18.6364	0.8523				20.7286	0.7931			
	AUC	sal	7067	164.1	15	1.924	**0.0001***	7770	183.1	13	1.065	0.3682
		coc	5666	118.3				8011	189			
Arborazing nodes	total number (SUM)	sal	560.81	21.9585	15	15.5	**0.0013***	654	29.4919	13	1.93	0.188
		coc	437.64	22.2839				599.62	25.7199			
Continuing nodes	total number (SUM)	sal	1115.17	43.3716	15	16.08	**0.0011***	1311.39	60.303	13	1.74	0.2099
		coc	867.39	44.0141				1205.83	52.5904			
Terminating nodes	total number (SUM)	sal	660.65	26.2874	15	15.14	**0.0014***	772.41	36.174	13	1.45	0.2504
		coc	514.91	26.6768				714.66	31.5475			
Bifurcations (all nodes)	total number (SUM)	sal	2336.64	91.3919	15	15.75	**0.0012***	2737.8	125.69	13	1.7	0.2144
		coc	1819.94	92.7459				2520.11	109.61			
Terminal points	total number (SUM)	sal	2501.46	98.6492	15	15.6	**0.0013***	2922.96	135.97	13	1.48	0.2455
		coc	1946.39	100.11				1703.51	118.58			
Filaments	length - total	sal	12387	449.46	15	21.91	**0.0003***	13985	567.69	13	1.12	0.3098
		coc	9389.48	456.12				13189	495.09			
Segments	total number (SUM)	sal	4859.45	190.99	15	15.66	**0.0013***	5700.52	263.17	13	1.7	0.2151
		coc	3782.52	193.82				5245.39	229.51			
	length - average	sal	5.0441	0.06532	15	4.54	0.0501	4.9037	0.08218	13	0.21	0.6546
		coc	4.8458	0.06629				4.9536	0.07167			

Chapter 3 “Changes in Astrocyte Branching Complexity …” Table 3

			Arborizing nodes			Continuing nodes			Terminating nodes		
3-way repeated measures ANOVA		variables	f-value	p-value	post hoc multiple comparison test (Bonferroni)	f-value	p-value	post hoc multiple comparison test (Bonferroni)	f-value	p-value	post hoc multiple comparison test (Bonferroni)
		distance	F (91, 2548) = 549.1	P<0.0001	N/A	F (3.163, 88.55) = 625.5	P<0.0001	N/A	F (2.678, 74.98) = 458.9	P<0.0001	N/A
		paradigm	F (1, 28) = 11.46	P=0.0021	N/A	F (1, 28) = 11.70	P=0.0019	N/A	F (1, 28) = 12.27	P=0.0016	N/A
		drug	F (1, 28) = 21.63	P<0.0001	N/A	F (1, 28) = 24.39	P<0.0001	N/A	F (1, 28) = 22.10	P<0.0001	N/A
		distance x paradigm	F (91, 2548) = 9.709	P<0.0001	N/A	F (91, 2548) = 9.772	P<0.0001	N/A	F (91, 2548) = 6.510	P<0.0001	N/A
		distance x drug	F (91, 2548) = 8.143	P<0.0001	N/A	F (91, 2548) = 10.33	P<0.0001	N/A	F (91, 2548) = 9.617	P<0.0001	N/A
		paradigm x drug	F (1, 28) = 1.404	P=0.2461	N/A	F (1, 28) = 1.472	P=0.2351	N/A	F (1, 28) = 0.02903	P=0.8659	N/A
		distance x paradigm x drug	F (91, 2548) = 0.6634	P=0.9939	N/A	F (91, 2548) = 0.6425	P=0.9965	N/A	F (91, 2548) = 0.4553	P>0.9999	N/A
2-way repeated measures ANOVA	ShA (sal v coc)	distance	F (91, 1274) = 264.4	P<0.0001	significant decrease between **18 and 27** µm (p<0.05)*	F (91, 1274) = 299.1	P<0.0001	significant decrease between **18 and 28** µm (p<0.05)*	F (91, 1274) = 198.3	P<0.0001	significant decrease between **20 and 29** µm (p<0.05)*
		drug	F (1, 14) = 5.391	**P=0.0358***		F (1, 14) = 6.072	**P=0.0273***		F (1, 14) = 7.529	**P=0.0158***	
		distance x drug	F (91, 1274) = 3.012	**P<0.0001***		F (91, 1274) = 3.602	**P<0.0001***		F (91, 1274) = 3.989	**P<0.0001***	
	LgA (sal v coc)	distance	F (91, 1274) = 296.6	P<0.0001	significant decrease between **8 and 32** µm (p<0.05)*	F (91, 1274) = 339.3	P<0.0001	significant decrease between **11 and 33** µm (p<0.05)*	F (91, 1274) = 290.9	P<0.0001	significant decrease between **16 and 35** µm (p<0.05)*
		drug	F (1, 14) = 19.20	**P=0.0006***		F (1, 14) = 22.02	**P=0.0003***		F (1, 14) = 18.48	**P=0.0007***	
		distance x drug	F (91, 1274) = 6.019	**P<0.0001***		F (91, 1274) = 7.736	**P<0.0001***		F (91, 1274) = 6.819	**P<0.0001***	
	Coc (ShA v LgA)	distance	F (91, 1365) = 257.3	P<0.0001	significant decrease between **24 and 43** µm (p<0.05)*	F (91, 1365) = 295.0	P<0.0001	significant decrease between **25 and 46** µm (p<0.05)*	F (91, 1365) = 248.4	P<0.0001	significant decrease between **26 and 46** µm (p<0.05)*
		paradigm	F (1, 15) = 10.87	**P=0.0049***		F (1, 15) = 11.31	**P=0.0043***		F (1, 15) = 10.71	**P=0.0051***	
		distance x paradigm	F (91, 1365) = 7.272	**P<0.0001***		F (91, 1365) = 7.309	**P<0.0001***		F (91, 1365) = 6.535	**P<0.0001***	
	Sal (Sha v LgA)	distance	F (91, 1183) = 286.6	P<0.0001	N/A (no effect of the paradigm)	F (91, 1183) = 324.0	P<0.0001	N/A (no effect of the paradigm)	F (91, 1183) = 214.2	P<0.0001	N/A (no effect of the paradigm)
		paradigm	F (1, 13) = 2.343	P=0.1498		F (1, 13) = 2.326	P=0.1512		F (1, 13) = 3.794	P=0.0734	
		distance x paradigm	F (91, 1183) = 3.585	**P<0.0001***		F (91, 1183) = 3.634	**P<0.0001***		F (91, 1183) = 1.783	**P<0.0001***	

			Sholl intersections			Terminal points		
3-way repeated measures ANOVA		variables	f-value	p-value	post hoc multiple comparison test (Bonferroni)	f-value	p-value	post hoc multiple comparison test (Bonferroni)
		distance	F (2.471, 69.19) = 621.3	P<0.0001	N/A	F (2.643, 73.99) = 645.5	P<0.0001	N/A
		paradigm	F (1, 28) = 2.460	P=0.1280	N/A	F (1, 28) = 10.47	P=0.0031	N/A
		drug	F (1, 28) = 17.17	P=0.0003	N/A	F (1, 28) = 21.87	P<0.0001	N/A
		distance x paradigm	F (93, 2604) = 10.96	P<0.0001	N/A	F (91, 2548) = 8.012	P<0.0001	N/A
		distance x drug	F (93, 2604) = 9.383	P<0.0001	N/A	F (91, 2548) = 9.953	P<0.0001	N/A
		paradigm x drug	F (1, 28) = 4.986	P=0.0337	N/A	F (1, 28) = 1.560	P=0.2220	N/A
		distance x paradigm x drug	F (93, 2604) = 1.334	**P=0.0194***	N/A	F (91, 2548) = 0.7792	P=0.9387	N/A
2-way repeated measures ANOVA	ShA (sal v coc)	distance	F (93, 1302) = 277.0	P<0.0001	N/A (no effect of the drug)	F (91, 1274) = 314.7	P<0.0001	significant decrease between **21 and 29** µm (p<0.05)*
		drug	F (1, 14) = 1.802	P=0.2009		F (1, 14) = 5.287	**P=0.0374***	
		distance x drug	F (93, 1302) = 1.994	**P<0.0001***		F (91, 1274) = 3.098	**P<0.0001***	
	LgA (sal v coc)	distance	F (93, 1302) = 365.2	P<0.0001	significant decrease between **11 and 35** µm (p<0.05)*	F (91, 1274) = 310.9	P<0.0001	significant decrease between **16 and 36** µm (p<0.05)*
		drug	F (1, 14) = 20.62	**P=0.0005***		F (1, 14) = 19.71	**P=0.0006**	
		distance x drug	F (93, 1302) = 9.623	**P<0.0001***		F (91, 1274) = 8.029	**P<0.0001**	
	Coc (ShA v LgA)	distance	F (93, 1395) = 340.4	P<0.0001	significant decrease between **25 and 46** µm (p<0.05)*	F (91, 1365) = 290.7	P<0.0001	significant decrease between **27 and 46** µm (p<0.05)*
		paradigm	F (1, 15) = 9.721	**P=0.0071***		F (1, 15) = 10.80	**P=0.0050***	
		distance x paradigm	F (93, 1395) = 9.900	**P<0.0001**		F (91, 1365) = 6.907	**P<0.0001***	
	Sal (Sha v LgA)	distance	F (93, 1209) = 286.0	P<0.0001	N/A (no effect of the paradigm)	F (91, 1183) = 349.6	P<0.0001	N/A (no effect of the paradigm)
		paradigm	F (1, 13) = 0.1677	P=0.6888		F (1, 13) = 1.842	P=0.1978	
		distance x paradigm	F (93, 1209) = 3.870	**P<0.0001***		F (91, 1183) = 2.431	**P<0.0001***	

REFERENCES

Ahmed SH, Koob GF. 1998. Transition from moderate to excessive drug intake: change in hedonic set point. *Science* 282: 298-300

Akhgari M, Sardari-Iravani F, Ghadipasha M. 2021. Trends in Poly Drug Use-associated Deaths based on Confirmed Analytical Toxicology Results in Tehran, Iran, in 2011-2016. *Addict Health* 13: 18-28

Allain F, Samaha AN. 2019. Revisiting long-access versus short-access cocaine self-administration in rats: intermittent intake promotes addiction symptoms independent of session length. *Addict Biol* 24: 641-51

Allen NJ. 2014. Synaptic plasticity: Astrocytes wrap it up. *Curr Biol* 24: R697-9

Allen NJ, Barres BA. 2009. Neuroscience: Glia - more than just brain glue. *Nature* 457: 675-7

Allen NJ, Eroglu C. 2017. Cell Biology of Astrocyte-Synapse Interactions. *Neuron* 96: 697-708

Ang CW, Koga M, Jacobs BC, Yuki N, van der Meche FG, van Doorn PA. 2001. Differential immune response to gangliosides in Guillain-Barre syndrome patients from Japan and The Netherlands. *J Neuroimmunol* 121: 83-7

Araque A, Parpura V, Sanzgiri RP, Haydon PG. 1999a. Tripartite synapses: glia, the unacknowledged partner. *Trends Neurosci* 22: 208-15

Araque A, Sanzgiri RP, Parpura V, Haydon PG. 1999b. Astrocyte-induced modulation of synaptic transmission. *Can J Physiol Pharmacol* 77: 699-706

Baker DA, McFarland K, Lake RW, Shen H, Tang XC, et al. 2003. Neuroadaptations in cystine-glutamate exchange underlie cocaine relapse. *Nat Neurosci* 6: 743-9

Banker GA. 1980. Trophic interactions between astroglial cells and hippocampal neurons in culture. *Science* 209: 809-10

Barker AJ, Ullian EM. 2010. Astrocytes and synaptic plasticity. *Neuroscientist* 16: 40-50

Barres BA. 2008. The mystery and magic of glia: a perspective on their roles in health and disease. *Neuron* 60: 430-40

Becquet D, Girardet C, Guillaumond F, Francois-Bellan AM, Bosler O. 2008. Ultrastructural plasticity in the rat suprachiasmatic nucleus. Possible involvement in clock entrainment. *Glia* 56: 294-305

Belin-Rauscent A, Fouyssac M, Bonci A, Belin D. 2016. How Preclinical Models Evolved to Resemble the Diagnostic Criteria of Drug Addiction. *Biol Psychiatry* 79: 39-46

Ben Haim L, Rowitch DH. 2017. Functional diversity of astrocytes in neural circuit regulation. *Nat Rev Neurosci* 18: 31-41

Benediktsson AM, Schachtele SJ, Green SH, Dailey ME. 2005. Ballistic labeling and dynamic imaging of astrocytes in organotypic hippocampal slice cultures. *J Neurosci Methods* 141: 41-53

Benesova J, Hock M, Butenko O, Prajerova I, Anderova M, Chvatal A. 2009. Quantification of astrocyte volume changes during ischemia in situ reveals two populations of astrocytes in the cortex of GFAP/EGFP mice. *J Neurosci Res* 87: 96-111

Bennett MV, Contreras JE, Bukauskas FF, Saez JC. 2003. New roles for astrocytes: gap junction hemichannels have something to communicate. *Trends Neurosci* 26: 610-7

Bespalov A, Steckler T, Altevogt B, Koustova E, Skolnick P, et al. 2016. Failed trials for central nervous system disorders do not necessarily invalidate preclinical models and drug targets. *Nat Rev Drug Discov* 15: 516

Bignami A, Dahl D. 1974. Astrocyte-specific protein and radial glia in the cerebral cortex of newborn rat. *Nature* 252: 55-6

Bird AD, Cuntz H. 2019. Dissecting Sholl Analysis into Its Functional Components. *Cell Rep* 27: 3081-96 e5

Bjornsson CS, Lin G, Al-Kofahi Y, Narayanaswamy A, Smith KL, et al. 2008. Associative image analysis: a method for automated quantification of 3D multi-parameter images of brain tissue. *J Neurosci Methods* 170: 165-78

Blanco-Calvo E, Rivera P, Arrabal S, Vargas A, Pavon FJ, et al. 2014. Pharmacological blockade of either cannabinoid CB1 or CB2 receptors prevents both cocaine-induced conditioned locomotion and cocaine-induced reduction of cell proliferation in the hippocampus of adult male rat. *Front Integr Neurosci* 7: 106

Blanpied TA, Ehlers MD. 2004. Microanatomy of dendritic spines: emerging principles of synaptic pathology in psychiatric and neurological disease. *Biol Psychiatry* 55: 1121-7

Block ML, Hong JS. 2007. Chronic microglial activation and progressive dopaminergic neurotoxicity. *Biochem Soc Trans* 35: 1127-32

Bondi H, Bortolotto V, Canonico PL, Grilli M. 2021. Complex and regional-specific changes in the morphological complexity of GFAP(+) astrocytes in middle-aged mice. *Neurobiol Aging* 100: 59-71

Bossert JM, Ghitza UE, Lu L, Epstein DH, Shaham Y. 2005. Neurobiology of relapse to heroin and cocaine seeking: an update and clinical implications. *Eur J Pharmacol* 526: 36-50

Bossert JM, Marchant NJ, Calu DJ, Shaham Y. 2013. The reinstatement model of drug relapse: recent neurobiological findings, emerging research topics, and translational research. *Psychopharmacology (Berl)* 229: 453-76

Boudreau AC, Wolf ME. 2005. Behavioral sensitization to cocaine is associated with increased

AMPA receptor surface expression in the nucleus accumbens. *J Neurosci* 25: 9144-51

Bowers MS, Kalivas PW. 2003. Forebrain astroglial plasticity is induced following withdrawal from repeated cocaine administration. *Eur J Neurosci* 17: 1273-8

Bridges RJ, Natale NR, Patel SA. 2012. System xc(-) cystine/glutamate antiporter: an update on molecular pharmacology and roles within the CNS. *Br J Pharmacol* 165: 20-34

Budde MD, Frank JA. 2012. Examining brain microstructure using structure tensor analysis of histological sections. *Neuroimage* 63: 1-10

Bushong EA, Martone ME, Ellisman MH. 2003. Examination of the relationship between astrocyte morphology and laminar boundaries in the molecular layer of adult dentate gyrus. *J Comp Neurol* 462: 241-51

Bushong EA, Martone ME, Ellisman MH. 2004. Maturation of astrocyte morphology and the establishment of astrocyte domains during postnatal hippocampal development. *Int J Dev Neurosci* 22: 73-86

Bushong EA, Martone ME, Jones YZ, Ellisman MH. 2002. Protoplasmic astrocytes in CA1 stratum radiatum occupy separate anatomical domains. *J Neurosci* 22: 183-92

Butt AM, Colquhoun K, Tutton M, Berry M. 1994. Three-dimensional morphology of astrocytes and oligodendrocytes in the intact mouse optic nerve. *J Neurocytol* 23: 469-85

Cadet JL, Bisagno V. 2014. Glial-neuronal ensembles: partners in drug addiction-associated synaptic plasticity. *Front Pharmacol* 5: 204

Cali C, Agus M, Kare K, Boges DJ, Lehvaslaiho H, et al. 2019. 3D cellular reconstruction of cortical glia and parenchymal morphometric analysis from Serial Block-Face Electron Microscopy of juvenile rat. *Prog Neurobiol* 183: 101696

Chai H, Diaz-Castro B, Shigetomi E, Monte E, Octeau JC, et al. 2017. Neural Circuit-Specialized Astrocytes: Transcriptomic, Proteomic, Morphological, and Functional Evidence. *Neuron* 95: 531-49 e9

Chan B, Kondo K, Freeman M, Ayers C, Montgomery J, Kansagara D. 2019. Pharmacotherapy for Cocaine Use Disorder-a Systematic Review and Meta-analysis. *J Gen Intern Med* 34: 2858-73

Chen BT, Hopf FW, Bonci A. 2010. Synaptic plasticity in the mesolimbic system: therapeutic implications for substance abuse. *Ann N Y Acad Sci* 1187: 129-39

Christopherson KS, Ullian EM, Stokes CC, Mullowney CE, Hell JW, et al. 2005. Thrombospondins are astrocyte-secreted proteins that promote CNS synaptogenesis. *Cell* 120: 421-33

Chung WS, Allen NJ, Eroglu C. 2015. Astrocytes Control Synapse Formation, Function, and

Elimination. *Cold Spring Harb Perspect Biol* 7: a020370

Clark KH, Wiley CA, Bradberry CW. 2013. Psychostimulant abuse and neuroinflammation: emerging evidence of their interconnection. *Neurotox Res* 23: 174-88

Cooper S, Robison AJ, Mazei-Robison MS. 2017. Reward Circuitry in Addiction. *Neurotherapeutics* 14: 687-97

Corkrum M, Covelo A, Lines J, Bellocchio L, Pisansky M, et al. 2020. Dopamine-Evoked Synaptic Regulation in the Nucleus Accumbens Requires Astrocyte Activity. *Neuron* 105: 1036-47 e5

Cornish JL, Kalivas PW. 2001a. Cocaine sensitization and craving: differing roles for dopamine and glutamate in the nucleus accumbens. *J Addict Dis* 20: 43-54

Cornish JL, Kalivas PW. 2001b. Repeated cocaine administration into the rat ventral tegmental area produces behavioral sensitization to a systemic cocaine challenge. *Behav Brain Res* 126: 205-9

Cui C, Shurtleff D, Harris RA. 2014. Neuroimmune mechanisms of alcohol and drug addiction. *Int Rev Neurobiol* 118: 1-12

Dachet F, Brown JB, Valyi-Nagy T, Narayan KD, Serafini A, et al. 2021. Selective time-dependent changes in activity and cell-specific gene expression in human postmortem brain. *Sci Rep* 11: 6078

Dafny N, Yang PB. 2006. The role of age, genotype, sex, and route of acute and chronic administration of methylphenidate: a review of its locomotor effects. *Brain Res Bull* 68: 393-405

Dallerac G, Zapata J, Rouach N. 2018. Versatile control of synaptic circuits by astrocytes: where, when and how? *Nat Rev Neurosci* 19: 729-43

Danbolt NC. 2001. Glutamate uptake. *Prog Neurobiol* 65: 1-105

De Pitta M, Brunel N, Volterra A. 2016. Astrocytes: Orchestrating synaptic plasticity? *Neuroscience* 323: 43-61

Derouiche A, Anlauf E, Aumann G, Muhlstadt B, Lavialle M. 2002. Anatomical aspects of glia-synapse interaction: the perisynaptic glial sheath consists of a specialized astrocyte compartment. *J Physiol Paris* 96: 177-82

Derouiche A, Pannicke T, Haseleu J, Blaess S, Grosche J, Reichenbach A. 2012. Beyond polarity: functional membrane domains in astrocytes and Muller cells. *Neurochem Res* 37: 2513-23

Dong Y, Taylor JR, Wolf ME, Shaham Y. 2017. Circuit and Synaptic Plasticity Mechanisms of Drug Relapse. *J Neurosci* 37: 10867-76

Dossi E, Vasile F, Rouach N. 2018. Human astrocytes in the diseased brain. *Brain Res Bull* 136: 139-56

Durkee CA, Araque A. 2019. Diversity and Specificity of Astrocyte-neuron Communication. *Neuroscience* 396: 73-78

Eichberg J, Shein HM, Hauser G. 1976. Lipid composition and metabolism of cultured hamster brain astrocytes. *J Neurochem* 27: 679-85

Eilam R, Aharoni R, Arnon R, Malach R. 2016. Astrocyte morphology is confined by cortical functional boundaries in mammals ranging from mice to human. *Elife* 5

Eroglu C, Allen NJ, Susman MW, O'Rourke NA, Park CY, et al. 2009. Gabapentin receptor alpha2delta-1 is a neuronal thrombospondin receptor responsible for excitatory CNS synaptogenesis. *Cell* 139: 380-92

Escartin C, Galea E, Lakatos A, O'Callaghan JP, Petzold GC, et al. 2021. Reactive astrocyte nomenclature, definitions, and future directions. *Nat Neurosci* 24: 312-25

Fan XC, Ma CN, Song JC, Liao ZH, Huang N, et al. 2021. Rac1 Signaling in Amygdala Astrocytes Regulates Fear Memory Acquisition and Retrieval. *Neurosci Bull* 37: 947-58

Fattore L, Puddu MC, Picciau S, Cappai A, Fratta W, et al. 2002. Astroglial in vivo response to cocaine in mouse dentate gyrus: a quantitative and qualitative analysis by confocal microscopy. *Neuroscience* 110: 1-6

Ferrario CR, Gorny G, Crombag HS, Li Y, Kolb B, Robinson TE. 2005. Neural and behavioral plasticity associated with the transition from controlled to escalated cocaine use. *Biol Psychiatry* 58: 751-9

Fields RD, Araque A, Johansen-Berg H, Lim SS, Lynch G, et al. 2014. Glial biology in learning and cognition. *Neuroscientist* 20: 426-31

Fischer-Smith KD, Houston AC, Rebec GV. 2012. Differential effects of cocaine access and withdrawal on glutamate type 1 transporter expression in rat nucleus accumbens core and shell. *Neuroscience* 210: 333-9

Florence CM, Baillie LD, Mulligan SJ. 2012. Dynamic volume changes in astrocytes are an intrinsic phenomenon mediated by bicarbonate ion flux. *PLoS One* 7: e51124

Fowler JS, Volkow ND, Wang GJ, Gatley SJ, Logan J. 2001. [(11)]Cocaine: PET studies of cocaine pharmacokinetics, dopamine transporter availability and dopamine transporter occupancy. *Nucl Med Biol* 28: 561-72

Friend DM, Keefe KA. 2013. Glial reactivity in resistance to methamphetamine-induced neurotoxicity. *J Neurochem* 125: 566-74

Gagnon D, Petryszyn S, Sanchez MG, Bories C, Beaulieu JM, et al. 2017. Striatal Neurons

Expressing D1 and D2 Receptors are Morphologically Distinct and Differently Affected by Dopamine Denervation in Mice. *Sci Rep* 7: 41432

Gameiro R, Costa S, Barroso M, Franco J, Fonseca S. 2019. Toxicological analysis of cocaine adulterants in blood samples. *Forensic Sci Int* 299: 95-102

Gatley SJ, Volkow ND, Gifford AN, Ding YS, Logan J, Wang GJ. 1997. Model for estimating dopamine transporter occupancy and subsequent increases in synaptic dopamine using positron emission tomography and carbon-11-labeled cocaine. *Biochem Pharmacol* 53: 43-52

Gillette TA, Ascoli GA. 2015. Topological characterization of neuronal arbor morphology via sequence representation: I--motif analysis. *BMC Bioinformatics* 16: 216

Grimm JW. 2020. Incubation of food craving in rats: A review. *J Exp Anal Behav* 113: 37-47

Grimm JW, Hope BT, Wise RA, Shaham Y. 2001. Neuroadaptation. Incubation of cocaine craving after withdrawal. *Nature* 412: 141-2

Halassa MM, Fellin T, Takano H, Dong JH, Haydon PG. 2007. Synaptic islands defined by the territory of a single astrocyte. *J Neurosci* 27: 6473-7

Halassa MM, Haydon PG. 2010. Integrated brain circuits: astrocytic networks modulate neuronal activity and behavior. *Annu Rev Physiol* 72: 335-55

Hama K, Arii T, Katayama E, Marton M, Ellisman MH. 2004. Tri-dimensional morphometric analysis of astrocytic processes with high voltage electron microscopy of thick Golgi preparations. *J Neurocytol* 33: 277-85

Hamby ME, Sofroniew MV. 2010. Reactive astrocytes as therapeutic targets for CNS disorders. *Neurotherapeutics* 7: 494-506

Hashemi M, Buibas M, Silva GA. 2008. Automated detection of intercellular signaling in astrocyte networks using the converging squares algorithm. *J Neurosci Methods* 170: 294-9

Haydon PG, Carmignoto G. 2006. Astrocyte control of synaptic transmission and neurovascular coupling. *Physiol Rev* 86: 1009-31

Heller JP, Michaluk P, Sugao K, Rusakov DA. 2017. Probing nano-organization of astroglia with multi-color super-resolution microscopy. *J Neurosci Res* 95: 2159-71

Heller JP, Rusakov DA. 2017. The Nanoworld of the Tripartite Synapse: Insights from Super-Resolution Microscopy. *Front Cell Neurosci* 11: 374

Hemby SE, Tang W, Muly EC, Kuhar MJ, Howell L, Mash DC. 2005. Cocaine-induced alterations in nucleus accumbens ionotropic glutamate receptor subunits in human and non-human primates. *J Neurochem* 95: 1785-93

Henneberger C, Bard L, Panatier A, Reynolds JP, Kopach O, et al. 2020. LTP Induction Boosts Glutamate Spillover by Driving Withdrawal of Perisynaptic Astroglia. *Neuron* 108: 919-36 e11

Hertz L. 1981. Features of astrocytic function apparently involved in the response of central nervous tissue to ischemia-hypoxia. *J Cereb Blood Flow Metab* 1: 143-53

Huang YH, Sinha SR, Tanaka K, Rothstein JD, Bergles DE. 2004. Astrocyte glutamate transporters regulate metabotropic glutamate receptor-mediated excitation of hippocampal interneurons. *J Neurosci* 24: 4551-9

Hyman SE. 2013. Psychiatric drug development: diagnosing a crisis. *Cerebrum* 2013: 5

Jaramillo AA, Agan VE, Makhijani VH, Pedroza S, McElligott ZA, Besheer J. 2018. Functional role for suppression of the insular-striatal circuit in modulating interoceptive effects of alcohol. *Addict Biol* 23: 1020-31

John Lin CC, Yu K, Hatcher A, Huang TW, Lee HK, et al. 2017. Identification of diverse astrocyte populations and their malignant analogs. *Nat Neurosci* 20: 396-405

Kalin NH. 2020. Substance Use Disorders and Addiction: Mechanisms, Trends, and Treatment Implications. *Am J Psychiatry* 177: 1015-18

Kalivas PW. 2004. Glutamate systems in cocaine addiction. *Curr Opin Pharmacol* 4: 23-9

Kalivas PW. 2007. Neurobiology of cocaine addiction: implications for new pharmacotherapy. *Am J Addict* 16: 71-8

Kalivas PW. 2009. The glutamate homeostasis hypothesis of addiction. *Nat Rev Neurosci* 10: 561-72

Kalivas PW, McFarland K. 2003. Brain circuitry and the reinstatement of cocaine-seeking behavior. *Psychopharmacology (Berl)* 168: 44-56

Kalivas PW, McFarland K, Bowers S, Szumlinski K, Xi ZX, Baker D. 2003. Glutamate transmission and addiction to cocaine. *Ann N Y Acad Sci* 1003: 169-75

Kalman D, Gomperts SN, Hardy S, Kitamura M, Bishop JM. 1999. Ras family GTPases control growth of astrocyte processes. *Mol Biol Cell* 10: 1665-83

Kang K, Lee SW, Han JE, Choi JW, Song MR. 2014. The complex morphology of reactive astrocytes controlled by fibroblast growth factor signaling. *Glia* 62: 1328-44

Kau KS, Madayag A, Mantsch JR, Grier MD, Abdulhameed O, Baker DA. 2008. Blunted cystine-glutamate antiporter function in the nucleus accumbens promotes cocaine-induced drug seeking. *Neuroscience* 155: 530-7

Kaur D, Sharma V, Deshmukh R. 2019. Activation of microglia and astrocytes: a roadway to

neuroinflammation and Alzheimer's disease. *Inflammopharmacology* 27: 663-77

Khakh BS, Beaumont V, Cachope R, Munoz-Sanjuan I, Goldman SA, Grantyn R. 2017. Unravelling and Exploiting Astrocyte Dysfunction in Huntington's Disease. *Trends Neurosci* 40: 422-37

Khakh BS, Deneen B. 2019. The Emerging Nature of Astrocyte Diversity. *Annu Rev Neurosci* 42: 187-207

Khakh BS, Sofroniew MV. 2015. Diversity of astrocyte functions and phenotypes in neural circuits. *Nat Neurosci* 18: 942-52

Kim R, Healey KL, Sepulveda-Orengo MT, Reissner KJ. 2018a. Astroglial correlates of neuropsychiatric disease: From astrocytopathy to astrogliosis. *Prog Neuropsychopharmacol Biol Psychiatry* 87: 126-46

Kim R, Sepulveda-Orengo MT, Healey KL, Williams EA, Reissner KJ. 2018b. Regulation of glutamate transporter 1 (GLT-1) gene expression by cocaine self-administration and withdrawal. *Neuropharmacology* 128: 1-10

Klein M, Lohr C, Droste D. 2020. Age-Dependent Heterogeneity of Murine Olfactory Bulb Astrocytes. *Front Aging Neurosci* 12: 172

Knackstedt LA, Kalivas PW. 2007. Extended access to cocaine self-administration enhances drug-primed reinstatement but not behavioral sensitization. *J Pharmacol Exp Ther* 322: 1103-9

Knackstedt LA, Melendez RI, Kalivas PW. 2010a. Ceftriaxone restores glutamate homeostasis and prevents relapse to cocaine seeking. *Biol Psychiatry* 67: 81-4

Knackstedt LA, Moussawi K, Lalumiere R, Schwendt M, Klugmann M, Kalivas PW. 2010b. Extinction training after cocaine self-administration induces glutamatergic plasticity to inhibit cocaine seeking. *J Neurosci* 30: 7984-92

Knuth M, Temme O, Daldrup T, Pawlik E. 2018. Analysis of cocaine adulterants in human brain in cases of drug-related death. *Forensic Sci Int* 285: 86-92

Kofuji P, Araque A. 2021. G-Protein-Coupled Receptors in Astrocyte-Neuron Communication. *Neuroscience* 456: 71-84

Koob GF. 2000. Neurobiology of addiction. Toward the development of new therapies. *Ann N Y Acad Sci* 909: 170-85

Korogod N, Petersen CC, Knott GW. 2015. Ultrastructural analysis of adult mouse neocortex comparing aldehyde perfusion with cryo fixation. *Elife* 4

Kruyer A, Dixon D, Angelis A, Amato D, Kalivas PW. 2021. Astrocytes in the ventral pallidum extinguish heroin seeking through GAT-3 upregulation and morphological plasticity at D1-MSN terminals. *Mol Psychiatry*

Kucukdereli H, Allen NJ, Lee AT, Feng A, Ozlu MI, et al. 2011. Control of excitatory CNS synaptogenesis by astrocyte-secreted proteins Hevin and SPARC. *Proc Natl Acad Sci U S A* 108: E440-9

Kulkarni PM, Barton E, Savelonas M, Padmanabhan R, Lu Y, et al. 2015. Quantitative 3-D analysis of GFAP labeled astrocytes from fluorescence confocal images. *J Neurosci Methods* 246: 38-51

Lacagnina MJ, Rivera PD, Bilbo SD. 2017. Glial and Neuroimmune Mechanisms as Critical Modulators of Drug Use and Abuse. *Neuropsychopharmacology* 42: 156-77

Lavialle M, Aumann G, Anlauf E, Prols F, Arpin M, Derouiche A. 2011. Structural plasticity of perisynaptic astrocyte processes involves ezrin and metabotropic glutamate receptors. *Proc Natl Acad Sci U S A* 108: 12915-9

Lee BR, Dong Y. 2011. Cocaine-induced metaplasticity in the nucleus accumbens: silent synapse and beyond. *Neuropharmacology* 61: 1060-9

Lenz JD, Lobo MK. 2013. Optogenetic insights into striatal function and behavior. *Behav Brain Res* 255: 44-54

Li X, Caprioli D, Marchant NJ. 2015. Recent updates on incubation of drug craving: a mini-review. *Addict Biol* 20: 872-6

Li Y, Li L, Wu J, Zhu Z, Feng X, et al. 2020. Activation of astrocytes in hippocampus decreases fear memory through adenosine A1 receptors. *Elife* 9

Liao Z, Tao Y, Guo X, Cheng D, Wang F, et al. 2017. Fear Conditioning Downregulates Rac1 Activity in the Basolateral Amygdala Astrocytes to Facilitate the Formation of Fear Memory. *Front Mol Neurosci* 10: 396

Lidow MS. 1995. Prenatal cocaine exposure adversely affects development of the primate cerebral cortex. *Synapse* 21: 332-41

Lipsky RH, Xu K, Zhu D, Kelly C, Terhakopian A, et al. 2001. Nuclear factor kappaB is a critical determinant in N-methyl-D-aspartate receptor-mediated neuroprotection. *J Neurochem* 78: 254-64

Little KY, Ramssen E, Welchko R, Volberg V, Roland CJ, Cassin B. 2009. Decreased brain dopamine cell numbers in human cocaine users. *Psychiatry Res* 168: 173-80

Liu JF, Li JX. 2018. Drug addiction: a curable mental disorder? *Acta Pharmacol Sin* 39: 1823-29

Logan CN, LaCrosse AL, Knackstedt LA. 2018. Nucleus accumbens GLT-1a overexpression reduces glutamate efflux during reinstatement of cocaine-seeking but is not sufficient to attenuate reinstatement. *Neuropharmacology* 135: 297-307

Logan J, Volkow ND, Fowler JS, Wang GJ, Fischman MW, et al. 1997. Concentration and

occupancy of dopamine transporters in cocaine abusers with [11C]cocaine and PET. *Synapse* 27: 347-56

Loweth JA, Tseng KY, Wolf ME. 2014. Adaptations in AMPA receptor transmission in the nucleus accumbens contributing to incubation of cocaine craving. *Neuropharmacology* 76 Pt B: 287-300

Lu L, Grimm JW, Hope BT, Shaham Y. 2004. Incubation of cocaine craving after withdrawal: a review of preclinical data. *Neuropharmacology* 47 Suppl 1: 214-26

Luscher C. 2016. The Emergence of a Circuit Model for Addiction. *Annu Rev Neurosci* 39: 257-76

Lynch WJ, Nicholson KL, Dance ME, Morgan RW, Foley PL. 2010. Animal models of substance abuse and addiction: implications for science, animal welfare, and society. *Comp Med* 60: 177-88

Maatouk L, Yi C, Carrillo-de Sauvage MA, Compagnion AC, Hunot S, et al. 2019. Glucocorticoid receptor in astrocytes regulates midbrain dopamine neurodegeneration through connexin hemichannel activity. *Cell Death Differ* 26: 580-96

Madayag A, Lobner D, Kau KS, Mantsch JR, Abdulhameed O, et al. 2007. Repeated N-acetylcysteine administration alters plasticity-dependent effects of cocaine. *J Neurosci* 27: 13968-76

Magistretti PJ, Allaman I. 2018. Lactate in the brain: from metabolic end-product to signalling molecule. *Nat Rev Neurosci* 19: 235-49

Mahmoud S, Gharagozloo M, Simard C, Gris D. 2019. Astrocytes Maintain Glutamate Homeostasis in the CNS by Controlling the Balance between Glutamate Uptake and Release. *Cells* 8

Mameli M, Luscher C. 2011. Synaptic plasticity and addiction: learning mechanisms gone awry. *Neuropharmacology* 61: 1052-9

Mantsch JR, Yuferov V, Mathieu-Kia AM, Ho A, Kreek MJ. 2004. Effects of extended access to high versus low cocaine doses on self-administration, cocaine-induced reinstatement and brain mRNA levels in rats. *Psychopharmacology (Berl)* 175: 26-36

Martin-Fernandez M, Jamison S, Robin LM, Zhao Z, Martin ED, et al. 2017. Synapse-specific astrocyte gating of amygdala-related behavior. *Nat Neurosci* 20: 1540-48

Martin M, Chen BT, Hopf FW, Bowers MS, Bonci A. 2006. Cocaine self-administration selectively abolishes LTD in the core of the nucleus accumbens. *Nat Neurosci* 9: 868-9

McBean GJ. 2002. Cerebral cystine uptake: a tale of two transporters. *Trends Pharmacol Sci* 23: 299-302

McFarland K, Kalivas PW. 2001. The circuitry mediating cocaine-induced reinstatement of drug-seeking behavior. *J Neurosci* 21: 8655-63

McGee AW, Bredt DS. 2003. Assembly and plasticity of the glutamatergic postsynaptic specialization. *Curr Opin Neurobiol* 13: 111-8

McKhann GM, 2nd, D'Ambrosio R, Janigro D. 1997. Heterogeneity of astrocyte resting membrane potentials and intercellular coupling revealed by whole-cell and gramicidin-perforated patch recordings from cultured neocortical and hippocampal slice astrocytes. *J Neurosci* 17: 6850-63

McLellan AT. 2017. Substance Misuse and Substance use Disorders: Why do they Matter in Healthcare? *Trans Am Clin Climatol Assoc* 128: 112-30

Miguel-Hidalgo JJ. 2009. The Role of Glial Cells in Drug Abuse. *Curr Drug Abuse Rev* 2: 76-82

Mitra S, Gobira PH, Werner CT, Martin JA, Iida M, et al. 2021. A role for the endocannabinoid enzymes monoacylglycerol and diacylglycerol lipases in cue-induced cocaine craving following prolonged abstinence. *Addict Biol* 26: e13007

Mogenson GJ, Jones DL, Yim CY. 1980. From motivation to action: functional interface between the limbic system and the motor system. *Prog Neurobiol* 14: 69-97

Moussawi K, Pacchioni A, Moran M, Olive MF, Gass JT, et al. 2009. N-Acetylcysteine reverses cocaine-induced metaplasticity. *Nat Neurosci* 12: 182-9

Munhoz CD, Garcia-Bueno B, Madrigal JL, Lepsch LB, Scavone C, Leza JC. 2008. Stress-induced neuroinflammation: mechanisms and new pharmacological targets. *Braz J Med Biol Res* 41: 1037-46

Murk K, Blanco Suarez EM, Cockbill LM, Banks P, Hanley JG. 2013. The antagonistic modulation of Arp2/3 activity by N-WASP, WAVE2 and PICK1 defines dynamic changes in astrocyte morphology. *J Cell Sci* 126: 3873-83

Murphy TR, Binder DK, Fiacco TA. 2017. Turning down the volume: Astrocyte volume change in the generation and termination of epileptic seizures. *Neurobiol Dis* 104: 24-32

Narayan PJ, Gibbons HM, Mee EW, Faull RL, Dragunow M. 2007. High throughput quantification of cells with complex morphology in mixed cultures. *J Neurosci Methods* 164: 339-49

Naskar S, Chattarji S. 2019. Stress Elicits Contrasting Effects on the Structure and Number of Astrocytes in the Amygdala versus Hippocampus. *eNeuro* 6

Nennig SE, Schank JR. 2017. The Role of NFkB in Drug Addiction: Beyond Inflammation. *Alcohol Alcohol* 52: 172-79

Nesse RM, Berridge KC. 1997. Psychoactive drug use in evolutionary perspective. *Science* 278: 63-6

Nestler EJ. 2001. Molecular basis of long-term plasticity underlying addiction. *Nat Rev Neurosci* 2: 119-28

O'Connor EC, Chapman K, Butler P, Mead AN. 2011. The predictive validity of the rat self-administration model for abuse liability. *Neurosci Biobehav Rev* 35: 912-38

O'Leary LA, Belliveau C, Davoli MA, Ma JC, Tanti A, et al. 2021. Widespread Decrease of Cerebral Vimentin-Immunoreactive Astrocytes in Depressed Suicides. *Front Psychiatry* 12: 640963

Octeau JC, Chai H, Jiang R, Bonanno SL, Martin KC, Khakh BS. 2018. An Optical Neuron-Astrocyte Proximity Assay at Synaptic Distance Scales. *Neuron* 98: 49-66 e9

Okada S, Hara M, Kobayakawa K, Matsumoto Y, Nakashima Y. 2018. Astrocyte reactivity and astrogliosis after spinal cord injury. *Neurosci Res* 126: 39-43

Omrani A, Melone M, Bellesi M, Safiulina V, Aida T, et al. 2009. Up-regulation of GLT-1 severely impairs LTD at mossy fibre--CA3 synapses. *J Physiol* 587: 4575-88

Panatier A, Arizono M, Nagerl UV. 2014. Dissecting tripartite synapses with STED microscopy. *Philos Trans R Soc Lond B Biol Sci* 369: 20130597

Panlilio LV, Goldberg SR. 2007. Self-administration of drugs in animals and humans as a model and an investigative tool. *Addiction* 102: 1863-70

Pannasch U, Freche D, Dallerac G, Ghezali G, Escartin C, et al. 2014. Connexin 30 sets synaptic strength by controlling astroglial synapse invasion. *Nat Neurosci* 17: 549-58

Parvaz MA, Moeller SJ, Goldstein RZ. 2016. Incubation of Cue-Induced Craving in Adults Addicted to Cocaine Measured by Electroencephalography. *JAMA Psychiatry* 73: 1127-34

Paterson NE, Markou A. 2003. Increased motivation for self-administered cocaine after escalated cocaine intake. *Neuroreport* 14: 2229-32

Pellegrino T, Bayer BM. 1998. In vivo effects of cocaine on immune cell function. *J Neuroimmunol* 83: 139-47

Perego C, Vanoni C, Bossi M, Massari S, Basudev H, et al. 2000. The GLT-1 and GLAST glutamate transporters are expressed on morphologically distinct astrocytes and regulated by neuronal activity in primary hippocampal cocultures. *J Neurochem* 75: 1076-84

Perez-Alvarez A, Navarrete M, Covelo A, Martin ED, Araque A. 2014. Structural and functional plasticity of astrocyte processes and dendritic spine interactions. *J Neurosci* 34: 12738-44

Periyasamy P, Guo ML, Buch S. 2016. Cocaine induces astrocytosis through ER stress-mediated activation of autophagy. *Autophagy* 12: 1310-29

Philips T, Rothstein JD. 2014. Glial cells in amyotrophic lateral sclerosis. *Exp Neurol* 262 Pt B:

111-20

Pickens CL, Airavaara M, Theberge F, Fanous S, Hope BT, Shaham Y. 2011. Neurobiology of the incubation of drug craving. *Trends Neurosci* 34: 411-20

Pirici D, Mogoanta L, Margaritescu O, Pirici I, Tudorica V, Coconu M. 2009. Fractal analysis of astrocytes in stroke and dementia. *Rom J Morphol Embryol* 50: 381-90

Popov A, Brazhe A, Denisov P, Sutyagina O, Li L, et al. 2021. Astrocyte dystrophy in ageing brain parallels impaired synaptic plasticity. *Aging Cell* 20: e13334

Popov A, Denisov P, Bychkov M, Brazhe A, Lyukmanova E, et al. 2020. Caloric restriction triggers morphofunctional remodeling of astrocytes and enhances synaptic plasticity in the mouse hippocampus. *Cell Death Dis* 11: 208

Potokar M, Kreft M, Li L, Daniel Andersson J, Pangrsic T, et al. 2007. Cytoskeleton and vesicle mobility in astrocytes. *Traffic* 8: 12-20

Potokar M, Morita M, Wiche G, Jorgacevski J. 2020. The Diversity of Intermediate Filaments in Astrocytes. *Cells* 9

Prochiantz A, Mallat M. 1988. Astrocyte diversity. *Ann N Y Acad Sci* 540: 52-63

Rajkowska G, Stockmeier CA. 2013. Astrocyte pathology in major depressive disorder: insights from human postmortem brain tissue. *Curr Drug Targets* 14: 1225-36

Reeves AM, Shigetomi E, Khakh BS. 2011. Bulk loading of calcium indicator dyes to study astrocyte physiology: key limitations and improvements using morphological maps. *J Neurosci* 31: 9353-8

Reichenbach A, Derouiche A, Kirchhoff F. 2010. Morphology and dynamics of perisynaptic glia. *Brain Res Rev* 63: 11-25

Reissner KJ, Brown RM, Spencer S, Tran PK, Thomas CA, Kalivas PW. 2014. Chronic administration of the methylxanthine propentofylline impairs reinstatement to cocaine by a GLT-1-dependent mechanism. *Neuropsychopharmacology* 39: 499-506

Reissner KJ, Gipson CD, Tran PK, Knackstedt LA, Scofield MD, Kalivas PW. 2015. Glutamate transporter GLT-1 mediates N-acetylcysteine inhibition of cocaine reinstatement. *Addict Biol* 20: 316-23

Reissner KJ, Kalivas PW. 2010. Using glutamate homeostasis as a target for treating addictive disorders. *Behav Pharmacol* 21: 514-22

Reissner KJ, Uys JD, Schwacke JH, Comte-Walters S, Rutherford-Bethard JL, et al. 2011. AKAP signaling in reinstated cocaine seeking revealed by iTRAQ proteomic analysis. *J Neurosci* 31: 5648-58

Rimmele TS, Rosenberg PA. 2016. GLT-1: The elusive presynaptic glutamate transporter. *Neurochem Int* 98: 19-28

Roberts DC, Brebner K, Vincler M, Lynch WJ. 2002. Patterns of cocaine self-administration in rats produced by various access conditions under a discrete trials procedure. *Drug Alcohol Depend* 67: 291-9

Roberts RC, Roche JK, McCullumsmith RE. 2014. Localization of excitatory amino acid transporters EAAT1 and EAAT2 in human postmortem cortex: a light and electron microscopic study. *Neuroscience* 277: 522-40

Roitman MF, Wheeler RA, Carelli RM. 2005. Nucleus accumbens neurons are innately tuned for rewarding and aversive taste stimuli, encode their predictors, and are linked to motor output. *Neuron* 45: 587-97

Rothstein JD, Patel S, Regan MR, Haenggeli C, Huang YH, et al. 2005. Beta-lactam antibiotics offer neuroprotection by increasing glutamate transporter expression. *Nature* 433: 73-7

Russo SJ, Wilkinson MB, Mazei-Robison MS, Dietz DM, Maze I, et al. 2009. Nuclear factor kappa B signaling regulates neuronal morphology and cocaine reward. *J Neurosci* 29: 3529-37

Salin A, Lardeux V, Solinas M, Belujon P. 2021. Protracted Abstinence From Extended Cocaine Self-Administration Is Associated With Hypodopaminergic Activity in the VTA but Not in the SNc. *Int J Neuropsychopharmacol* 24: 499-504

Sanchis-Segura C, Spanagel R. 2006. Behavioural assessment of drug reinforcement and addictive features in rodents: an overview. *Addict Biol* 11: 2-38

Santello M, Toni N, Volterra A. 2019. Astrocyte function from information processing to cognition and cognitive impairment. *Nat Neurosci* 22: 154-66

Saunders BT, Richard JM, Janak PH. 2015. Contemporary approaches to neural circuit manipulation and mapping: focus on reward and addiction. *Philos Trans R Soc Lond B Biol Sci* 370: 20140210

Saur L, Baptista PP, Bagatini PB, Neves LT, de Oliveira RM, et al. 2016. Experimental Post-traumatic Stress Disorder Decreases Astrocyte Density and Changes Astrocytic Polarity in the CA1 Hippocampus of Male Rats. *Neurochem Res* 41: 892-904

Schitine C, Nogaroli L, Costa MR, Hedin-Pereira C. 2015. Astrocyte heterogeneity in the brain: from development to disease. *Front Cell Neurosci* 9: 76

Schiweck J, Eickholt BJ, Murk K. 2018. Important Shapeshifter: Mechanisms Allowing Astrocytes to Respond to the Changing Nervous System During Development, Injury and Disease. *Front Cell Neurosci* 12: 261

Scofield MD, Boger HA, Smith RJ, Li H, Haydon PG, Kalivas PW. 2015. Gq-DREADD Selectively Initiates Glial Glutamate Release and Inhibits Cue-induced Cocaine Seeking.

Biol Psychiatry 78: 441-51

Scofield MD, Heinsbroek JA, Gipson CD, Kupchik YM, Spencer S, et al. 2016a. The Nucleus Accumbens: Mechanisms of Addiction across Drug Classes Reflect the Importance of Glutamate Homeostasis. *Pharmacol Rev* 68: 816-71

Scofield MD, Kalivas PW. 2014. Astrocytic dysfunction and addiction: consequences of impaired glutamate homeostasis. *Neuroscientist* 20: 610-22

Scofield MD, Li H, Siemsen BM, Healey KL, Tran PK, et al. 2016b. Cocaine Self-Administration and Extinction Leads to Reduced Glial Fibrillary Acidic Protein Expression and Morphometric Features of Astrocytes in the Nucleus Accumbens Core. *Biol Psychiatry* 80: 207-15

Self DW, Choi KH, Simmons D, Walker JR, Smagula CS. 2004. Extinction training regulates neuroadaptive responses to withdrawal from chronic cocaine self-administration. *Learn Mem* 11: 648-57

Sepulveda-Orengo MT, Healey KL, Kim R, Auriemma AC, Rojas J, et al. 2018. Riluzole Impairs Cocaine Reinstatement and Restores Adaptations in Intrinsic Excitability and GLT-1 Expression. *Neuropsychopharmacology : official publication of the American College of Neuropsychopharmacology* 43: 1212-23

Sethian JA. 1996. A fast marching level set method for monotonically advancing fronts. *Proc Natl Acad Sci U S A* 93: 1591-5

Shaham Y, Shalev U, Lu L, de Wit H, Stewart J. 2003. The reinstatement model of drug relapse: history, methodology and major findings. *Psychopharmacology (Berl)* 168: 3-20

Shibasaki K, Ikenaka K, Tamalu F, Tominaga M, Ishizaki Y. 2014. A novel subtype of astrocytes expressing TRPV4 (transient receptor potential vanilloid 4) regulates neuronal excitability via release of gliotransmitters. *J Biol Chem* 289: 14470-80

Shigetomi E, Bushong EA, Haustein MD, Tong X, Jackson-Weaver O, et al. 2013. Imaging calcium microdomains within entire astrocyte territories and endfeet with GCaMPs expressed using adeno-associated viruses. *J Gen Physiol* 141: 633-47

Shigetomi E, Kracun S, Khakh BS. 2010. Monitoring astrocyte calcium microdomains with improved membrane targeted GCaMP reporters. *Neuron Glia Biol* 6: 183-91

Simard M, Nedergaard M. 2004. The neurobiology of glia in the context of water and ion homeostasis. *Neuroscience* 129: 877-96

Singh A, Abraham WC. 2017. Astrocytes and synaptic plasticity in health and disease. *Exp Brain Res* 235: 1645-55

Sinha R. 2011. New findings on biological factors predicting addiction relapse vulnerability. *Curr Psychiatry Rep* 13: 398-405

Siracusa R, Fusco R, Cuzzocrea S. 2019. Astrocytes: Role and Functions in Brain Pathologies. *Front Pharmacol* 10: 1114

Smaga I, Wydra K, Frankowska M, Fumagalli F, Sanak M, Filip M. 2020. Cocaine Self-Administration and Abstinence Modulate NMDA Receptor Subunits and Active Zone Proteins in the Rat Nucleus Accumbens. *Molecules* 25

Smith BA, Daugherty-Clarke K, Goode BL, Gelles J. 2013. Pathway of actin filament branch formation by Arp2/3 complex revealed by single-molecule imaging. *Proc Natl Acad Sci U S A* 110: 1285-90

Sofroniew MV. 2015. Astrocyte barriers to neurotoxic inflammation. *Nat Rev Neurosci* 16: 249-63

Sofroniew MV, Vinters HV. 2010. Astrocytes: biology and pathology. *Acta Neuropathol* 119: 7-35

Spanagel R. 2017. Animal models of addiction. *Dialogues Clin Neurosci* 19: 247-58

Stockmeier CA, Rajkowska G. 2004. Cellular abnormalities in depression: evidence from postmortem brain tissue. *Dialogues Clin Neurosci* 6: 185-97

Su ZZ, Leszczyniecka M, Kang DC, Sarkar D, Chao W, et al. 2003. Insights into glutamate transport regulation in human astrocytes: cloning of the promoter for excitatory amino acid transporter 2 (EAAT2). *Proc Natl Acad Sci U S A* 100: 1955-60

Sullivan RJ, Hagen EH. 2002. Psychotropic substance-seeking: evolutionary pathology or adaptation? *Addiction* 97: 389-400

Swanson CJ, Baker DA, Carson D, Worley PF, Kalivas PW. 2001. Repeated cocaine administration attenuates group I metabotropic glutamate receptor-mediated glutamate release and behavioral activation: a potential role for Homer. *J Neurosci* 21: 9043-52

Tang XC, Kalivas PW. 2003. Bidirectional modulation of cystine/glutamate exchanger activity in cultured cortical astrocytes. *Ann N Y Acad Sci* 1003: 472-5

Tannu N, Mash DC, Hemby SE. 2007. Cytosolic proteomic alterations in the nucleus accumbens of cocaine overdose victims. *Mol Psychiatry* 12: 55-73

Tannu NS, Howell LL, Hemby SE. 2010. Integrative proteomic analysis of the nucleus accumbens in rhesus monkeys following cocaine self-administration. *Mol Psychiatry* 15: 185-203

Tasdemir-Yilmaz OE, Freeman MR. 2014. Astrocytes engage unique molecular programs to engulf pruned neuronal debris from distinct subsets of neurons. *Genes Dev* 28: 20-33

Testen A, Ali M, Sexton HG, Hodges S, Dubester K, et al. 2019. Region-Specific Differences in Morphometric Features and Synaptic Colocalization of Astrocytes During Development. *Neuroscience* 400: 98-109

Testen A, Kim R, Reissner KJ. 2020. High-Resolution Three-Dimensional Imaging of Individual Astrocytes Using Confocal Microscopy. *Curr Protoc Neurosci* 91: e92

Testen A, Sepulveda-Orengo MT, Gaines CH, Reissner KJ. 2018. Region-Specific Reductions in Morphometric Properties and Synaptic Colocalization of Astrocytes Following Cocaine Self-Administration and Extinction. *Front Cell Neurosci* 12: 246

Theparambil SM, Hosford PS, Ruminot I, Kopach O, Reynolds JR, et al. 2020. Astrocytes regulate brain extracellular pH via a neuronal activity-dependent bicarbonate shuttle. *Nat Commun* 11: 5073

Toda S, Alguacil LF, Kalivas PW. 2003. Repeated cocaine administration changes the function and subcellular distribution of adenosine A1 receptor in the rat nucleus accumbens. *J Neurochem* 87: 1478-84

Toda S, Shen HW, Peters J, Cagle S, Kalivas PW. 2006. Cocaine increases actin cycling: effects in the reinstatement model of drug seeking. *J Neurosci* 26: 1579-87

Turner DA, Adamson DC. 2011. Neuronal-astrocyte metabolic interactions: understanding the transition into abnormal astrocytoma metabolism. *J Neuropathol Exp Neurol* 70: 167-76

Tzschentke TM. 2007. Measuring reward with the conditioned place preference (CPP) paradigm: update of the last decade. *Addict Biol* 12: 227-462

Udomuksorn W, Mukem S, Kumarnsit E, Vongvatcharanon S, Vongvatcharanon U. 2011. Effects of alcohol administration during adulthood on parvalbumin and glial fibrillary acidic protein immunoreactivity in the rat cerebral cortex. *Acta Histochem* 113: 283-9

Uhl GR, Koob GF, Cable J. 2019. The neurobiology of addiction. *Ann N Y Acad Sci* 1451: 5-28

Uys JD, Reissner KJ. 2011. Glutamatergic neuroplasticity in cocaine addiction. *Prog Mol Biol Transl Sci* 98: 367-400

Venniro M, Caprioli D, Shaham Y. 2016. Animal models of drug relapse and craving: From drug priming-induced reinstatement to incubation of craving after voluntary abstinence. *Prog Brain Res* 224: 25-52

Venniro M, Zhang M, Shaham Y, Caprioli D. 2017. Incubation of Methamphetamine but not Heroin Craving After Voluntary Abstinence in Male and Female Rats. *Neuropsychopharmacology* 42: 1126-35

Verkhratsky A, Nedergaard M. 2018. Physiology of Astroglia. *Physiol Rev* 98: 239-389

Vivino FB, Carsons SE, Foulks G, Daniels TE, Parke A, et al. 2016. New Treatment Guidelines for Sjogren's Disease. *Rheum Dis Clin North Am* 42: 531-51

Volkow ND, Wang GJ, Fischman MW, Foltin RW, Fowler JS, et al. 1997a. Relationship between subjective effects of cocaine and dopamine transporter occupancy. *Nature* 386: 827-30

Volkow ND, Wang GJ, Fowler JS. 1997b. Imaging studies of cocaine in the human brain and studies of the cocaine addict. *Ann N Y Acad Sci* 820: 41-54; discussion 54-5

Volkow ND, Wang GJ, Fowler JS, Logan J, Gatley SJ, et al. 1997c. Decreased striatal dopaminergic responsiveness in detoxified cocaine-dependent subjects. *Nature* 386: 830-3

Wahis J, Baudon A, Althammer F, Kerspern D, Goyon S, et al. 2021. Astrocytes mediate the effect of oxytocin in the central amygdala on neuronal activity and affective states in rodents. *Nat Neurosci* 24: 529-41

Wang GJ, Volkow ND, Fowler JS, Fischman M, Foltin R, et al. 1997. Cocaine abusers do not show loss of dopamine transporters with age. *Life Sci* 61: 1059-65

Wang J, Holt LM, Huang HH, Sesack SR, Nestler EJ, Dong Y. 2021. Astrocytes in cocaine addiction and beyond. *Mol Psychiatry*

Wang ZJ, Martin JA, Gancarz AM, Adank DN, Sim FJ, Dietz DM. 2017. Activin A is increased in the nucleus accumbens following a cocaine binge. *Sci Rep* 7: 43658

Webster MJ, O'Grady J, Kleinman JE, Weickert CS. 2005. Glial fibrillary acidic protein mRNA levels in the cingulate cortex of individuals with depression, bipolar disorder and schizophrenia. *Neuroscience* 133: 453-61

Wilkin GP, Marriott DR, Cholewinski AJ. 1990. Astrocyte heterogeneity. *Trends Neurosci* 13: 43-6

Wolf ME. 2003. Effects of psychomotor stimulants on glutamate receptor expression. *Methods Mol Med* 79: 13-31

Wolf ME. 2016. Synaptic mechanisms underlying persistent cocaine craving. *Nat Rev Neurosci* 17: 351-65

Wolf ME, Ferrario CR. 2010. AMPA receptor plasticity in the nucleus accumbens after repeated exposure to cocaine. *Neurosci Biobehav Rev* 35: 185-211

Wolff JR, Nemecek S. 1970. [New information on the ultrastructure and function of astroglia]. *Cesk Neurol* 33: 74-9

Zhang LY, Zhou YQ, Yu ZP, Zhang XQ, Shi J, Shen HW. 2021. Restoring glutamate homeostasis in the nucleus accumbens via endocannabinoid-mimetic drug prevents relapse to cocaine seeking behavior in rats. *Neuropsychopharmacology* 46: 970-81

Zhang Y, Barres BA. 2010. Astrocyte heterogeneity: an underappreciated topic in neurobiology. *Curr Opin Neurobiol* 20: 588-94

Zlatkine P, Mehul B, Magee AI. 1997. Retargeting of cytosolic proteins to the plasma membrane by the Lck protein tyrosine kinase dual acylation motif. *J Cell Sci* 110 (Pt 5): 673-9